A&A 438, 685–704 (2005)
DOI: 10.1051/0004-6361:20042126

Astronomy & Astrophysics

The sensitivity of Lick indices to abundance variations⋆

A. J. Korn⋆⋆, C. Maraston⋆⋆⋆, and D. Thomas⋆⋆⋆

Max-Planck-Institut für extraterrestrische Physik (MPE), Giessenbachstraße, 85748 Garching, Germany
e-mail: akorn@mpe.mpg.de

Received 6 October 2004 / Accepted 17 April 2005

Abstract. We present results of model atmosphere/line formation calculations which quantitatively test how the 21 classical and four higher-order Balmer-line Lick/IDS indices (Worthey et al. 1994, ApJS, 94, 687; Worthey & Ottaviani 1997, ApJS, 111, 377) depend on individual elemental abundances (of carbon, nitrogen, oxygen, magnesium, iron, calcium, sodium, silicon, chromium, titanium) and overall metallicity in various stellar evolutionary stages and at various metallicities. At low metallicities the effects of an overall enhancement of α-elements are also investigated. The general results obtained by Tripicco & Bell (1995, ApJ, 110, 3035) at solar metallicity are confirmed, while details do differ. Tables are given detailing to which element every index reacts significantly, as a function of evolutionary stage and composition.
This work validates a number of assumptions implicitly made in the stellar population models of Thomas et al. (2003a, MNRAS, 339, 897), which utilized the results of Tripicco & Bell (1995) to include the effects of element abundance ratios variations. In particular, these computations confirm that fractional changes to index strengths computed at solar metallicity (and solar age) can be applied over a wide range of abundances and ages, also to model old stellar populations with non-solar abundance ratios. The use of metallicity-dependent response functions not only leads to a higher degree of self-consistency in the stellar population models, but is even required for the proper modelling of the Balmer-line indices. We find that the latter become increasingly sensitive to element abundances with increasing metallicity and decreasing wavelength. While Hβ still responds only moderately to abundance ratio variations, the higher-order Balmer-line indices Hγ and Hδ display very strong dependencies at high metallicities. As shown in Thomas et al. (2004, MNRAS, 351, L19), this result allows to remove systematic effects in age determinations based on different Balmer-line indices.

Key words. radiative transfer – line: formation – stars: late-type – galaxies: abundances – galaxies: evolution – galaxies: fundamental parameters

1. Introduction

In order to constrain galaxy formation models, and with it the cosmological evolution of the baryonic Universe, the analysis of stellar populations is of primary importance, because it provides the unique way of measuring the metal enrichment and the epoch(s) of star formation. Furthermore, if it was possible to measure the relative abundances of individual elements in integrated spectra, in the same way one does for single stars (e.g. magnesium, iron, calcium, oxygen), this would provide further important information on the detailed chemical enrichment. In massive galaxies the situation is, however, more complicated. The dispersion of the velocity distribution significantly reduces the *intrinsic* spectral resolution, in other words single absorption lines are not resolved. Typical galaxy spectra exhibit relatively broad absorption features, that contain a huge number of lines from a large variety of chemical elements. This obviously complicates the chemical abundance analysis.

Substantial progress in exploiting galaxy spectra has been made by the Lick group who defined a set of so-called absorption-line indices in the visual region (4000 Å $\lesssim \lambda \lesssim$ 6400 Å) with relatively wide band-passes on the feature ($\Delta\lambda \sim$ 20–40 Å) and two windows blue- and redward of the band-pass defining pseudo-continua (Burstein et al. 1984). The various indices were measured on a large sample of Milky Way stars, mostly located in the solar vicinity, and were related with the stellar parameters, effective temperature ($T_{\rm eff}$), surface gravity (g), total metallicity (Z), by analytical relations, known as the Lick fitting functions (Gorgas et al. 1993; Worthey et al. 1994). The latter are then plugged into an evolutionary synthesis code which produces integrated Lick indices for stellar population models (Worthey 1994). The comparison of galaxy data with these models allows one in principle to quantify the metallicity of the galaxy.

It had been realized from the very start, that the interpretation of the Lick indices would not be as simple as the naming of the indices suggests. The modelled Lick indices fail to match

⋆ Tables 6–32 are only available in electronic form at http://www.edpsciences.org and at http://www-astro.physics.ox.ac.uk/~dthomas

⋆⋆ Leopoldina fellow at Uppsala Astronomical Observatory, Box 515, 751 20 Uppsala, Sweden.
⋆⋆⋆ *Present address*: University of Oxford, Denys Wilkinson Building, Keble Road, Oxford OX1 3RH, UK.

the data of elliptical galaxies (Worthey et al. 1994; Davies et al. 1993; Carollo & Danziger 1994), more specifically magnesium indices were found to be much stronger than predicted by the models at a given iron index. The calibration of the models with globular cluster (GC) data having abundance patterns known from high-resolution spectroscopy have secured the conclusion that the mismatch is indeed caused by an elemental abundance effect, in particular an enhanced [α/Fe] ratio (Maraston et al. 2003). There are several astrophysical environments that have non-solar elemental proportions, which urges the computation of models for a variety of chemical mixtures. This task is difficult to accomplish empirically by using observed spectra, because these are bound to trace the specific chemical history of the portion of Universe the stars were born in (cf. efforts of Borges et al. 1995; Idiart et al. 1997; Lejeune et al. 1997; and LeBorgne et al. 2004).

The theoretical approach has the undoubted advantage of allowing a much larger variety of chemical mixtures and ages, and was the way embarked on by the seminal study of Tripicco & Bell (1995, hereafter TB95). The authors investigated how the 21 original indices depend upon individual abundance variations for representative positions along a solar-metallicity 5 Gyr isochrone. On the whole, their calculations succeeded in reproducing many of the observed index strengths, while some deficits were uncovered.

Thomas et al. (2003a, hereafter TMB03) have implemented the results by TB95 for the individual stars in a theoretical scheme, using an extension of the method introduced by Trager et al. (2000). This allows the computation of a complete stellar population model, thereby providing integrated Lick indices for a variety of chemical mixtures. In first applications, α/Fe and Ca/Fe ratios of early-type galaxies have been derived (Thomas et al. 2003b, 2004).

Although the models have been carefully calibrated to reproduce the absorption lines of globular clusters with known element abundance ratios, a number of approximations have entered their modelling, due to the limited range of results published by TB95.

Firstly, TB95 measured the index variations for solar metallicity only, while the corresponding partial derivatives have been applied by TMB03 to a large range of chemical compositions. Although the calibrating GCs span a wide range in metallicities, super-solar metallicities are not covered, while they are very important for many applications. Also, the very low metallicities encountered in Halo GCs ([Z/H] ~ -2) remain to be calibrated.

Secondly, TB95 selected the three representative stars, a main-sequence dwarf, a turnoff and a giant star on a 5 Gyr isochrone (shown to match the colour–magnitude diagram of the open cluster M 67), while TMB03 used the results for these stars to compute models for a wide range of ages from 1 to 15 Gyr (and thus a range of stellar parameters as well).

Thirdly, TB95 analysed the classical Lick indices, while absorption indices in other wavelength ranges are nowadays in wide use, and especially for high-redshift galaxies bluer wavelength settings are required.

The principle goal of the present paper is to verify and extend the work of TB95, the prior by using an independent model atmosphere code, the latter by investigating how all 25 Lick indices react to abundance variations at different metallicities. That is, we extend the computations to include the four higher-order Balmer-line indices H$\gamma_{\rm A}$, H$\gamma_{\rm F}$, H$\delta_{\rm A}$, H$\delta_{\rm F}$ defined by Worthey & Ottaviani (1997) and the modification of the Fe5270 index by the SAURON collaboration (Davies et al. 2001; Falcon-Barroso et al. 2004; H. Kuntschner, private communication).

Section 2 describes the computations we have performed and confronts the synthetic spectra with high-resolution spectra of the Sun and Arcturus. In Sect. 3 the derived index values are compared with the computations by TB95 and the empirical fitting functions (relating line index strengths and stellar parameters, hereafter referred to as FFs) of Worthey et al. (1994). The behaviour of every index to abundance variations is subsequently discussed individually. Section 4 puts the new computations in the context of stellar population models, while Sect. 5 summarizes our results.

2. Computations

2.1. Model atmospheres

All spectra and indices presented below are based on the model atmosphere code originally written by Gehren (Gehren 1975a,b) and later named MAFAGS. Just like e.g. ATLAS (Kurucz 1993a) or MARCS (Gustafsson et al. 1975), this code produces model temperature structures for the photospheres of cool stars assuming a plane-parallel geometry in hydrostatic equilibrium and LTE. The models are flux-conserving and line blanketed by means of Opacity Distribution Functions (ODFs, Kurucz 1993b). As these ODFs were computed assuming[1] $\log \varepsilon(\mathrm{Fe}) = 7.67$, we rescale them by -0.16 dex to account for the low solar iron abundance of $\log \varepsilon(\mathrm{Fe}) = 7.50 \pm 0.05$ as given by Grevesse & Sauval (1998). For all models of all metallicities ODFs with a microturbulence of 1 km s^{-1} were used, while the microturbulence entering the line formation calculation was allowed to vary between 1 km s^{-1} and 2.5 km s^{-1}.

Convection is approximated by mixing-length theory (Böhm-Vitense 1958). No overshooting is considered. Unlike in the other codes mentioned above, a mixing length $\alpha_{\rm conv} = l/H_{\rm p} = 0.5$ is used in order to simultaneously model Hα and the higher Balmer lines (cf. Fuhrmann et al. 1993; van't Veer-Menneret & Mégessier 1996). This choice has little effect on metal lines, as they, in contrast to Hβ and higher members of the Balmer series, form at optical depths in which the flux is predominantly carried by radiation. A low convective efficiency leads to a steeper temperature gradient at high optical depths which alters the line formation of Hβ and the higher-order Balmer lines (see below and Sect. 3).

It is worth noticing that in the framework of a refined theory of convection (Canuto & Mazzitelli 1992) a single value of $\alpha_{\rm conv}$ is capable of fulfilling the constraints of stellar evolution (i.e., reproducing the solar radius at the solar age) and Balmer profile fitting (Bernkopf 1998).

Following TB95, we have calculated model atmospheres with solar abundance ratios and ones with the abundances of

[1] $\log \varepsilon(\mathrm{Fe}) = \log (n_{\rm Fe}/n_{\rm H}) + 12$.

carbon, nitrogen, oxygen, magnesium, iron, calcium, sodium, silicon, chromium and titanium each doubled in turn. In addition, we have also increased the overall metallicity [Z/H] of the model by +0.3 dex from each base metallicity[2] [Fe/H] of {+0.67, +0.35, 0.0, −0.35, −1.35, −2.25}. Only in the latter case the ODF was changed according to the modified metallicity isolating the abundance effect whenever a single elemental abundance was varied. This assumes that the element whose abundance is varied behaves like a trace element and its variation has no effect on the temperature structure of the atmosphere. For most of the elements considered here, this is a valid assumption. It is not in two cases: iron and carbon. As iron is responsible for more than half of all line blanketing effects, the true index change due to varying the iron abundance will be somewhere between what is tabulated as "Fe" and "[Z/H]".

Carbon is an even more complicated case. Enhancing C by 0.3 dex brings the C/O ratio so close to unity that a carbon star is produced. While the according changes to the molecular equilibria of C_2, CH, CO and CN are properly accounted for in the line formation, the feedback of the significantly modified line blanketing of carbon-star spectra on the underlying atmospheric structure cannot be modelled in an ODF approach to calculating model atmospheres. This can lead to dramatically overestimated (or underestimated) index strengths. Worthey (2005) argues that the excess of carbon (the fraction not locked up in CO) in the C-enhanced models of TB95 overestimates the true sensitivity of certain indices to carbon, as the Swan bands of C_2 react quadratically to the carbon abundance. This is correct, but not the main cause for a potential overestimation of the sensitivity. Rather, we believe it is caused by the shortcomings inherent to the ODF approach (also adopted by TB95) when applied to carbon stars.

To guide the reader in an attempt to assess the reliability of the index variations due to carbon, we have computed additional sequences for the solar-metallicity stars tabulated in Tables 12−14: carbon was enhanced by 0.15 dex only (Col. 15). This smaller increase will not produce a carbon star and reflects the approach taken by Houdashelt et al. (2002). Another attempt was performed by increasing both carbon and oxygen by 0.3 dex, thus preventing the formation of a carbon star. The "C0.15" sequence ought to correctly predict the sensitivity to an increase of carbon by 40%. "C+O0.3" − "O" (Col. 16−Col. 6) is deemed a better proxy to the actual C variation that what is tabulated in Col. 4. As carbon was not varied in TMB03, this whole problem has no impact on the scientific results published so far.

For solar metallicity, three representative models along a 1 Gyr isochrone were also computed. They allow an assessment of the overall influence the parameter "age" has on the index strengths, mainly via increased turnoff temperatures.

For the two lowest metallicities additional sequences were computed in which a global enhancement of the α elements by a factor of two was assumed. This change in abundance was assumed not to influence the stellar parameters, to be able to isolate the effect of α enhancement. To be consistent with previous assumptions (TMB03), α elements were chosen to include O, Ne, Mg, Si, S, Ar, Ca, Ti (particles that are build up with α-particle nuclei) plus the elements N and Na. The abundance of C was kept fixed at the base metallicity, such that the α enhancement is compensated for by a deficit of iron-group elements. For more details on this point, see TMB03.

[2] $[\mathrm{Fe/H}] = \log \varepsilon(\mathrm{Fe})_\star - \log \varepsilon(\mathrm{Fe})_\odot$.

2.2. Synthetic spectra

For computing the emergent spectral energy distribution we utilize the line formation code LINFOR which is derived from MAFAGS. It has to be realized that the traditional two-step approach to calculating spectra (step 1: determining the temperature structure and partial pressures, step 2: calculating the spectrum) is a convenient, but artificial, separation of the one task of solving the radiative transfer equation with boundary conditions. It is convenient, as (in codes like ATLAS or MAFAGS) a resolution of 20 Å (the resolution of the ODFs) is enough to compute realistically blanketed model temperature structures in step 1, while the use of a line formation code (like SYNTHE for ATLAS, SSG for MARCS or LINFOR for MAFAGS) in principle allows one to compute spectra at arbitrary resolutions.

LINFOR considers the formation of lines for 37 elements and 14 diatomic molecules: H_2, CH, NH, OH, C_2, CN, CO, N_2, NO, O_2, MgH, SiH, CaH and TiO. Triatomic molecules are currently not included. All important external broadening mechanisms are considered, i.e. Doppler, van-der-Waals, resonance and Stark broadening. In the specific case of Fe I, $\log C_6$ values were determined to be 0.15 dex smaller than those proposed by Anstee & O'Mara (1995) and changed accordingly (see Gehren et al. 2001 for more details). For most of the other elements, $\log C_6$ values according to Unsöld (1968) or Kurucz (1992) are used.

The line list serving as input to LINFOR is not, strictly speaking, fully consistent with the ODFs used in the model atmosphere computation. This is because the atomic data of individual lines has been modified over the years based on constraints arising from the reproduction of the solar spectrum. However, the vast majority of lines still has unaltered atomic data most of which taken from Kurucz & Peytremann (1975), Kurucz (1992) and Kurucz & Bell (1995). Our line list does not contain TiO (Kurucz (2002) quotes his list to contain close to 40 million lines due to this molecule alone), therefore we refrain from discussing the two TiO indices in Sect. 3 at great length.

2.3. The Sun and Arcturus

The Sun clearly constitutes the most important point of reference for our calculations. We have therefore compared our synthetic spectra with the most commonly used solar flux atlas, the Kitt Peak atlas (Kurucz et al. 1984), in two ways. Firstly, we can compare the spectra by eye. This way individual lines obviously missing from our line list were identified and added utilizing online compilations for atomic data like those of the National (American) Institute of Standards and Technology, NIST. We, however, refrained from adding

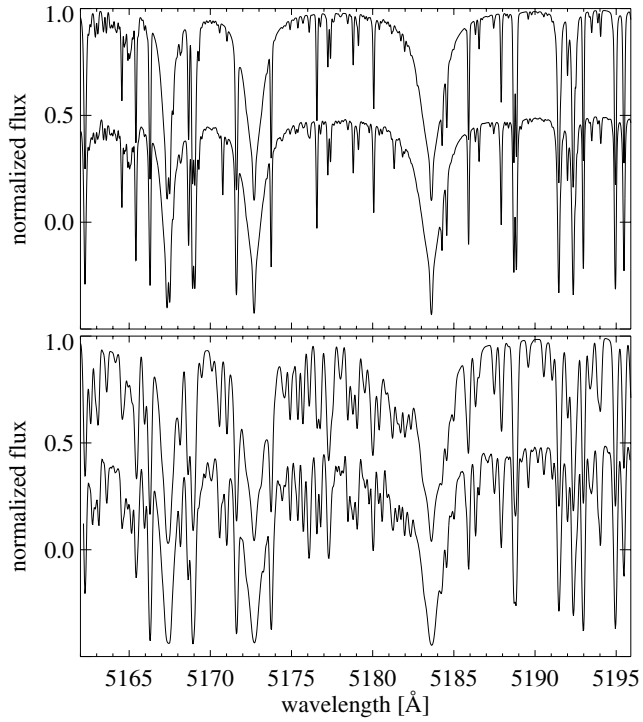

Fig. 1. A comparison between observed and computed spectra around the Mg I*b* lines. *Upper panel*: the Sun, *lower panel*: Arcturus. In both panels the observations are offset by −0.5 units.

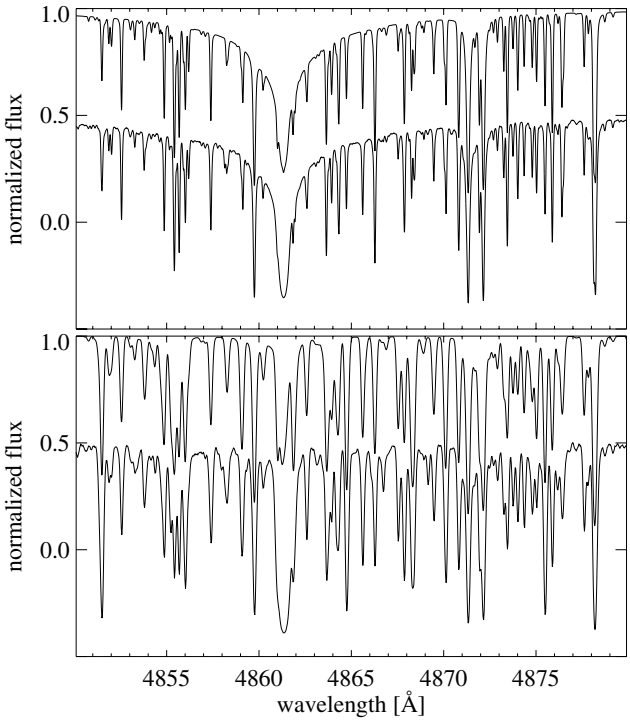

Fig. 2. A comparison between observed and computed spectra around Hβ. *Upper panel*: the Sun, *lower panel*: Arcturus. In both panels the observations are offset by −0.5 units. Due to unmodelled physics, the line strength of Hβ comes out too low in Arcturus.

artificial lines as substitutes for unidentified lines in the Sun of which there are still thousands in the optical (a good example is the line at 5170.76 Å, cf. Fig. 1). Figures 1 and 2 give a qualitative indication of how well our modelling performs. These figures can be directly compared to Figs. 1 and 2 of TB95 and show that the performance of the two independent codes is quite comparable.

Secondly, since the position of the continuum is known in both the observed and the theoretical spectrum of the Sun, we can directly compare the equivalent widths W_λ of the band-passes of the 25 Lick indices without the use of the pseudo-continua. This comparison was done after folding the theoretical spectra with a projected rotational velocity $v \sin i$ of 1.8 km s^{-1} and a macroturbulence $\Xi_{\rm rt}$ of 3.5 km s^{-1} in the radial-tangential approximation (Gray 1977) to account for the observed solar line broadening. The results are given in Table 1 with the last column indicating that there is a general absorption deficit in our modelling of (15 ± 5)%. Some indices deviate markedly from this mean value: C_2 4668, NaD and the two TiO indices have significantly higher ΔW_λ[3], G4300, Hβ, Mg_2, Mg*b* and HγF perform better than average. There is no clear trend with wavelength. We note that using $\alpha_{\rm conv}$ = 1.5 would result in a ΔW_λ twice as large for Hβ (14.1%) and 4−8% larger for the higher-order Balmer-line indices.

[3] The spectral regions around Fe5709 and Fe5782 were re-rectified by +1.0 respectively +1.8% to account for an unmodelled global suppression of the observed continuum in the Kitt Peak atlas. This procedure reduces the ΔW_λ values for these two indices.

The cause of this absorption deficit is not to be found primarily in individual strong lines that are missing in our line list; rather is has to be attributed to many unmodelled lines of low oscillator strength and small equivalent width. To make progress in this context significantly larger line lists would have to be implemented (cf. efforts by Kurucz 2002) which is beyond the scope of this project.

The lower panels of Figs. 1 and 2 compare theory and observation for the thick-disk standard star Arcturus, a first-ascent red giant. The spectrum was obtained with the FOCES spectrograph (Pfeiffer et al. 1998) on the Calar Alto 2.2 m telescope in May 2000 (kindly made available by K. Fuhrmann). The spectrum covers 4200 Å < λ < 9000 Å and has a resolving power of R = 60 000. The signal-to-noise ratio (*S/N*) varies between 70 in the bluest part of the spectrum and 430 in the near-IR; at the wavelengths presented here it is around 230 (Mg Ib lines) and 200 (Hβ), respectively.

For the modelling we take stellar parameters from the literature: $T_{\rm eff}$ = 4300 K (Peterson et al. 1993), log g = 1.6 (between Peterson et al. 1993; and Decin et al. 1997), [Fe/H] = −0.5, $\xi_{\rm mic}$ = 1.7 km s^{-1}. The abundances of O, Mg, Si and Ca were enhanced by 0.3 dex to account for Arcturus' α enhancement.

As can be appreciated from the lower panels of Figs. 1 and 2, our model for Arcturus is, within its limitations, an appropriate representation of the conditions in this cool red giant. One marked exception is the Hβ line itself with obvious modelling deficits that have to be attributed to unmodelled physics

Table 1. Direct integration of the Lick index band-passes, both on the observed spectrum of the Sun (Kitt Peak National Observatory, KPNO) and on the theoretical spectrum computed using the MAFAGS atmosphere code ($T_{\rm eff}$ = 5780, log g = 4.44, [Fe/H] = 0, $\xi_{\rm mic}$ = 1.0 km s^{-1}, $\alpha_{\rm conv}$ = 0.5). The final column gives the absorption deficit $\Delta W_\lambda = 100\,(W_\lambda({\rm KPNO}) - W_\lambda({\rm MAFAGS}))/W_\lambda({\rm KPNO})$. All numbers are rounded to the first decimal place.

Lick index	W_λ(KPNO) [Å]	W_λ(MAFAGS) [Å]	ΔW_λ [%]
CN_1, CN_2	9.1	7.4	18.0
Ca4227	4.0	3.7	9.4
G4300	14.1	13.2	6.5
Fe4383	12.7	11.3	11.2
Ca4455	4.4	3.9	11.5
Fe4531	6.8	5.6	17.9
C_2 4668	11.2	7.6	31.9
Hβ	5.9	5.5	7.1
Fe5015	10.0	8.6	14.2
Mg_1	6.7	5.7	13.8
Mg_2	7.7	7.3	5.0
Mgb	6.7	6.4	4.5
Fe5270	5.0	4.3	13.9
Fe5335	3.5	3.0	13.6
Fe5406	2.8	2.4	12.7
Fe5709	1.5	1.3	13.5
Fe5782	1.0	0.8	21.0
NaD	2.5	1.9	25.6
TiO_1	1.7	0.7	57.4
TiO_2	3.0	1.9	37.2
Hγ A	11.9	10.5	11.9
Hγ F	6.1	5.7	6.8
Hδ A	10.3	9.3	10.3
Hδ F	6.5	5.9	9.3

(non-LTE and/or chromospheric contributions, see Przybilla & Butler 2004). The overall good correspondence between theory and observation shows that the choices for transition probabilities and damping constants made for the Sun are essentially correct. Absorption deficits of similar magnitude as in the solar case are, however, also encountered for Arcturus.

2.4. Spectral indices

The output spectra are normalized and have a flux point spacing of 0.1 Å, just like those of TB95. To put them onto the Lick/IDS system, they were convolved with Gaussians of variable FWHM interpolated among the values given in Table 8 of Worthey & Ottaviani (1997). This ought to not have a significant influence on the comparison with TB95 (see below). The final flux point spacing is typically 0.5 Å, a factor of two higher than that of the IDS spectrograph.

Table 2. Stellar parameters used in the computation of the synthetic Lick indices.

[Z/H]	Age [Gyr]	Stage	$T_{\rm eff}$	log g	[α/Fe]
+0.67	5	MS	4667	4.59	0.0
		TO	5694	4.16	
		RG	4590	3.42	
+0.35	5	MS	4543	4.58	0.0
		TO	5969	4.18	
		RG	4236	2.00	
+0.00	5	MS	4575	4.60	0.0
		TO	6200	4.10	
		RG	4255	1.90	
+0.00	1	MS	5297	4.56	0.0
		TO	8048	3.91	
		RG	4336	1.83	
−0.35	13	MS	4466	4.60	0.0
		TO	5822	4.22	
		RG	4414	1.77	
−1.35	13	MS	4385	4.83	0.0/+0.3
		TO	6383	4.16	
		RG	4662	1.83	
−2.25	13	MS	5124	4.70	0.0/+0.3
		TO	6724	4.15	
		RG	4822	1.83	

We did not run calculations testing the influence of microturbulence, offsets, FWHM, continuum and resolution on the index values. The reader is referred to Tables 1−3 of TB95 for a thorough evaluation of these aspects. Note, however, that the dependence on FWHM, continuum and resolution was found to be below the 2σ (twice the observed standard error) level in all cases. This leaves microturbulence and potential wavelengths distortions/offsets as additional sources of systematic error.

936 Lick indices were computed at each base metallicity making it 8424 spectral indices in total.

3. Results

3.1. Comparison with TB95

Tables 12–14 give the Lick index name (Col. 1), the computed index strength (Col. 2), the standard error taken from TB95 (Col. 3) and the absolute variation of the index strengths upon increasing the abundance of the element given at the top of the column by 0.3 dex. [Z/H] (Col. 14) refers to an overall increase in metallicity by 0.3 dex. The Tables can be compared with Tables 4−6 of TB95. Note, however, that we chose to tabulate the absolute index changes, i.e., not the ones normalized to the assumed standard error.

Common and disparate features of the two data sets are discussed below, first globally, then index by index.

In comparing the computed index values given in Col. 2 to those of TB95, one notices agreement at the 2σ level in 2/3 of all cases (42 out of 63).

Table 3. Sensitivity of individual indices to abundance variations in the dwarf phase of evolution. Only the significant (>one standard error) top three elements are given. For Fe5270(Sauron), the standard error of Fe5270(Lick) was assumed to be applicable.

Index	+0.67	+0.35	0.00	−0.35	−1.35	−1.35 α-enh.	−2.25	−2.25 α-enh.
CN_1	C, O, N	C, O, N	C, N, O	C, N				
CN_2	C, O, N	C, O, N	C, N, O	C, N				
Ca4227	Ca, [Z/H], C	Ca, [Z/H], C	Ca, C, [Z/H]	Ca, [Z/H], C	Ca, [Z/H], C	Ca, [Z/H], C		
G4300	C, O, Ti	C, O, Ti	C, O, Fe	C, O, Ti	C, O	C, O	C, [Z/H], O	C, [Z/H], O
Fe4383	Fe, Mg, [Z/H]	Fe, Mg, [Z/H]	Fe, Mg, [Z/H]	Fe, Mg, [Z/H]	Fe, [Z/H]	Fe, [Z/H]	[Z/H], Fe	
Ca4455								
Fe4531	Ti, [Z/H], Mg	Ti, [Z/H], Mg	Ti, [Z/H]	Ti, [Z/H]	[Z/H], Ti	[Z/H], Ti		
C_2 4668	C, O	C	C	C				
Hβ								
Fe5015	Ti, [Z/H], Mg	Ti, [Z/H], Mg	Ti, [Z/H], Mg	Ti, [Z/H], Mg	Ti, Mg, [Z/H]	Ti, Mg, [Z/H]		
Mg_1	C, Mg, Fe	C, Mg, [Z/H]	C, Mg, Fe	Mg, C, Fe	Mg, [Z/H], Fe	Mg, [Z/H]		
Mg_2	Mg, [Z/H], Fe	Mg, [Z/H], Fe	Mg, [Z/H], Fe	Mg, [Z/H], Fe	Mg, [Z/H], Fe	Mg, [Z/H], Fe	Mg, [Z/H]	Mg, [Z/H]
Mg *b*	Mg, Fe, [Z/H]	Mg, Fe, Cr	Mg, Fe, Cr	Mg, Fe, Cr	Mg, [Z/H], Cr	Mg, [Z/H], Cr	Mg, [Z/H]	Mg, [Z/H]
Fe5270	Fe, [Z/H], Mg	Fe, [Z/H], Mg	Fe, [Z/H], Mg	Fe, [Z/H], Mg	[Z/H], Fe	[Z/H], Fe		
Fe5270(Sauron)	Fe, [Z/H], Mg	Fe, [Z/H], Mg	Fe, [Z/H], Mg	Fe, [Z/H], Mg	[Z/H], Fe	[Z/H], Fe		
Fe5335	Fe, [Z/H], Mg	Fe, [Z/H], Mg	Fe, [Z/H], Mg	Fe, [Z/H], Mg	Fe, [Z/H]	Fe, [Z/H]		
Fe5406	Fe, [Z/H], Mg	Fe, [Z/H], Mg	Fe, [Z/H], Mg	Fe, [Z/H], Mg	Fe, [Z/H]	Fe, [Z/H]		
Fe5709	[Z/H]	[Z/H]	[Z/H]	[Z/H]				
Fe5782	Cr	Cr	Cr	Cr				
Na D	Na, [Z/H], Mg	Na, [Z/H], Mg	Na, [Z/H], Mg	Na, [Z/H], Mg	Na, [Z/H]	Na, [Z/H]		
TiO_1								
TiO_2								
Hγ A	Fe, Mg, [Z/H]	Fe, Mg, [Z/H]	Fe, Mg, [Z/H]	Fe, Mg, C	C, [Z/H], Fe	C, [Z/H], Fe	C, [Z/H]	C, [Z/H]
Hγ F	Fe, C, Mg	Fe, C, Mg	Fe, C, Mg	Fe, C, Mg	C, Fe, O	C, O, Fe	C, [Z/H]	C
Hδ A	Fe, Mg, [Z/H]	Fe, Mg, [Z/H]	Fe, Mg, [Z/H]	Fe, C, Mg	Fe, [Z/H], C	Fe, [Z/H], C		
Hδ F	Fe, [Z/H], Mg	Fe, [Z/H], Mg	Fe, [Z/H], Mg	Fe, [Z/H], Mg	Fe, [Z/H]	Fe, [Z/H]		

For the *turnoff star* (6200/4.1, Table 13), the agreement is always within 2σ, in 2/3 of all cases (14 out of 21) even within 1σ. It was expected that the turnoff star would show the highest degree of consistency as *a)* the temperature structure and electron pressure is robust to small changes in the assumed composition and *b)* molecules play a significantly reduces rôle in computing the spectra. Therefore, it does not come as a surprise either that the fractional changes show a similar overall behaviour: in 17 out of the 21 cases the sensitivity is found to be highest for the same particular element. The seemingly discrepant cases are Ca4227, Fe5335, NaD an TiO_2. We find Ca4227 and NaD to depend more strongly on the name-giving element than on metallicity (TB95 vice versa), in the case of Fe5335 it is the other way around. The two TiO indices do not significantly depend on any of the 12 elements, neither in this study nor in TB95 (in the M-star regime, they would naturally depend on Ti and O).

Turning to the *main sequence star* (4575/4.6), there are two indices which turn out more than 2σ stronger than their TB95 counterparts: Hβ and Fe5015. In both cases, this strengthening turns out to bring these indices into much better agreement with both the observational data on M 67 and the Worthey et al. FFs. The index strength of Fe5015 is still 1 Å short of the FF for the dwarf, but the scatter among the M 67 dwarfs is of the same order (cf. Fig. 13 of TB95).

Seven indices have I_0 values smaller by more than 2σ: CN_1, CN_2, Ca4227, G4300, Ca4455, C_2 4668 and NaD. In two cases (Ca4227 and NaD), the new values lie closer to the corresponding FF and the M 67 data. Two other cases (the two CN indices) are now in better agreement with M 67, but move away from the FF. The remaining three cases (G4300, Ca4455 and C_2 4668) perform worse with respect to both references.

Comparing the sensitivity to particular abundance variations, agreement is found on the element causing the largest index change in 16 cases. In two cases (Fe5015 and Mg_1) the element in first and second place trade places, and we find Ca4455 to (insignificantly) react more strongly to Ca itself than to metallicity, Cr or Fe. Furthermore, no sensitivity to C is found in the two TiO indices (as claimed by TB95). In fact, no significant sensitivity is found at all for any of these indices, neither for Ca4455 and Hβ (cf. the red giant).

Table 4. Sensitivity of individual indices to abundance variations in the turnoff phase of evolution. Only the significant (>one standard error) top three elements are given. For Fe5270(Sauron), the standard error of Fe5270(Lick) was assumed to be applicable.

Index	+0.67	+0.35	0.00	−0.35	−1.35	−1.35 α-enh.	−2.25	−2.25 α-enh.
CN_1	N, C, [Z/H]	N, [Z/H], C						
CN_2	N, C, [Z/H]	N, [Z/H], C						
Ca4227	C, Ca, N	Ca						
G4300	C, Fe	C, Fe	C, [Z/H]	C		[Z/H]		
Fe4383	Fe, [Z/H]	Fe		[Z/H]				
Ca4455								
Fe4531	[Z/H]	[Z/H]	[Z/H]	[Z/H]				
C_2 4668	C, [Z/H], O	C, [Z/H]	C	C				
Hβ	[Z/H]	[Z/H]	[Z/H]					
Fe5015	[Z/H]	[Z/H]	[Z/H]	[Z/H]				
Mg_1	C, [Z/H], O	C, [Z/H], Fe	C	C				
Mg_2	Mg, [Z/H], C	[Z/H], Mg, C	Mg, [Z/H]	Mg, [Z/H], C				
Mg *b*	Mg, [Z/H], C	Mg, [Z/H]	Mg, [Z/H]	Mg, [Z/H]				
Fe5270	[Z/H], Fe	[Z/H], Fe	[Z/H]	[Z/H]				
Fe5270(Sauron)	[Z/H], Fe, Ca	[Z/H], Fe, Ca	[Z/H], Fe, Ca	[Z/H], Fe, Ca	[Z/H], Ca, Fe	[Z/H], Ca, Fe	[Z/H], Fe, Ca	[Z/H], Fe, Ca
Fe5335	Fe, [Z/H]	[Z/H], Fe	[Z/H]	[Z/H]				
Fe5406	Fe, [Z/H]							
Fe5709	[Z/H]	[Z/H]						
Fe5782								
Na D	Na, [Z/H]	Na, [Z/H]	Na	Na				
TiO_1								
TiO_2								
Hγ A	C, Fe, Mg	C	C	C, [Z/H]				
Hγ F	C	C	C	C				
Hδ A	Fe							
Hδ F	Fe							

In the *red giant* (4255/1.9), four indices are significantly stronger: Fe4531, Hβ, Fe5015 and Fe5335. Just like in the case of the main sequence star, Hβ and Fe5015 are now in excellent agreement with the M 67 fiducials of TB95. Fe4531 and Fe5335 are 2 Å respectively 1 Å too large to be in accord with M 67 and the FF.

The same seven indices that were found to be more than 2σ weaker in the dwarf are also weaker in the giant; TiO_2 has to be added to this list. Four indices (CN_1, Ca4455, C_2 4668 and TiO_2) clearly perform worse, the new strength of NaD places it on the opposite side of the distribution of giants in M 67 from TB95 and about equally close to the FF, and three indices (CN_2, Ca4227 and G4300) fare better using MAFAGS.

Turning to the abundance variations, the dominant rôle of a particular element found by TB95 is recovered for 11 indices. In a further 5 cases (Fe5015, Fe5270, Fe5335, Fe5406 and Fe5782) the order of the first two element is reversed (sometimes making them most sensitive to Fe, sometimes to [Z/H]), in one case (Ca4227) that of the dominant three. In four cases (Ca4455, Hβ, TiO_1 and TiO_2) we find no significant sensitivity to any of the elements studied. For Hβ this is confirmation of the TB95 result.

Overall, the one-by-one comparison shows that the computations presented here are on par with those published by TB95. Irrespective of whether improvements were found or not, understanding the cause of disparate results would bring on progress. Since we do not have access to R. Bell's version of the MARCS code nor to the line-formation code SSG and the line list used, this is unfortunately not possible. Taken at face value, the differences certainly tell us something about the uncertainties involved in the modelling of Lick indices. As a rule of thumb, we conclude that the bluest classical indices except Fe4383[4] (that is, CN_1, CN_2, Ca4227, G4300, Ca4455, Fe4531 and C_2 4668) bear higher modelling uncertainties than the other 13 indices. Together with the wavelength independence of ΔW_λ (see Table 1), this indicates that line-list differences are largest in regions of high line density, as one might have expected.

[4] Fe4383 can be considered an exception. We agree with TB95 that this index is best suited for the determination of the iron abundance.

Table 5. Sensitivity of individual indices to abundance variations in the giant phase of evolution. Only the significant (>one standard error) top three elements are given. For Fe5270(Sauron), the standard error of Fe5270(Lick) was assumed to be applicable.

Index	+0.67	+0.35	0.00	−0.35	−1.35	−1.35 α-enh.	−2.25	−2.25 α-enh.
CN_1	C, O, N	C, O, N	C, O, N	C, N, O	N, C	N, C, [Z/H]		
CN_2	C, O, N	C, O, N	C, O, N	C, N, O	N, [Z/H], C	N, [Z/H], C		
Ca4227	Ca, [Z/H], C	Ca, [Z/H], C	Ca, [Z/H], C	C, Ca, [Z/H]	C	C		
G4300	C, O, Fe	C, O, Fe	C, O	C, O	C		C, [Z/H]	C, [Z/H]
Fe4383	Fe, Mg, [Z/H]	Fe, [Z/H], Mg	Fe, [Z/H], Mg	Fe, [Z/H]	[Z/H], C	C, [Z/H]		
Ca4455								
Fe4531	[Z/H], Ti	[Z/H], Ti	[Z/H], Ti	[Z/H]	[Z/H]	[Z/H]	[Z/H]	
C_2 4668	C, O, [Z/H]	C, O, [Z/H]	C, O, [Z/H]	C, [Z/H], O	C	C		
Hβ								
Fe5015	[Z/H], Ti, Mg	[Z/H], Ti, Mg	[Z/H], Ti, Mg	[Z/H], Fe, Mg	[Z/H]	[Z/H]	[Z/H]	[Z/H]
Mg_1	C, Mg, [Z/H]	C, Mg, [Z/H]	C, [Z/H], Mg	C, [Z/H], Mg	C, [Z/H]	C, [Z/H]		
Mg_2	Mg, [Z/H], C	Mg, [Z/H], C	Mg, [Z/H], C	Mg, [Z/H], C	[Z/H], C	[Z/H], Mg, C		
Mg b	Mg, Fe, [Z/H]	Mg, [Z/H], Fe	Mg, [Z/H], Fe	Mg, [Z/H], C		Mg		
Fe5270	Fe, [Z/H]	Fe, [Z/H]	Fe, [Z/H]	[Z/H], Fe	[Z/H]	[Z/H]		
Fe5270(Sauron)	Fe, [Z/H], Mg	Fe, [Z/H], Mg	Fe, [Z/H], Mg	[Z/H], Fe, Mg	[Z/H], Fe, Ca	[Z/H], Fe, Ca	[Z/H], Fe, Ca	[Z/H], Ca, Fe
Fe5335	[Z/H], Fe, Mg	[Z/H], Fe	[Z/H], Fe	[Z/H], Fe	[Z/H]			
Fe5406	[Z/H], Fe	[Z/H], Fe	[Z/H], Fe	[Z/H], Fe	[Z/H]			
Fe5709	[Z/H]	[Z/H]	[Z/H]	[Z/H]	[Z/H]			
Fe5782	Cr, [Z/H]	Cr	Cr, [Z/H]	Cr, [Z/H]				
Na D	Na, [Z/H], Mg	Na, [Z/H]	Na, [Z/H]	Na, [Z/H]				
TiO_1								
TiO_2								
Hγ A	Fe, [Z/H], Mg	Fe, [Z/H], Mg	Fe, [Z/H], Mg	[Z/H], Fe	[Z/H]	[Z/H]	[Z/H], C	[Z/H], C
Hγ F	Fe, C	[Z/H], Fe, C	Fe, [Z/H]				C, [Z/H]	C, [Z/H]
Hδ A	Fe, [Z/H], Mg	Fe, [Z/H]	Fe, [Z/H]	Fe, [Z/H]	C	C		
Hδ F	Fe, [Z/H], Mg	[Z/H], Fe, Mg	[Z/H], Fe	[Z/H], Fe				

3.2. Comparison with Fitting Functions at various metallicities

Table 2 gives details of the stellar parameters used for the computation of the synthetic Lick indices. The data pairs $\{T_{\rm eff}, \log g\}$ were read off from isochrones of the given metallicity and age (from Cassisi et al. 1997; and Salasnich et al. 2000 for the highest metallicity, see Maraston 1998, 2005 for details) for dwarf and turnoff stars. For the giants, they represent average locations in which the fuel consumption on the Red Giant Branch is maximum (see Maraston 2005).

Tables 6–32 give the index values and index variations for representative dwarfs (MS), turnoff stars (TO) and red giants (RG) for metallicities ranging from +0.67 to −2.25. At solar metallicity Tables 15−17 give additional values for objects of age 1 Gyr. At metallicities −1.35 and −2.25 Tables 24−26 and 30−32 contain additional data sets computed under the assumption of a general enhancement of α elements. Tables 3−5 give an overview of the sensitivity of Lick indices to abundance variations (including sensitivity to [Z/H]).

Figures 4–8 are a graphical representation of the metallicity dependence of the index and the corresponding FF values. They may serve as an at-a-glance source of information on where modelling deficits are practically absent or dominating. Modelled index strengths are denoted by the (coloured) boxes, the bullets are the corresponding FF values with IDS standard errors of Worthey et al. (1994). The diamonds indicate the absolute index change that results from a 0.3 dex increase of the element producing the highest index change. This dominant element was sometimes found to vary with evolutionary phase, see e.g. Hβ.

Offsets between our results and the FFs beyond 1σ are found in 2/3 of all cases (cf. Figs. 4–8). Note that it is practically impossible to name the cause for a mismatch between theory and observation. This is because a high index strength can be caused by too few absorbers in the continuum band-passes or too many in the band-pass itself. A mismatch can also result from ill-determined stellar parameters in the sample of stars defining the FFs such that one is not comparing like with like. There certainly is room for the latter at the

low-metallicity end where absolute effective temperatures are still uncertain at the 200 K level (see e.g. Barklem et al. 2002) and where the FFs are poorly constrained owing to the lack of stars in the Lick library.

In what follows the 25 indices are discussed individually.

CN_1 and CN_2 (Fig. 4)

The index is most sensitive to the abundances of C and N. It is also sensitive to O via the preferred formation of CO. Metallicity plays some rôle in the turnoff phase.

Contrary to TB95, our computations underpredict the index strengths at high metallicity, in particular for the dwarfs and the giants. Interestingly, this behaviour is reversed in the low-metallicity dwarfs making the dependence on metallicity rather weak. The FFs do show such a weak trend for the turnoff stars where our modelling is in good agreement with them. The metallicity trend for the giants is more or less recovered with an offset of 0.1 mag. An increase of 0.2 dex in C would be sufficient to account for this offset at high metallicities. However, as mixing with CN-cycled material on the giant branch would lower the C abundance, this can not serve as an explanation for the low index values predicted here.

Ca4227 (Fig. 4)

Ca, C and [Z/H] dominate the overall index strength, α-enhancement has no effect on it.

The index strengths for the dwarfs rise steeper than the FFs and do not saturate. At solar metallicity, the agreement is acceptable (within the 0.3 dex variation of Ca), somewhat better than in TB95. In the giants, a steeper rise with metallicity is also predicted which starts at higher metallicities only.

G4300 (Fig. 4)

This index is very sensitive to the C abundance, O and Fe are important contributors as well. The sensitivity to α-enhancement is generally low.

The turnoff stars and dwarfs are compatible with the FFs within a 0.3 dex variation of the C abundance. The high-metallicity giants are also consistent and are in fact in better agreement with the FFs than in the study of TB95. Yet the index strengths are significantly overestimated at low metallicities. The saturation in index strength takes place at much lower metallicities than what is deduced from the FFs.

Fe4383 (Fig. 4)

This index is particularly sensitive to the iron abundance itself which is no surprise given the intrinsic strength of Fe I 4383 and Fe I 4404 (both multiplet 41). Metallicity [Z/H] and the Mg abundance also influence the index strength, the latter one via its influence on the continuous opacity arising from H^-.

There is a very slight tendency for the index strength to be too high in the turnoff stars and giants, a clear one in the case of the dwarfs. Here, the dynamic response to α-enhancement is also overestimated, whereas it is well reproduced in the evolved stages of evolution.

Ca4455 (Fig. 5)

This index is not very sensitive to any of the elements studied, at all times below the level of 1σ. The highest variations are due to Ca (dwarf phase), [Z/H] (turnoff phase) and Fe and Cr (giant phase).

In the absence of a significant response to varying elemental abundances it is particularly troublesome to see the index perform increasingly badly towards high metallicities, in all stages of evolution. TB95 note the strong dependence on bandpass placement, the highest found for any of the 21 classical Lick indices. The size of the variation (between 4 and 8σ for a -3 Å wavelength shift in the giant and dwarf, respectively) is in principle fully sufficient to account for the offsets found. This might or might not be the sole source of the discrepancy; in any case, it tells us that one has to be careful in using this index, as also noted from the comparison with globular cluster data (Maraston et al. 2003, TMB03).

Fe4531 (Fig. 5)

For this index, variations of Ti and [Z/H] are important. All other elements cause an index response at or below the 1σ level.

The agreement between our model predictions and the FFs is good in the case of the dwarfs, excellent for the turnoff stars, but mediocre for the giants. Here, the index strengths are overpredicted at high metallicities, which goes into the opposite direction from TB95.

C_2 4668 (formerly Fe4668) (Fig. 5)

This index is almost exclusively a measure of the carbon abundance. It shows practically no dependence on α-enhancement.

The dwarfs do not follow the FFs at all: values too high at low metallicity, values too low at high metallicity. At [Z/H] = 0, C_2 4668(TB95) is at 2 Å rather than 1 Å as here, whereas the FF is close to 5 Å. The turnoff stars, on the other hand, are well-matched. A variation of C by 0.2 dex is enough to bring the giants into concordance with the FF values. Yet, it is quite obvious that the metallicity dependence is not properly accounted for. TB95 succeed remarkably well in reproducing the FFs and the data on giants in M 67. Just like in the case of Fe4531, our respective baseline values fall on opposite sides of the FFs.

Hβ (Fig. 5)

This index is hardly changed by any of the studied elemental variations, α-enhancement has no effect, either (see Thomas et al. 2004). The dominant variations presented in Fig. 5 are at or below $1/3\sigma$ and therefore hard to trace observationally.

The expected behaviour of the index is reproduced well for all evolutionary stages, even at low temperatures where TB95

found systematic offsets of around 1 Å. We have no explanation for the 1 Å offset encountered in the $Z = 0.05\,Z_\odot$ dwarf.

The seemingly non-monotonic behaviour of the Hβ index (most apparent in the turnoff stars) is a direct consequence of our choice of representative stars: they are non-monotonic in $T_{\rm eff}$ causing the temperature sensitivity of the Hβ line to carry through to the index strength.

Fe5015 (Fig. 5)

In the turnoff stars, this index is only sensitive to [Z/H], in the cooler stars also to Ti and Mg. This supports the findings of TB95. α-enhancement has some effect on the overall index strength, in good agreement with the FFs.

This index was considered to be the overall poorest fit by TB95. On the contrary, the FFs of all stages of evolution are reasonably well-matched by our computations. All discrepancies can be removed by a 0.3 dex increase in Ti alone. This is, however, not to say that all stars defining the FFs show super-solar [Ti/Fe] abundance ratios (which is unlikely at or above solar metallicity). We note that the high sensitivity to offsets in wavelength found in the TB95 dwarf (5 standard errors per −3 Å) cannot explain the residual discrepancies.

Mg_1 (Fig. 6)

C, Mg, [Z/H] and Fe dominate the behaviour of this index in decreasing order of importance. It is interesting to see how the relative sensitivity to Mg (MgH) wins over that to C (C_2) towards lower metallicities in the dwarf phase.

The overall correspondence between FFs and theoretical index strengths is good, except for two areas: the I_0 values are systematically too low in the metal-poor dwarfs and systematically too high in the metal-rich giants. The latter was also found by TB95.

Mg_2 (Fig. 6)

As the Mg_2 band-pass covers the Mgb lines, the sensitivity to Mg is higher than in the case of Mg_1. It is also influenced by [Z/H], C and Fe.

The behaviour of Mg_2 as a function of metallicity is very similar to Mg_1. Among the dwarfs, only the most metal-poor star shows a significant discrepancy, among the giants it is once more the solar and super-solar ones. In this case, no offset was reported by TB95 at solar metallicity.

Mgb (Fig. 6)

The most dominant species are Mg, [Z/H] and Fe (plus Cr in the dwarfs). α enhancement has an effect on the $Z = 0.005\,Z_\odot$ dwarfs and giants which is well-modelled.

The turnoff and red giant stars are well accounted for, in this index the dwarfs are off the FFs. This is then a feature common to all three Mg indices. At the lowest metallicity, our calculation predict values far below the FFs, which is due to the FFs largely overestimating the index strengths with respect to real stars (see Fig. 3 in Maraston et al. 2003). At high metallicities, the behaviour of all three Mg indices is also similar (Mgb performs best) and – in contrast to the low-metallicity cases in the dwarf phase – stays within a 0.3 dex variation of Mg.

Fe5270 (Fig. 6)

This index is most sensitive to Fe, [Z/H] and Mg. A response to α-enhancement is practically only visible in the dwarfs where its dynamic range are predicted correctly.

The fit is overall acceptable, displaying the same shortcomings as in TB95: the index strengths is predicted to be somewhat too high at low effective temperatures, both in the dwarfs and giants (the TB95 values for giants come closer to the FFs).

Fe5335 (Fig. 6)

This index behaves very much like Fe5270. Its response is dominated by [Z/H], Fe and Mg. The effect of α-enhancement is more pronounced in the computations than what is encoded in the FFs.

Just like in Fe5270, the theoretical indices for high-metallicity dwarfs and giants are too strong by typically 1 Å. Again, the results of TB95 are closer to the FFs.

Fe5406 (Fig. 7)

The response of this index is practically identical to that of Fe5335 (see above). For a direct comparison, Fe5270, Fe5335 and Fe5406 are all plotted on the same scale in Figs. 6 and 7.

This index performs best of the three above-mentioned iron indices. Deficits only exist in the high-metallicity giants where the index strengths of the FFs are overpredicted by 0.5 Å. Considering that the overall index strength is smaller than in the case of Fe5270 and Fe5335, the fractional deficits are all of the same size. It is then observationally easier to use Fe5270 or Fe5335.

Fe5709 (Fig. 7)

Another iron index quite similar to Fe5406, but with lower sensitivity to Fe. Interestingly, in the high-metallicity giants it is more sensitive to Ti than to Fe itself. All variations cease to be significant at $Z = 0.005\,Z_\odot$. The dependence on α-enhancement is well-modelled.

The high-metallicity giants are once again predicted to have index strengths some 0.5 Å larger than what is observed. This finding is not shared by TB95, although their prediction keeps rising towards cooler temperatures while the FF level off and decline at around 4200 K.

Fe5782 (Fig. 7)

As already noted by TB95, this index measures Cr rather than Fe, [Z/H] plays some rôle as well.

The predictions are too low at high metallicity and vice versa making the metallicity trends generally flatter than in the FFs. Except for the lowest-metallicity dwarfs and giants, all indices are compatible with the FF within the dynamic range of a 0.3 dex variation in Cr.

Na D (Fig. 8)

This index depends strongly on Na, other than that most significantly on [Z/H]. α-enhancement has little effect whatsoever.

The reproduction of the FFs presented here is quite good overall, in the case of the dwarfs (where deficits are clearly present) better than by TB95. Except for the lowest-metallicity point, all deficits are confined to a $\pm$0.3 dex variation in Na.

TiO_1 and TiO_2 (Fig. 7)

In the absence of TiO lines from our line list, the results we get are quite comparable to those of TB95. However, we do not find a pronounced sensitivity to C.

While TiO_2 is well-reproduced in the turnoff stars, there is a general deficit of $\approx$0.01 mag in TiO1 for all evolutionary phases rising to $\approx$0.03 mag in the super-solar giant. Presumably, this rise is entirely due to the increased importance of TiO at low effective temperatures.

Hγ A (Fig. 8)

The most crucial elements for this index are Fe, C, Mg and metallicity [Z/H]. Some dependence on α-enhancement is predicted (e.g. 1.3 Å difference between the two $Z = 0.005\,Z_\odot$ dwarfs).

When it comes to stellar populations, this index is dominated by the contribution of the turnoff (by the horizontal branch where applicable). It is therefore reassuring to see that indices for the turnoff stars are predicted correctly (within the 0.3 dex variation of the element dominating the index strength). Both the dwarfs and giants fall short of the FFs by several Å.

Hγ F (Fig. 8)

Overall, Hγ F behaves quite similar to Hγ A. The dependence on C is, however, more pronounced.

The turnoff stars are well-matched (on par with Hγ A), the deficits in the dwarfs and giants are smaller here (in relative terms). On the other hand, the difference in index strengths between dwarfs/giants and turnoff stars (as read off from the FFs) is not as large as in Hγ A. Taking these two competing properties into account, it is not easy to decide which index is to be preferred.

Hδ A (Fig. 8)

The three elements to which this pair of indices is most sensitive are Fe, [Z/H] and Mg.

What was said about the behaviour of dwarfs and giants in Hγ also holds true here. The theoretical sequence for the giants is in better agreement with the FF at high metallicities, but does not come close to the FFs for the metal-poor objects. At the lowest metallicities, the FFs predict the indices of the giants to compete with those of the turnoff stars, a finding not supported by our calculations.

Hδ F (Fig. 8)

This index is less sensitive to Fe than Hδ A. Additionally, the difference in index strengths between dwarfs/giants and turnoff stars is not as large as in Hδ A. Therefore, Hδ A is to be preferred, if one wants to use this band-pass.

4. Stellar population models

The index responses presented a here are the key ingredient for the stellar population models with variable element abundance ratios presented in TMB03. In these models the index response functions of TB95 have been used, which have, as mentioned in the Introduction, the major shortcoming to be calculated only for a 5 Gyr isochrone with solar metallicity. The main motivation for this work was to improve on these simplifications. In this section, we discuss the impact of the present paper on stellar population models, and compare stellar population models using the new response functions of this work with the models presented in TMB03 based on TB95.

4.1. Inclusion of the response functions

Before, we briefly summarize, how the calculations of this paper are included in stellar population models. For details we refer to TMB03.

4.1.1. The evolutionary phases

Like TB95, we have measured on each model star – dwarfs, turnoff, giants – the absolute Lick index value I_0. Doubling in turn the abundances X_i of the dominant elements C, N, O, Mg, Fe, Ca, Na, Si, Cr, and Ti, we determine the index changes $\delta I(i)$. The abundance effects are therefore isolated at a given temperature and surface gravity. In this way, we obtain the first partial derivative $\partial I/\partial[X_i]$ of the index I_0 for the logarithmic element abundance increment $\delta[X_i] \equiv \log X_i^1/X_i^0 = \log 2 = 0.3$ dex.

As discussed in the previous sections, the I_0 values of our calculations (like in TB95) do not always match the ones derived from the (purely empirical) FFs. In TMB03, it was therefore decided to rely on the values in a differential sense, and adopt only the index variations $((\partial I/\partial[X_i]) \times 0.3$. The absolute I_0 values for the three evolutionary phases, instead, are taken from our underlying 5 Gyr, $Z_\odot$ SSP model.

The model index is computed by splitting the basic SSP model in the three evolutionary phases, dwarfs, turnoff stars and giants. We compute the Lick indices of the base model for each phase separately, and modify them using the fractional responses $\delta I/I_0$.

4.1.2. Negative indices

As extensively discussed in TMB03, this approach assumes that the index approaches asymptotically the value zero for very low element abundances, i.e. $I \rightarrow 0$ for $X_i \rightarrow 0$ or $[X_i] \rightarrow -\infty$. This condition, however, is not generally fulfilled for Lick indices. They can become negative, depending on the definition of line and pseudo-continuum windows. This typically happens at young ages and/or low abundances, and must be corrected before applying fractional index responses. In TMB03 this problem is solved by shifting negative index values such that they approach zero at zero element abundances. After applying the response functions, the index is scaled back (see TMB03 for details). Indices with positive values were assumed to reach the value zero at zero abundances and therefore did not require any correction. This approach seems a bit approximative, but turns out to work very well.

The fact that we have response functions at every metallicity allows us now to improve on this method. We now apply the fractional responses to the flux in the absorption line directly, as the latter is always positive. The absorption index I (measured in Å) is linked with the fluxes in line F_l and continuum F_c through the following equation (Δ is the bandwidth, see Maraston et al. (2003) for more details and for the equivalent definition for indices measured in magnitudes):

$$I = \Delta \cdot (1 - F_\mathrm{l}/F_\mathrm{c}). \quad (1)$$

The index variations tabulated in Tables 6–32 are converted to variations in F_l with the following equation which can be derived from Eq. (1):

$$\frac{\delta F_\mathrm{l}}{F_\mathrm{l}^0} = \frac{\delta I}{I_0 - \Delta}. \quad (2)$$

Equivalent to Eq. (7) in TMB03, the fractional responses of the flux in the line are then multiplied as follows:

$$F_\mathrm{l}^\mathrm{new} = F_\mathrm{l} \prod_{i=1}^{n} \exp\left\{\frac{1}{F_\mathrm{l}^0}\frac{\partial F_\mathrm{l}}{\partial [X_i]}\, 0.3\right\}^{(\Delta[X_i]/0.3)}. \quad (3)$$

The new index is then computed from $F_\mathrm{l}^\mathrm{new}$ with Eq. (1). We have verified that the resulting stellar population models are not significantly affected when compared to models based on the method used in TMB03. This consistency can be taken as further evidence that the approximation originally used in TMB03 has been successful at dealing with negative absorption line indices.

4.2. Metallicity dependence

In TMB03, it had to be assumed that the fractional responses $\delta I/I_0$ are independent of metallicity. This approximation is sensible in the linear part of the growth curve, in which equivalent width of the absorption line and element abundance are linearly related. In particular at metallicities well above solar, it is not clear whether this assumption is still valid. The calculations of this paper allow to test the validity of this simplification, as we have now at hand response function in the whole metallicity range $-2.25 \leq [Z/\mathrm{H}] \leq 0.67$.

4.3. Age dependence

TB95 calculated the index response functions for stellar parameter pairs that correspond to an isochrone of 5 Gyr, and in TMB03 it is assumed that this age restriction does not significantly impact on the resulting SSP model. In this paper we have now the tools available to check the validity of this assumption. For this purpose, we have additionally computed index response functions for a 1 Gyr isochrone at solar metallicity (Tables 15−17). The resulting α/Fe enhanced SSP model (age 1 Gyr) is in perfect agreement with the 1 Gyr model based on the response functions from the 5 Gyr isochrone (Tables 12−14). Deviations are about 1 per cent for G4300 and Fe4383, significantly below that value for all other indices.

4.4. Symmetry

TB95 computed index variations upon enhancing the abundance of an individual element by 0.3 dex. We also performed test calculations in which the abundance was diminished instead. No significant changes were found in the absolute index changes. This means that the index variations can be used to trace element abundances both above and below the base abundance.

4.5. Classical Lick indices

The resulting stellar population models calibrated with galactic globular clusters are shown in Fig. 3, which is the equivalent of Fig. 2 in TMB03. We plot models for constant age (12 Gyr) and constant α/Fe ratios in the metallicity range $-2.25 \leq [Z/\mathrm{H}] \leq 0.67$. Three models with $[\alpha/\mathrm{Fe}] = 0.0,\ 0.3,\ 0.5$ are shown in blue, green, and red, respectively (see labels). Models with solar abundance ratios ($[\alpha/\mathrm{Fe}] = 0.0$) and models with $[\alpha/\mathrm{Fe}] = 0.5$ are those with the lowest and highest Mgb indices, respectively. Solid lines are the TMB03 models using the new response functions of this paper, dotted lines are the models of TMB03 based on the TB95 response functions. Filled squares are globular cluster data, the open square is the integrated Bulge light (both from Puzia et al. 2002), small grey dots are the Lick data of giant elliptical galaxies from Trager et al. (1998).

We recall here that the Galactic globular clusters are α/Fe enhanced by about a factor 2, hence the model can be considered well calibrated when the model with $[\alpha/\mathrm{Fe}] = 0.3$ (middle green line) fits the observational data (squares). As discussed in detail in TMB03, not all of the Lick absorption line indices show a satisfactory calibration and can be considered adequate for stellar population studies. For the aim of this paper, we are more interested in the direct comparison with the TMB03 models based on the TB95 response functions.

The main conclusion is the following: the assumption of TMB03 that the fractional response is independent of metallicity is generally confirmed for the whole metallicity range considered. The convergence to minimal index variations at the lowest metallicities and the corresponding expansion of the models with different α/Fe ratios at high metallicities is present also in the models with the metallicity-dependent

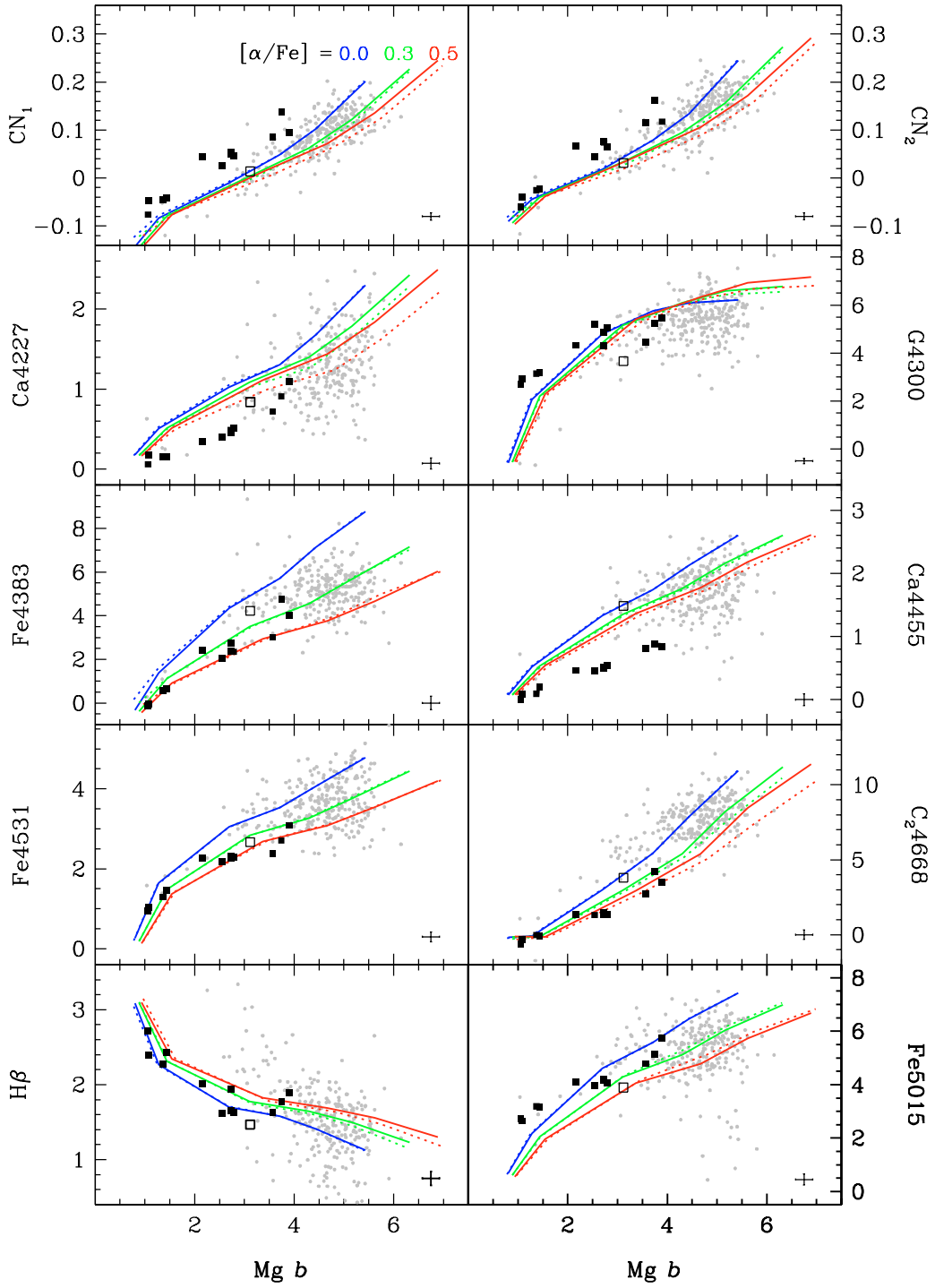

Fig. 3. Mg*b* index versus the other 20 Lick indices. Solid lines are the TMB03 models using the new response functions of this paper, dotted lines are the models of TMB03 based on the TB95 response functions. They are plotted for constant age (12 Gyr) and constant α/Fe ratios in the metallicity range $-2.25 \leq [Z/H] \leq 0.67$. The three models with $[\alpha/Fe] = 0.0,\ 0.3,\ 0.5$ are shown in blue, green, and red, respectively (see labels). Models with solar abundance ratios ($[\alpha/Fe] = 0.0$) and models with $[\alpha/Fe] = 0.5$ are those with the lowest and highest Mg*b* indices, respectively. Filled squares are globular cluster data, the open square is the integrated Bulge light from Puzia et al. (2002), small grey dots are the Lick data of giant elliptical galaxies from Trager et al. (1998). Error bars indicate typical errors of the globular cluster data. The figure is the equivalent of Fig. 2 in TMB03 and continues on the next page.

response functions presented here. For most indices, the two models are well consistent within the calibration uncertainty introduced by observational errors. If discrepancies are present, they do not originate from the neglect of the metallicity dependence, but are caused by differences between the response functions presented here and those of TB95.

The indices CN_1, CN_2, Hβ, Mg*b*, Mg_2, Fe5270, NaD, and TiO_2 exhibit only relatively small offsets, while the

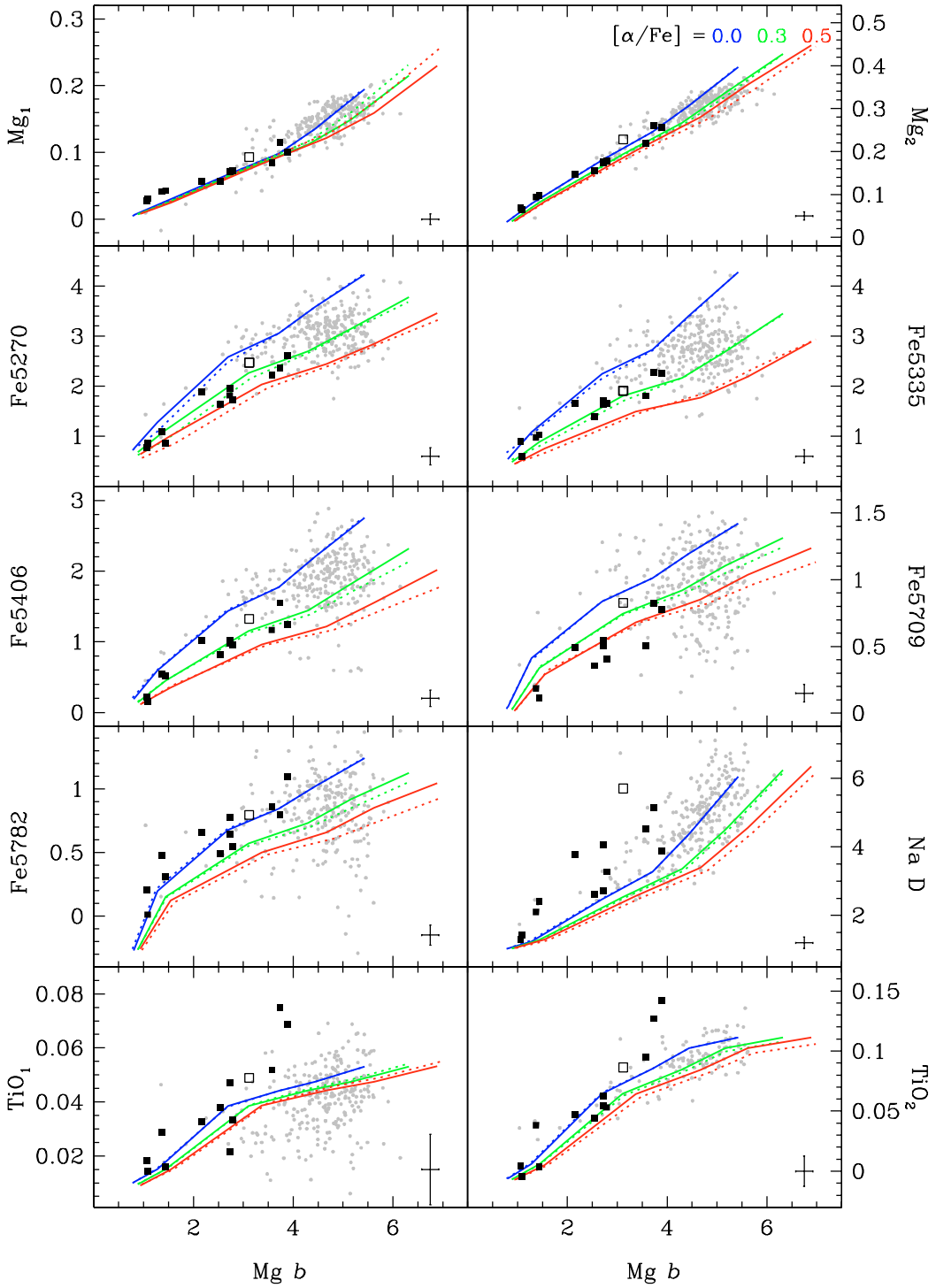

Fig. 3. continued.

indices G4300, Fe4383, Ca4455, Fe4531, Fe5015, Fe5335, and TiO_1 basically did not change. Largest differences are found for Ca4227, C_2 4668, Mg_1, Fe5406, Fe5709, and Fe5782.

Ca4227 and C_2 4668 have become more sensitive to α/Fe ratio, and increase now slightly with increasing α/Fe ratios. In both cases, the main reason is a more pronounced negative response to the element Cr, the abundance of which decreases relative to the α-elements in the enhanced models. As mentioned earlier, Ca4227 and C_2 4668 are most sensitive to their name-giving elements, Ca and C, respectively, which do not vary significantly in the α/Fe enhanced mixtures of the TMB03 models.

Mg_1 is now somewhat less sensitive to α/Fe because of slightly smaller responses to both Mg and Fe in the response function of this work. Fe5406 and Fe5709 decrease less strongly with increasing α/Fe because the sensitivity to the element Fe is less pronounced. Fe5782 is interesting, as

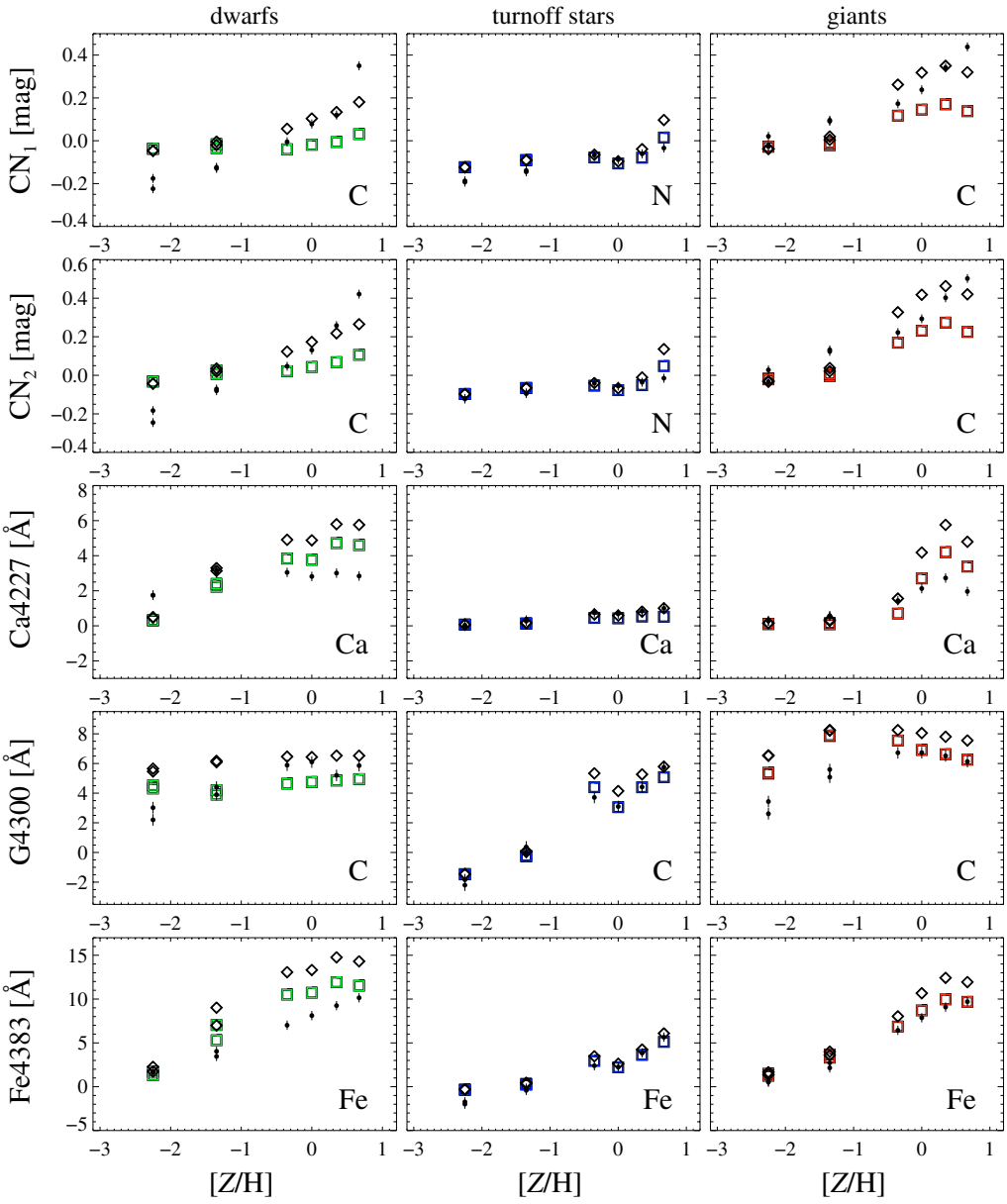

Fig. 4. Theoretical index-strength variations as a function of metallicity for CN1, CN2, Ca4227, G4300 and Fe4383 in the three evolutionary stages dwarf (*left*), turnoff (*middle*) and giant phase (*right*). Squares denote index strengths from this work, diamonds the respective index strength obtained by enhancing the index-dominating element (given in the lower right corner) by 0.3 dex. Bullets are the FFs with IDS standard errors of Worthey et al. (1994).

its sensitivity to α/Fe ratio comes only from the positive response to abundance changes of the element Cr. In the response functions of this paper, Fe5782 even decreases with increasing Fe abundances, hence counterbalances the positive response to Cr, which leads to the lower sensitivity to α/Fe ratios. For all the three Fe indices, this effect slightly increases with increasing metallicity.

Hβ is the only case, in which the metallicity dependence of the response functions leaves a small, but measurable trace. The higher the metallicity, the larger is the Hβ strength of the α/Fe enhanced models with the new metallicity-dependent response functions relative to the ones based on TB95. The reason is the negative response to Cr, due to a Cr line at 4885 Å in the red pseudo-continuum of the index definition. It makes indeed sense that the influence of metallic lines on a Balmer-line index increases with increasing metallicity. Still, the effect is small. In the highest metallicity model ([Z/H] = 0.67), where the effect is maximized, the doubling of the α/Fe ratio leads to an increase of the Hβ index by less than 10 per cent.

This is significantly less than the increase of about 100 per cent recently claimed by Tantalo & Chiosi (2004) on the basis of the TB95 response functions (in contrast to the results in TMB03). According to Tantalo & Chiosi (2004) this dramatic increase of Hβ results from a strong sensitivity of Hβ

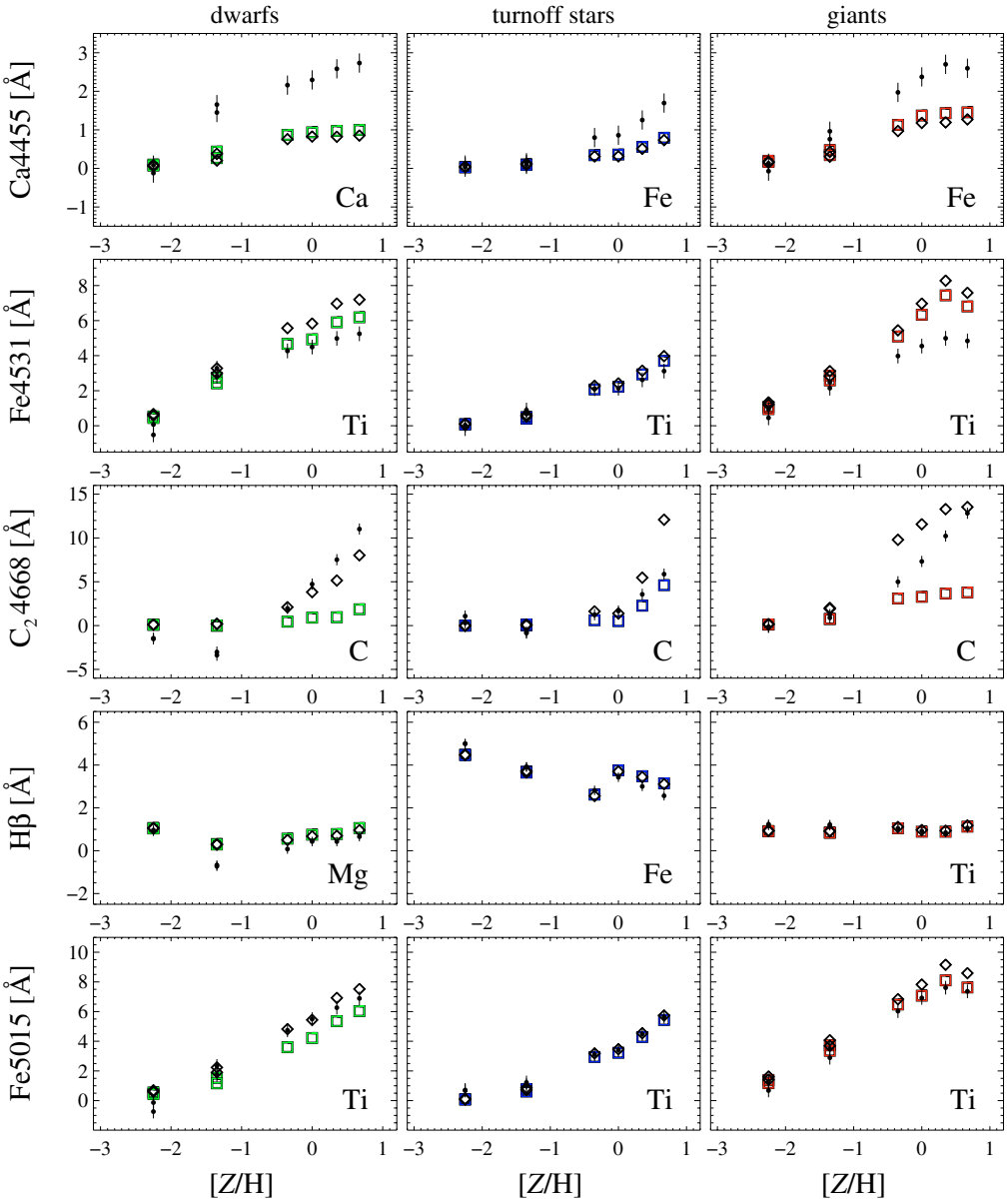

Fig. 5. Same as Fig. 4, here for Ca4455, Fe4531, C_2 4668, Hβ and Fe5015.

to Ti abundance in the dwarf evolutionary phase. Inspecting the response function of TB95, however, reveals that Hβ in the dwarfs actually decreases with increasing Ti, which leads to the conclusion that the result of Tantalo & Chiosi (2004) is likely a numerical artefact. It should also be noted that the models of Tantalo & Chiosi (2004) predict such strong Hβ indices (of the order of 2 Å) that the vast majority of early-type galaxies would be about 30 Gyr old, which is significantly older than the Universe. It is very important to note that in the response functions of this work, the sensitivity of Hβ to Ti abundance does not exceed the few per cent level in all evolutionary phases.

4.6. Higher-order Balmer-line indices

As mentioned earlier, Hβ shows little sensitivity to element ratio variations as well as to total metallicity, because of the lack of strong metallic lines in the wavelength range of the index definition. At bluer wavelengths, this situation naturally changes. The higher-order Balmer-line indices Hγ and Hδ around 4340 and 4100 Å as defined in Worthey & Ottaviani (1997) are significantly more affected by metallic lines. A well-known direct consequence is that these indices are more sensitive to metallicity than Hβ. But they are also significantly more sensitive to the α/Fe ratio as shown here. With increasing metallicity, the influence of metallic lines rises. As a consequence, unlike for Hβ, the fractional index responses increase considerably with metallicity as can be appreciated by comparing Figs. 5 and 8. The impact on the stellar population models is dramatic as shown in Thomas et al. (2004). This effect cannot be neglected when these line indices are used to derive the ages of metal-rich, unresolved stellar populations like early-type galaxies. In Thomas et al. (2004) we show that consistent

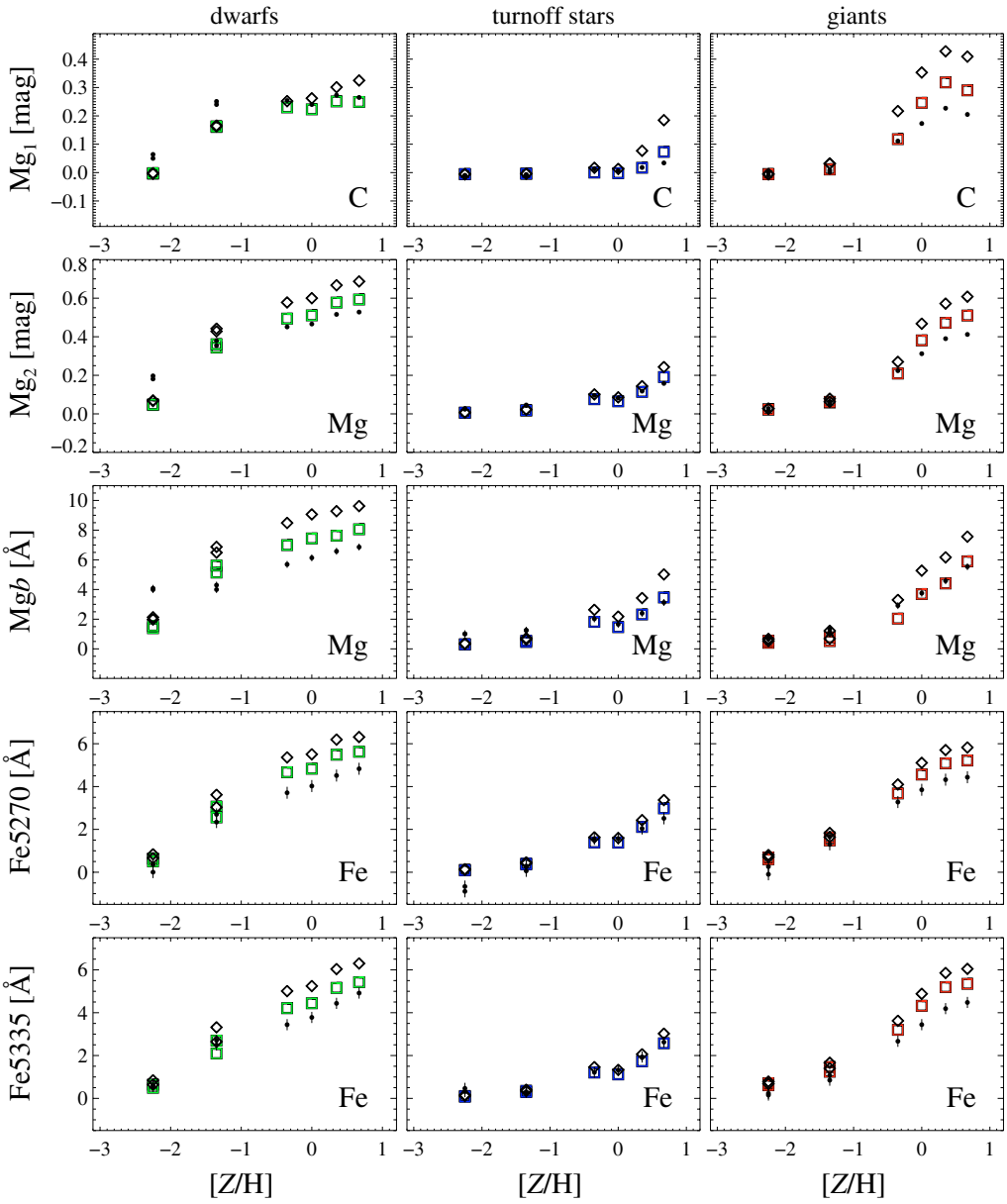

Fig. 6. Same as Fig. 4, here for Mg_1, Mg_2, Mg*b*, Fe5270 and Fe5335.

age estimates from Hβ and Hγ_A are obtained, only if the effect of α/Fe enhancement on Hγ_A is taken into account in the models. This result rectifies a problem currently present in the literature, namely that Hγ and Hδ have up to now led to significantly younger ages for early-type galaxies than Hβ (see Thomas et al. 2004 for more details).

5. Conclusions

We have computed line indices for the 21 classical and 4 higher-order Balmer-line Lick/IDS indices at six different metallicities ranging from −2.25 to +0.67 in [Z/H]. At the lowest two metallicities (−2.25 and −1.35) we also computed indices with a general enhancement of α elements. For all of these, we have varied individual elemental abundances of ten elements (plus overall metallicity) and tabulated the index changes. At solar metallicity, we compare our results with the work of Tripicco & Bell (1995). In the majority of cases, we confirm the findings to TB95. By tabulating index changes for all 25 Lick indices for a wide range of metallicities, we significantly extend the work of TB95.

The major assumptions of TMB03 were checked and verified by these calculations: the use of fractional changes produces accurate results over a wide range of abundances and ages. They can also be used to compute response functions with enhanced or diminished abundances of individual elements (notably α elements). Still, the metallicity-dependent response functions presented here do lead to a higher degree of self-consistency in the stellar population models. Furthermore, their

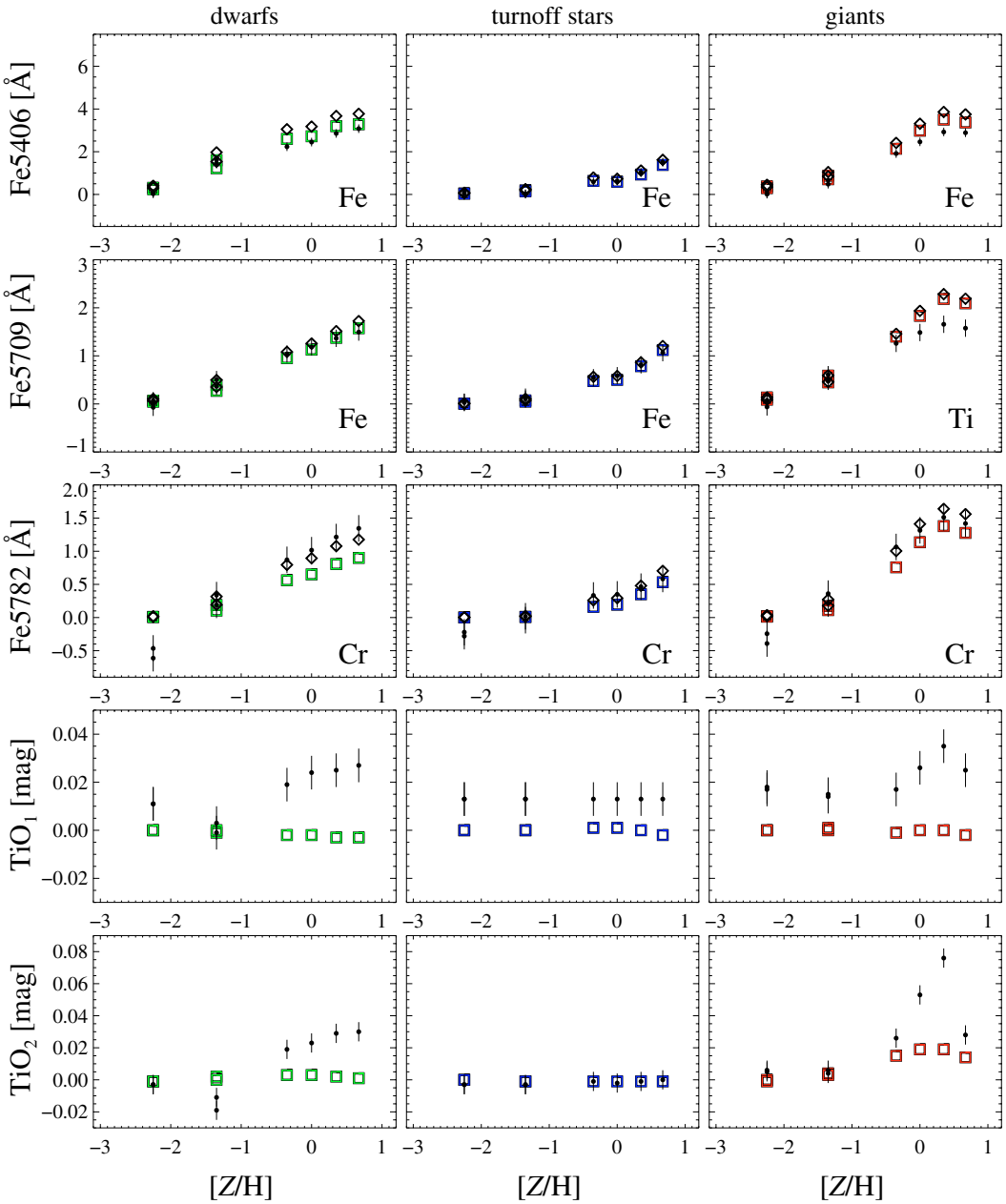

Fig. 7. Same as Fig. 4, here for Fe5406, Fe5709, Fe5782, TiO_1 and TiO_2.

use turns out to be of particular importance for the Balmer-line indices. We find that, different from the metallic indices, the Balmer-line indices become increasingly sensitive to element abundances with increasing metallicity and decreasing wavelength.

Hence, while the Hβ index only responds moderately (below 10 per cent) to abundance ratio variations, the higher-order Balmer-line indices Hγ and Hδ display very strong dependencies at high metallicities. More specifically, Hγ and Hδ significantly increase with increasing alpha/Fe ratio. This effect must not be neglected when these indices are used as age indicators of unresolved stellar systems. As shown in Thomas et al. (2004), the response functions of this work allow for a proper modelling of these indices, which helped to remove systematic effects in age determinations based on different Balmer-line indices previously present in the literature.

With the general availability of huge, homogeneous sets of galaxy spectra (e.g. Madgwick et al. 2003), direct synthesis of large wavelength ranges will become a more wide-spread analysis technique. To extract useful information from the spectra, the behaviour of different regions to individual abundance changes will have to be established. As a starting point and reference, the Lick indices serve an important purpose in this sense. By defining how they are expected to react to abundance changes under a variety of circumstances, we hope to shed light on the chemical evolution of galaxies throughout the Hubble sequence.

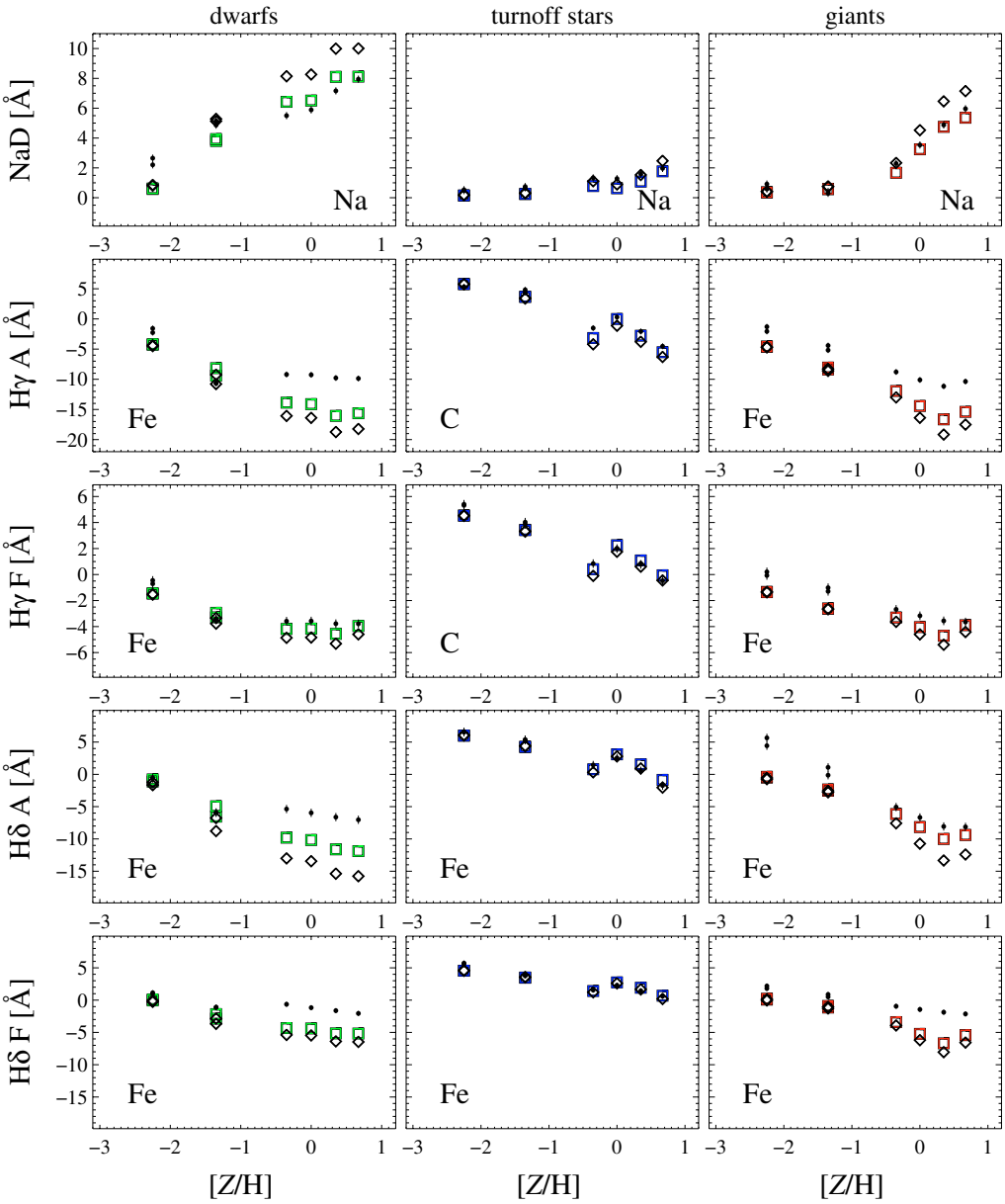

Fig. 8. Same as Fig. 4, here for NaD, Hγ A, Hγ F, Hδ A and Hδ F.

Acknowledgements. We would like to thank Thomas Gehren (Universitäts-Sternwarte München) for continuous support with his atmospheric code MAFAGS. Laura Greggio, Alvio Renzini and Scott Trager are thanked for repeated fruitful discussions. The referee, Guy Worthey, is thanked for stressing the carbon-star difficulty which prompted us to perform some extra computations. This work was in part supported by the Deutsche Akademie der Naturforscher Leopoldina (Halle, Germany) under grant BMBF-LPD 9901/8-87.

References

Anstee, S. D., & O'Mara, B. J. 1995, MNRAS, 276, 859
Barklem, P. S., Stempels, H. C., Allende Prieto, C., et al. 2002, A&A, 385, 951
Bernkopf, J. 1998, A&A, 332, 127
Böhm-Vitense, E. 1958, Z. Astrophys., 46, 108
Borges, A. C., Idiart, T. P., & de Freitas Pacheco, J. A., Thévenin, F. 1995, AJ, 110, 2408
Burstein, D., Faber, S. M., Gaskell, C. M., & Krumm, N. 1984, ApJ, 287, 586
Canuto, V. M., & Mazzitelli, I. 1992, ApJ, 389, 724
Carollo, C. M., & Danziger, I. J. 1994, MNRAS, 270, 523
Cassisi, S., Castellani, M., & Castellani, V. 1997, A&A, 317, 10
Davies, R. L., Kuntschner, H., et al. 2001, ApJ, 548, L33
Davies, R. L., Sadler, E. M., & Peletier, R. F. 1993, MNRAS, 262, 650
Decin, L., Cohen, M., Eriksson, K., et al. 1997, in Proc. of the first ISO workshop on Analytical Spectroscopy, ed. A. M. Heras, K. Leech, N. R. Trams, & M. Perry, ESA (Noordwijk, The Netherlands), 185
Falcon-Barroso, J., Peletier, R. F., Emsellem, E., et al. 2004, MNRAS, 350, 35
Fuhrmann, K., Axer, M., & Gehren, T. 1993, A&A, 271, 451

Gehren, T. 1975a, LTE-Sternatmosphärenmodelle (I), University of Kiel, Germany
Gehren, T. 1975b, LTE-Sternatmosphärenmodelle (II), University Kiel, Germany
Gehren, T., Korn, A. J., & Shi, J. 2001, A&A, 380, 645
Gray, D. F. 1977, ApJ, 218, 530
Grevesse, N., & Sauval, A. J. 1998, Space Sci. Rev., 85, 161
Gorgas, J., Faber, S. M., Burstein, D., et al. 1993, ApJS, 86, 153
Gustafsson, B., Bell, R. A., Eriksson, K., & Nordlund, Å. 1975, A&A, 42, 407
Houdashelt, M. L., Trager, S. C., Worthey, G., & Bell, R. A. 2002, BAAS, 34, 1118
Idiart, T. P., Thévenin, F., & de Freitas Pacheco, J. A. 1997, AJ, 113, 1066
Kurucz, R. L. 1992, Rev. Mex. Astron. Astrof., 23, 45
Kurucz, R. L. 1993a, CD-ROM No. 13, ATLAS9, Smithonian Astrophysical Observatory, Cambridge, USA
Kurucz, R. L. 1993b, CD-ROMs, Opacities for stellar atmospheres, Smithonian Astrophysical Observatory, Cambridge, USA
Kurucz, R. L. 2002, in Atomic and Molecular Data and their Applications, ed. D. R. Schultz, P. S. Krstic, & F. Ownby, AIP Conf. Proc., 636, 134
Kurucz, R. L., & Bell, B. 1995, CD-ROM No. 23, Atomic Line List, Smithonian Astrophysical Observatory, Cambridge, USA
Kurucz, R. L., Furenlid, I., Brault, J., & Testerman, L. 1984, Solar Flux Atlas from 296 to 1300 nm, Kitt Peak National Solar Observatory
Kurucz, R. L., & Peytremann, E. 1975, SAO Spec. Rep., 362, 1219
LeBorgne, D., Rocca-Volmerange, B., Prugniel, P., et al. 2004, A&A, 425, 881
Lejeune, T., Cuisinier, F., & Buser, R. 1997, A&AS, 125, 229
Madgwick, D. S., Coil, A. L., Conselice, C. J., et al. 2003, ApJ, 599, 997
Maraston, C. 1998, MNRAS, 300, 872
Maraston, C. 2005, MNRAS, in press
Maraston, C., Greggio, L., Renzini, A., et al. 2003, A&A, 400, 823
Peterson, R. C., Dalle Ore, C. M., & Kurucz, R. L. 1993, ApJ, 404, 333
Pfeiffer, M. J., Frank, C., Baumüller, D., Fuhrmann, K., & Gehren, T. 1998, A&AS, 130, 381
Przybilla, N., & Butler, K. 2004, ApJ, 610, 61
Salasnich, B., Girardi, L., Weiss, A., & Chiosi, C. 2000, A&A, 361, 1023
Tantalo, R., & Chiosi, C. 2004, MNRAS, 353, 917
Thomas, D., Maraston, C., & Bender, R. 2003a, MNRAS, 339, 897 (TMB03)
Thomas, D., Maraston, C., & Bender, R. 2003b, MNRAS, 343, 279
Thomas, D., Maraston, C., & Korn, A. 2004, MNRAS, 351, L19
Thomas, D., Maraston, C., Bender, R., & Mendes de Oliveira, C. 2005, ApJ, 621, 673
Tripicco, M. J., & Bell, R. A. 1995, ApJ, 110, 3035
Unsöld, A. 1968, in Physik der Sternatmosphären (Berlin: Springer)
van't Veer-Menneret, C., & Mégessier, C. 1996, A&A, 309, 879
Worthey, G. 2004, AJ, 128, 2826
Worthey, G., Faber, S. M., & González, J. J. 1992, ApJ, 398, 69
Worthey, G., Faber, S. M., González, J. J., & Burstein, D. 1994, ApJS, 94, 687
Worthey, G., & Ottaviani, D. L. 1997, ApJS, 111, 377

Online Material

Table 6. Spectral index response: Cool dwarf (4667/4.59/+0.67/0.00).

(1)	(2)	(3)	(4)	(5)	(6)	(7)	(8)	(9)	(10)	(11)	(12)	(13)	(14)
Index	I_0	Error	C	N	O	Mg	Fe	Ca	Na	Si	Cr	Ti	[Z/H][1]
CN_1	0.031	0.021	0.150	0.046	−0.058	−0.006	−0.010	−0.009	−0.001	0.008	−0.020	0.001	−0.020
CN_2	0.106	0.023	0.159	0.048	−0.061	−0.013	−0.012	−0.013	−0.003	0.015	−0.021	0.002	−0.029
Ca4227	4.606	0.270	−0.638	−0.143	0.281	−0.075	−0.077	1.158	−0.043	−0.077	−0.201	−0.030	−0.741
G4300	4.942	0.390	1.584	0.001	−0.697	−0.208	−0.499	0.466	−0.071	−0.048	−0.205	0.534	−0.108
Fe4383	11.525	0.530	0.156	0.005	0.043	−1.110	2.784	−0.737	−0.231	−0.209	−0.275	−0.043	−0.895
Ca4455	0.997	0.250	−0.050	0.000	0.012	−0.039	−0.042	−0.144	−0.019	−0.006	0.055	−0.001	−0.010
Fe4531	6.188	0.420	0.011	0.002	0.008	−0.475	0.336	−0.172	−0.076	−0.097	0.164	1.014	−0.827
C_2 4668	1.859	0.640	6.167	−0.001	−0.921	−0.266	0.110	0.155	−0.047	−0.225	−0.315	0.063	−0.369
Hβ	1.058	0.220	−0.020	0.001	0.010	−0.100	−0.012	−0.050	−0.018	−0.011	−0.096	0.020	−0.089
Fe5015	6.032	0.460	−0.082	0.002	0.022	−0.887	0.274	0.031	−0.050	−0.109	−0.016	1.488	−1.015
Mg_1	0.249	0.007	0.076	0.000	−0.012	0.031	−0.025	−0.006	−0.006	−0.004	−0.005	−0.001	−0.024
Mg_2	0.593	0.008	0.033	0.001	−0.004	0.094	−0.038	−0.016	−0.016	−0.011	−0.009	0.002	−0.065
Mg *b*	8.058	0.230	−0.046	0.009	0.049	1.566	−0.661	−0.184	−0.217	−0.121	−0.529	−0.038	−0.547
Fe5270	5.623	0.280	0.007	0.003	0.023	−0.358	0.691	0.272	−0.110	−0.076	−0.011	0.031	−0.539
Fe5270(Sauron)	4.834		0.006	0.002	0.021	−0.308	0.588	0.250	−0.095	−0.065	0.004	−0.018	−0.455
Fe5335	5.424	0.260	0.003	0.002	0.020	−0.435	0.875	−0.116	−0.134	−0.097	0.275	0.010	−0.633
Fe5406	3.283	0.200	−0.017	0.001	0.013	−0.236	0.493	−0.075	−0.077	−0.060	0.154	0.015	−0.374
Fe5709	1.575	0.180	0.000	0.000	0.002	−0.006	0.150	0.007	−0.135	−0.018	0.004	0.054	−0.237
Fe5782	0.899	0.200	0.002	0.000	0.003	0.001	−0.111	−0.042	−0.016	0.000	0.277	−0.032	−0.143
Na D	8.115	0.240	0.019	0.006	0.057	−0.329	−0.227	−0.196	1.893	−0.112	−0.044	−0.088	−1.252
TiO_1	−0.003	0.007	0.000	0.000	0.000	0.000	0.000	−0.002	0.000	0.001	0.000	0.002	0.001
TiO_2	0.001	0.006	0.000	0.000	0.000	0.000	0.001	−0.005	0.000	0.000	0.000	0.001	0.001
Hγ A	−15.625	0.480	−1.258	−0.006	0.603	1.643	−2.608	−0.289	0.338	0.241	0.205	−0.603	1.517
Hγ F	−3.959	0.330	−0.573	0.000	0.293	0.374	−0.639	−0.139	0.074	0.038	0.213	−0.096	0.256
Hδ A	−11.880	0.640	−0.365	0.136	0.305	1.209	−3.885	0.357	0.343	0.595	0.093	−0.187	1.198
Hδ F	−5.170	0.400	−0.237	−0.029	0.114	0.523	−1.292	0.236	0.154	0.135	−0.019	−0.197	0.623

[1] Overall metallicity *decreased* by 0.3 dex.

Table 7. Spectral index response: Turnoff star (5694/4.16/+0.67/0.00).

(1)	(2)	(3)	(4)	(5)	(6)	(7)	(8)	(9)	(10)	(11)	(12)	(13)	(14)
Index	I_0	Error	C	N	O	Mg	Fe	Ca	Na	Si	Cr	Ti	[Z/H][1]
CN_1	0.015	0.021	0.079	0.082	−0.025	−0.017	−0.017	−0.006	−0.002	−0.008	−0.005	0.004	−0.044
CN_2	0.048	0.023	0.083	0.088	−0.026	−0.019	−0.018	−0.008	−0.002	−0.007	−0.005	0.004	−0.049
Ca4227	0.517	0.270	−0.492	−0.345	0.151	0.107	0.153	0.490	0.008	0.047	−0.103	−0.009	−0.010
G4300	5.079	0.390	0.714	−0.001	−0.282	−0.272	−0.508	0.122	−0.044	−0.158	−0.103	0.091	0.056
Fe4383	5.114	0.530	0.394	0.001	−0.051	−0.277	0.970	−0.173	0.025	−0.153	−0.099	0.161	−0.531
Ca4455	0.795	0.250	−0.030	0.000	0.004	−0.023	−0.061	−0.024	−0.008	−0.007	0.070	0.051	−0.128
Fe4531	3.701	0.420	−0.026	0.000	0.003	−0.078	0.186	−0.004	0.023	−0.040	0.093	0.274	−0.479
C_2 4668	4.607	0.640	7.481	−0.003	−1.086	−0.399	−0.311	−0.001	0.271	−0.471	−0.103	0.129	−1.349
Hβ	3.149	0.220	−0.028	0.002	0.018	−0.058	−0.040	−0.011	−0.005	−0.021	−0.067	0.051	−0.292
Fe5015	5.433	0.460	−0.339	0.001	0.030	−0.175	0.443	0.082	0.019	−0.076	−0.006	0.302	−0.785
Mg_1	0.073	0.007	0.112	0.000	−0.019	0.000	−0.010	−0.001	−0.001	−0.006	−0.001	0.000	−0.033
Mg_2	0.191	0.008	0.041	0.000	−0.009	0.052	−0.011	−0.001	0.000	−0.007	−0.003	0.001	−0.041
Mg *b*	3.462	0.230	−0.349	0.003	0.069	1.556	−0.257	−0.011	−0.043	−0.102	−0.166	−0.017	−0.512
Fe5270	2.981	0.280	−0.005	0.001	0.008	−0.065	0.391	0.134	−0.004	−0.046	−0.034	0.057	−0.474
Fe5270(Sauron)	2.457		−0.004	0.001	0.007	−0.061	0.359	0.118	−0.004	−0.042	0.003	0.019	−0.364
Fe5335	2.572	0.260	−0.023	0.001	0.012	−0.062	0.451	−0.006	−0.004	−0.041	0.097	0.024	−0.446
Fe5406	1.379	0.200	−0.058	0.000	0.009	−0.018	0.243	−0.002	−0.001	−0.032	0.044	0.014	−0.219
Fe5709	1.121	0.180	−0.005	0.000	0.002	0.032	0.084	0.017	−0.032	−0.001	0.017	0.037	−0.208
Fe5782	0.533	0.200	0.010	0.000	0.000	0.036	−0.100	−0.012	0.000	0.011	0.171	−0.020	−0.121
Na D	1.768	0.240	−0.004	0.001	0.010	−0.057	−0.032	−0.043	0.704	−0.064	0.013	−0.004	−0.346
TiO_1	−0.002	0.007	0.000	0.000	0.000	0.000	0.000	−0.001	0.000	0.000	0.000	0.001	0.001
TiO_2	−0.001	0.006	0.000	0.000	0.000	0.000	−0.001	−0.001	0.000	0.000	0.000	0.001	0.000
Hγ A	−5.515	0.480	−0.780	0.002	0.300	0.526	−0.567	−0.089	0.004	0.219	0.011	−0.196	0.319
Hγ F	−0.055	0.330	−0.396	0.002	0.150	0.188	−0.162	−0.035	0.008	0.074	−0.029	−0.007	−0.058
Hδ A	−0.854	0.640	−0.306	0.086	0.124	0.268	−1.190	0.051	0.017	0.169	−0.012	−0.182	0.303
Hδ F	0.683	0.400	−0.124	−0.030	0.052	0.103	−0.500	0.027	0.006	0.064	−0.041	−0.143	0.128

[1] Overall metallicity *decreased* by 0.3 dex.

Table 8. Spectral index response: Cool giant (4590/3.42/+0.67/0.00).

(1)	(2)	(3)	(4)	(5)	(6)	(7)	(8)	(9)	(10)	(11)	(12)	(13)	(14)
Index	I_0	Error	C	N	O	Mg	Fe	Ca	Na	Si	Cr	Ti	[Z/H][1]
CN_1	0.138	0.021	0.182	0.063	−0.080	−0.016	−0.021	−0.010	−0.002	0.010	−0.016	0.002	−0.034
CN_2	0.225	0.023	0.195	0.067	−0.087	−0.024	−0.026	−0.014	−0.003	0.021	−0.016	0.003	−0.047
Ca4227	3.380	0.270	−0.810	−0.187	0.384	0.014	0.015	1.416	0.015	−0.068	−0.175	−0.024	−0.879
G4300	6.254	0.390	1.300	0.000	−0.704	−0.129	−0.459	0.238	−0.037	−0.025	−0.213	0.270	0.133
Fe4383	9.680	0.530	0.276	0.003	−0.018	−0.844	2.260	−0.443	−0.094	−0.172	−0.279	0.041	−0.721
Ca4455	1.455	0.250	−0.044	0.000	0.012	−0.018	−0.183	−0.061	−0.009	−0.003	0.149	0.067	−0.071
Fe4531	6.808	0.420	−0.027	0.000	0.002	−0.307	0.304	−0.049	−0.005	−0.060	0.125	0.779	−0.803
C_2 4668	3.785	0.640	9.748	−0.002	−1.783	−0.552	−0.139	0.058	−0.131	−0.369	−0.381	0.078	−0.719
Hβ	1.124	0.220	−0.028	0.000	0.010	−0.105	−0.017	−0.032	−0.014	0.007	−0.118	0.057	−0.091
Fe5015	7.624	0.460	−0.132	−0.001	0.011	−0.953	0.549	0.097	0.034	−0.053	0.080	0.965	−0.972
Mg_1	0.290	0.007	0.119	0.000	−0.022	0.043	−0.028	−0.006	−0.005	−0.007	−0.003	0.000	−0.043
Mg_2	0.510	0.008	0.046	0.000	−0.009	0.098	−0.030	−0.010	−0.008	−0.010	−0.006	0.004	−0.067
Mg *b*	5.899	0.230	−0.196	0.006	0.049	1.663	−0.717	−0.106	−0.131	−0.096	−0.487	0.017	−0.531
Fe5270	5.217	0.280	0.001	0.001	0.011	−0.241	0.608	0.163	−0.039	−0.053	−0.111	0.051	−0.431
Fe5270(Sauron)	4.235		0.002	0.001	0.012	−0.215	0.558	0.140	−0.036	−0.047	−0.042	−0.004	−0.363
Fe5335	5.348	0.260	−0.003	0.001	0.010	−0.319	0.699	−0.053	−0.053	−0.070	0.238	0.061	−0.700
Fe5406	3.368	0.200	−0.035	0.001	0.010	−0.160	0.383	−0.032	−0.028	−0.046	0.106	0.032	−0.395
Fe5709	2.093	0.180	−0.001	0.000	0.001	−0.006	0.093	0.032	−0.055	−0.002	0.020	0.096	−0.316
Fe5782	1.276	0.200	0.003	0.000	0.000	0.019	−0.145	−0.018	−0.004	0.013	0.284	−0.044	−0.205
Na D	5.362	0.240	0.010	0.004	0.035	−0.249	−0.138	−0.102	1.785	−0.086	0.017	−0.062	−1.069
TiO_1	−0.002	0.007	0.000	0.000	0.000	0.000	0.000	−0.001	0.000	0.000	0.000	0.003	0.000
TiO_2	0.014	0.006	0.000	0.000	0.000	0.000	0.000	−0.003	0.000	0.000	0.000	0.002	0.000
Hγ A	−15.396	0.480	−0.825	−0.003	0.625	1.113	−2.113	−0.151	0.126	0.140	0.030	−0.339	1.327
Hγ F	−3.894	0.330	−0.491	0.000	0.317	0.285	−0.525	−0.070	0.036	0.031	−0.011	−0.007	0.307
Hδ A	−9.397	0.640	−0.102	0.350	0.258	0.785	−3.009	0.124	0.133	0.665	0.018	−0.347	1.094
Hδ F	−5.415	0.400	−0.212	0.014	0.173	0.463	−1.149	0.130	0.077	0.118	−0.073	−0.298	0.872

[1] Overall metallicity *decreased* by 0.3 dex.

Table 9. Spectral index response: Cool dwarf (4543/4.58/+0.35/0.00).

(1)	(2)	(3)	(4)	(5)	(6)	(7)	(8)	(9)	(10)	(11)	(12)	(13)	(14)
Index	I_0	Error	C	N	O	Mg	Fe	Ca	Na	Si	Cr	Ti	[Z/H]
CN_1	−0.006	0.021	0.140	0.040	−0.040	0.000	−0.010	−0.010	0.000	0.010	−0.020	0.000	0.010
CN_2	0.068	0.023	0.150	0.040	−0.050	−0.010	−0.010	−0.010	0.000	0.020	−0.020	0.000	0.020
Ca4227	4.718	0.270	−0.640	−0.130	0.230	−0.080	−0.080	1.080	−0.030	−0.050	−0.190	−0.010	0.660
G4300	4.848	0.390	1.680	0.000	−0.710	−0.210	−0.500	0.430	−0.080	−0.040	−0.220	0.560	0.170
Fe4383	11.923	0.530	0.100	0.000	0.040	−1.150	2.840	−0.800	−0.270	−0.180	−0.240	−0.020	0.850
Ca4455	0.972	0.250	−0.050	0.000	0.010	−0.040	−0.030	−0.150	−0.020	−0.010	0.050	−0.010	−0.020
Fe4531	5.902	0.420	0.020	0.000	0.000	−0.480	0.310	−0.190	−0.060	−0.060	0.190	1.070	0.800
C_2 4668	0.946	0.640	4.200	0.000	−0.500	−0.220	0.220	0.170	−0.020	−0.140	−0.310	0.120	0.210
Hβ	0.778	0.220	−0.020	0.000	0.000	−0.080	0.030	−0.040	−0.010	0.000	−0.090	0.020	0.070
Fe5015	5.352	0.460	−0.030	0.000	0.000	−0.870	0.270	0.000	−0.030	−0.070	0.010	1.570	1.040
Mg_1	0.251	0.007	0.050	0.000	−0.010	0.030	−0.020	−0.010	−0.010	0.000	0.000	0.000	0.020
Mg_2	0.577	0.008	0.020	0.000	0.000	0.090	−0.040	−0.020	−0.020	−0.010	−0.010	0.000	0.050
Mg *b*	7.628	0.230	−0.040	0.000	0.030	1.650	−0.630	−0.200	−0.200	−0.080	−0.520	−0.040	0.480
Fe5270	5.485	0.280	0.000	0.000	0.010	−0.360	0.710	0.230	−0.110	−0.060	0.010	0.050	0.500
Fe5270(Sauron)	4.716		0.000	0.000	0.010	−0.310	0.590	0.220	−0.100	−0.050	0.020	0.000	0.420
Fe5335	5.158	0.260	0.000	0.000	0.010	−0.390	0.880	−0.140	−0.130	−0.070	0.300	0.030	0.590
Fe5406	3.194	0.200	−0.010	0.000	0.010	−0.240	0.480	−0.090	−0.080	−0.040	0.170	0.030	0.350
Fe5709	1.375	0.180	0.000	0.000	0.000	−0.010	0.140	0.000	−0.120	−0.010	0.020	0.060	0.210
Fe5782	0.807	0.200	0.000	0.000	0.000	0.000	−0.100	−0.040	−0.010	0.000	0.270	−0.030	0.130
Na D	8.099	0.240	0.010	0.000	0.030	−0.330	−0.220	−0.210	1.890	−0.070	0.000	−0.050	1.220
TiO_1	−0.003	0.007	0.000	0.000	0.000	0.000	0.000	0.000	0.000	0.000	0.000	0.000	0.000
TiO_2	0.002	0.006	0.000	0.000	0.000	0.000	0.000	0.000	0.000	0.000	0.000	0.000	0.000
Hγ A	−16.066	0.480	−1.280	0.000	0.620	1.680	−2.670	−0.180	0.390	0.210	0.180	−0.680	−1.640
Hγ F	−4.565	0.330	−0.580	0.000	0.290	0.430	−0.750	−0.100	0.110	0.050	0.240	−0.110	−0.310
Hδ A	−11.612	0.640	−0.680	0.020	0.360	1.240	−3.760	0.440	0.370	0.540	0.060	−0.230	−1.120
Hδ F	−5.153	0.400	−0.280	−0.040	0.100	0.530	−1.230	0.270	0.160	0.140	−0.030	−0.220	−0.580

Table 10. Spectral index response: Turnoff star (5969/4.18/+0.35/0.00).

(1)	(2)	(3)	(4)	(5)	(6)	(7)	(8)	(9)	(10)	(11)	(12)	(13)	(14)
Index	I_0	Error	C	N	O	Mg	Fe	Ca	Na	Si	Cr	Ti	[Z/H]
CN_1	−0.079	0.021	0.030	0.040	0.000	−0.010	−0.010	0.000	0.000	0.000	0.000	0.000	0.030
CN_2	−0.051	0.023	0.030	0.040	0.000	−0.010	−0.010	0.000	0.000	0.000	0.000	0.000	0.030
Ca4227	0.529	0.270	−0.260	−0.200	0.030	0.050	0.120	0.280	0.000	0.030	−0.080	0.000	0.030
G4300	4.397	0.390	0.870	0.000	−0.120	−0.280	−0.440	0.090	−0.040	−0.210	−0.070	0.080	0.040
Fe4383	3.627	0.530	0.380	0.000	−0.030	−0.160	0.620	−0.120	0.030	−0.110	−0.060	0.160	0.480
Ca4455	0.560	0.250	−0.020	0.000	0.000	−0.010	−0.050	−0.010	−0.010	0.000	0.050	0.040	0.130
Fe4531	2.933	0.420	−0.010	0.000	0.000	−0.040	0.110	0.000	0.010	−0.020	0.100	0.210	0.450
C_2 4668	2.268	0.640	3.200	0.000	−0.210	−0.370	−0.260	−0.270	−0.330	−0.250	−0.340	−0.150	1.110
Hβ	3.478	0.220	−0.020	0.000	0.010	−0.020	−0.040	−0.010	0.000	−0.010	−0.050	0.050	0.310
Fe5015	4.285	0.460	−0.090	0.000	0.000	−0.060	0.350	0.070	0.020	−0.050	−0.040	0.260	0.760
Mg_1	0.017	0.007	0.060	0.000	0.000	0.000	−0.010	0.000	0.000	0.000	0.000	0.000	0.030
Mg_2	0.114	0.008	0.030	0.000	0.000	0.030	−0.010	0.000	0.000	0.000	0.000	0.000	0.030
Mg *b*	2.318	0.230	−0.170	0.000	0.020	1.110	−0.120	−0.010	−0.030	−0.060	−0.110	−0.020	0.430
Fe5270	2.115	0.280	0.000	0.000	0.000	−0.020	0.320	0.110	0.000	−0.020	0.010	0.070	0.470
Fe5270(Sauron)	1.786		0.000	0.000	0.000	−0.020	0.280	0.090	0.000	−0.020	0.030	0.030	0.350
Fe5335	1.729	0.260	−0.020	0.000	0.010	−0.020	0.330	0.000	0.000	−0.020	0.060	0.020	0.390
Fe5406	0.932	0.200	−0.040	0.000	0.000	0.000	0.190	0.000	0.000	−0.010	0.040	0.020	0.200
Fe5709	0.785	0.180	0.000	0.000	0.000	0.030	0.080	0.010	−0.020	0.010	0.010	0.010	0.200
Fe5782	0.350	0.200	0.010	0.000	0.000	0.040	−0.070	−0.010	0.000	0.020	0.130	−0.010	0.120
Na D	1.078	0.240	0.000	0.000	0.000	−0.030	−0.020	−0.030	0.450	−0.040	0.010	0.000	0.270
TiO_1	0.000	0.007	0.000	0.000	0.000	0.000	0.000	0.000	0.000	0.000	0.000	0.000	0.000
TiO_2	−0.001	0.006	0.000	0.000	0.000	0.000	0.000	0.000	0.000	0.000	0.000	0.000	0.000
Hγ A	−2.781	0.480	−1.010	0.000	0.130	0.450	−0.210	−0.050	0.010	0.260	0.000	−0.190	−0.210
Hγ F	1.087	0.330	−0.480	0.000	0.060	0.190	−0.050	−0.020	0.010	0.110	−0.020	−0.020	0.090
Hδ A	1.555	0.640	−0.390	−0.090	0.030	0.200	−0.630	−0.020	0.010	0.140	−0.030	−0.130	−0.100
Hδ F	1.914	0.400	−0.090	−0.020	0.010	0.080	−0.250	0.030	0.000	0.060	−0.040	−0.090	0.000

Table 11. Spectral index response: Red giant (4236/2.00/+0.35/0.00).

(1)	(2)	(3)	(4)	(5)	(6)	(7)	(8)	(9)	(10)	(11)	(12)	(13)	(14)
Index	I_0	Error	C	N	O	Mg	Fe	Ca	Na	Si	Cr	Ti	[Z/H]
CN_1	0.170	0.021	0.180	0.060	−0.080	−0.020	−0.020	−0.010	0.000	0.010	−0.020	0.000	0.030
CN_2	0.273	0.023	0.190	0.060	−0.090	−0.030	−0.030	−0.010	0.000	0.020	−0.020	0.000	0.040
Ca4227	4.200	0.270	−0.730	−0.150	0.330	0.080	0.050	1.560	0.040	−0.060	−0.180	−0.020	1.210
G4300	6.623	0.390	1.180	0.000	−0.670	−0.080	−0.400	0.190	−0.030	0.000	−0.220	0.370	−0.030
Fe4383	9.961	0.530	0.270	0.000	−0.040	−0.710	2.460	−0.360	−0.080	−0.140	−0.260	0.050	1.140
Ca4455	1.434	0.250	−0.040	0.000	0.010	0.000	−0.240	−0.040	−0.010	0.000	0.150	0.090	−0.010
Fe4531	7.441	0.420	−0.030	0.000	0.000	−0.280	0.360	−0.030	0.000	−0.050	0.100	0.840	1.120
C_2 4668	3.655	0.640	9.640	0.000	−1.870	−0.660	−0.160	0.050	−0.130	−0.400	−0.410	0.050	0.780
Hβ	0.885	0.220	−0.020	0.000	0.000	−0.080	0.000	−0.020	−0.010	0.020	−0.110	0.050	0.050
Fe5015	8.105	0.460	−0.130	0.000	0.010	−0.890	0.620	0.090	0.040	−0.040	0.100	1.050	1.360
Mg_1	0.318	0.007	0.110	0.000	−0.020	0.040	−0.020	−0.010	−0.010	−0.010	0.000	0.000	0.040
Mg_2	0.472	0.008	0.040	0.000	−0.010	0.100	−0.030	−0.010	−0.010	−0.010	−0.010	0.000	0.070
Mg *b*	4.408	0.230	−0.250	0.000	0.030	1.760	−0.530	−0.090	−0.110	−0.070	−0.500	0.020	0.660
Fe5270	5.085	0.280	0.000	0.000	0.000	−0.180	0.620	0.110	−0.030	−0.040	−0.120	0.050	0.480
Fe5270(Sauron)	4.007		0.000	0.000	0.000	−0.170	0.580	0.100	−0.030	−0.040	−0.050	0.000	0.400
Fe5335	5.196	0.260	0.000	0.000	0.000	−0.250	0.660	−0.040	−0.040	−0.050	0.230	0.060	0.800
Fe5406	3.503	0.200	−0.040	0.000	0.010	−0.130	0.360	−0.030	−0.020	−0.040	0.100	0.020	0.410
Fe5709	2.185	0.180	0.000	0.000	0.000	0.000	0.080	0.030	−0.030	0.000	0.020	0.100	0.330
Fe5782	1.379	0.200	0.000	0.000	0.000	0.020	−0.140	−0.010	0.000	0.010	0.260	−0.040	0.200
Na D	4.750	0.240	0.000	0.000	0.010	−0.120	−0.040	−0.060	1.710	−0.060	0.020	−0.050	1.410
TiO_1	0.000	0.007	0.000	0.000	0.000	0.000	0.000	0.000	0.000	0.000	0.000	0.000	0.000
TiO_2	0.019	0.006	0.000	0.000	0.000	0.000	0.000	0.000	0.000	0.000	0.000	0.000	0.000
Hγ A	−16.649	0.480	−0.400	0.000	0.520	0.840	−2.510	−0.150	0.100	0.070	−0.090	−0.450	−2.470
Hγ F	−4.709	0.330	−0.350	0.000	0.280	0.240	−0.690	−0.060	0.030	0.020	−0.090	−0.020	−0.710
Hδ A	−10.003	0.640	−0.230	0.350	0.260	0.630	−3.330	0.030	0.100	0.610	0.020	−0.360	−1.920
Hδ F	−6.687	0.400	−0.240	0.030	0.190	0.430	−1.370	0.120	0.070	0.120	−0.080	−0.310	−1.390

Table 12. Spectral index response: Cool dwarf (4575/4.60/0.00/0.00).

(1)	(2)	(3)	(4)	(5)	(6)	(7)	(8)	(9)	(10)	(11)	(12)	(13)	(14)	(15)	(16)
Index	I_0	Error	C	N	O	Mg	Fe	Ca	Na	Si	Cr	Ti	[Z/H]	C0.15	C+O0.3
CN_1	−0.019	0.021	0.123	0.037	−0.033	−0.004	−0.007	−0.007	0.000	0.010	−0.017	0.002	0.014	0.038	0.009
CN_2	0.043	0.023	0.130	0.039	−0.034	−0.009	−0.008	−0.010	−0.002	0.017	−0.018	0.004	0.022	0.040	0.010
Ca4227	3.763	0.270	−0.669	−0.148	0.202	−0.087	−0.069	1.118	−0.028	−0.058	−0.175	−0.007	0.653	−0.212	−0.039
G4300	4.749	0.390	1.687	0.000	−0.768	−0.196	−0.470	0.323	−0.063	−0.035	−0.205	0.453	0.073	0.591	0.040
Fe4383	10.723	0.530	0.199	0.001	0.003	−1.060	2.595	−0.642	−0.183	−0.168	−0.179	0.024	0.890	0.047	0.042
Ca4455	0.936	0.250	−0.052	0.000	0.012	−0.046	−0.021	−0.109	−0.020	−0.007	0.050	−0.007	0.038	−0.017	−0.011
Fe4531	4.930	0.420	0.032	0.000	−0.006	−0.413	0.272	−0.125	−0.036	−0.055	0.168	0.902	0.723	0.010	0.007
C_2 4668	0.906	0.640	2.914	0.000	−0.311	−0.169	0.228	0.118	−0.036	−0.105	−0.229	0.129	0.141	0.730	0.555
Hβ	0.748	0.220	−0.012	0.000	0.003	−0.074	0.026	−0.035	−0.011	−0.013	−0.072	0.024	0.063	−0.005	−0.006
Fe5015	4.220	0.460	−0.025	0.000	0.005	−0.801	0.336	0.026	0.001	−0.048	0.007	1.216	0.891	−0.008	−0.004
Mg_1	0.223	0.007	0.039	0.000	−0.004	0.032	−0.021	−0.005	−0.004	−0.002	−0.004	0.000	0.019	0.010	0.007
Mg_2	0.511	0.008	0.020	0.000	−0.001	0.089	−0.032	−0.013	−0.011	−0.007	−0.004	0.004	0.055	0.005	0.004
Mg *b*	7.440	0.230	−0.084	0.001	0.008	1.623	−0.688	−0.149	−0.150	−0.077	−0.552	−0.089	0.355	−0.051	−0.043
Fe5270	4.831	0.280	0.001	0.001	0.005	−0.336	0.677	0.203	−0.081	−0.052	0.027	0.040	0.490	0.001	0.007
Fe5270(Sauron)	4.162		0.001	0.000	0.005	−0.292	0.572	0.195	−0.071	−0.045	0.036	0.000	0.417	0.000	0.006
Fe5335	4.440	0.260	0.000	0.000	0.004	−0.380	0.806	−0.059	−0.092	−0.062	0.243	0.022	0.549	0.000	0.005
Fe5406	2.723	0.200	−0.008	0.000	0.003	−0.213	0.456	−0.063	−0.054	−0.037	0.153	0.031	0.350	−0.002	0.000
Fe5709	1.130	0.180	0.000	0.000	0.000	−0.009	0.128	−0.005	−0.094	−0.005	0.019	0.058	0.202	0.000	0.000
Fe5782	0.650	0.200	0.000	0.000	0.001	0.005	−0.081	−0.033	−0.008	0.002	0.244	−0.027	0.125	0.000	0.001
Na D	6.509	0.240	0.004	0.001	0.013	−0.313	−0.207	−0.160	1.751	−0.058	−0.005	−0.039	1.125	0.002	0.017
TiO_1	−0.002	0.007	0.000	0.000	0.000	0.000	0.000	−0.001	0.000	0.000	0.000	0.002	−0.001	0.000	0.000
TiO_2	0.003	0.006	0.000	0.000	0.000	0.000	0.001	−0.004	0.000	0.000	0.000	0.001	−0.001	0.000	0.000
Hγ A	−14.121	0.480	−1.311	−0.001	0.691	1.446	−2.269	−0.134	0.247	0.166	0.156	−0.549	−1.381	−0.475	0.027
Hγ F	−4.159	0.330	−0.588	0.000	0.319	0.390	−0.679	−0.081	0.072	0.038	0.207	−0.084	−0.269	−0.218	0.011
Hδ A	−10.165	0.640	−0.942	−0.063	0.368	1.109	−3.277	0.306	0.249	0.515	0.056	−0.220	−1.089	−0.372	−0.133
Hδ F	−4.386	0.400	−0.301	−0.044	0.090	0.471	−1.077	0.189	0.109	0.120	−0.015	−0.203	−0.546	−0.104	−0.037

Table 13. Spectral index response: Turnoff star (6200/4.10/0.00/0.00).

(1)	(2)	(3)	(4)	(5)	(6)	(7)	(8)	(9)	(10)	(11)	(12)	(13)	(14)	(15)	(16)
Index	I_0	Error	C	N	O	Mg	Fe	Ca	Na	Si	Cr	Ti	[Z/H]	C0.15	C+O0.3
CN_1	−0.106	0.021	0.001	0.010	0.000	−0.001	−0.002	−0.002	0.000	−0.001	−0.001	0.001	−0.002	0.000	0.000
CN_2	−0.077	0.023	0.000	0.010	0.000	−0.001	−0.003	−0.002	0.000	−0.001	−0.001	0.002	−0.001	−0.001	0.000
Ca4227	0.426	0.270	−0.076	−0.052	0.002	0.008	0.057	0.160	0.001	0.006	−0.055	0.004	0.071	−0.032	−0.071
G4300	3.053	0.390	1.092	0.000	−0.034	−0.199	−0.258	0.065	−0.020	−0.158	−0.046	0.101	0.406	0.553	1.059
Fe4383	2.212	0.530	0.280	0.000	−0.016	−0.082	0.408	−0.072	0.017	−0.050	−0.030	0.129	0.459	0.125	0.261
Ca4455	0.359	0.250	−0.009	0.000	0.000	−0.011	−0.045	−0.005	−0.005	0.001	0.035	0.019	0.109	−0.004	−0.009
Fe4531	2.222	0.420	0.003	0.000	0.000	−0.017	0.090	0.002	0.006	0.000	0.102	0.198	0.440	0.001	0.002
C_2 4668	0.504	0.640	0.883	0.000	−0.015	0.259	0.174	0.029	−0.002	−0.095	−0.061	0.107	0.595	0.303	0.830
Hβ	3.757	0.220	−0.011	0.000	0.002	0.008	−0.060	−0.003	0.000	0.004	−0.024	0.051	0.252	−0.005	−0.009
Fe5015	3.222	0.460	−0.015	0.000	−0.007	−0.005	0.241	0.057	0.019	−0.018	−0.037	0.241	0.669	−0.005	−0.021
Mg_1	−0.002	0.007	0.015	0.000	0.000	0.000	−0.004	0.000	0.000	0.000	−0.002	0.000	0.006	0.005	0.014
Mg_2	0.065	0.008	0.008	0.000	0.000	0.021	−0.001	0.000	0.000	−0.001	−0.002	0.001	0.019	0.003	0.008
Mg *b*	1.461	0.230	−0.047	0.000	0.004	0.717	−0.053	−0.002	−0.019	−0.027	−0.065	−0.012	0.329	−0.016	−0.041
Fe5270	1.382	0.280	0.001	0.000	0.000	0.000	0.217	0.081	0.000	0.000	0.024	0.057	0.384	0.000	0.002
Fe5270(Sauron)	1.228		0.001	0.000	0.001	−0.004	0.170	0.074	0.000	−0.003	0.027	0.033	0.285	0.000	0.001
Fe5335	1.119	0.260	−0.012	0.000	−0.061	−0.002	0.212	−0.001	0.000	−0.001	0.034	−0.053	0.270	−0.005	−0.072
Fe5406	0.591	0.200	−0.023	0.000	0.000	0.007	0.143	0.000	0.000	−0.001	0.027	0.010	0.159	−0.010	−0.022
Fe5709	0.500	0.180	−0.002	0.000	0.000	0.029	0.082	0.004	−0.019	0.010	0.006	0.005	0.157	−0.001	−0.002
Fe5782	0.192	0.200	0.008	0.000	0.000	0.029	−0.045	−0.007	0.000	0.014	0.101	−0.007	0.097	0.003	0.007
Na D	0.630	0.240	−0.002	0.000	0.001	−0.011	−0.014	−0.025	0.262	−0.025	0.004	−0.005	0.163	−0.001	−0.001
TiO_1	0.001	0.007	0.000	0.000	0.000	0.000	0.000	0.000	0.000	0.000	0.000	0.001	0.000	0.000	0.000
TiO_2	−0.001	0.006	0.000	0.000	0.000	0.000	0.000	0.000	0.000	0.000	0.000	0.000	0.000	0.000	0.000
Hγ A	−0.012	0.480	−1.115	0.000	0.034	0.303	−0.118	−0.036	0.005	0.185	−0.007	−0.167	−0.427	−0.554	−1.079
Hγ F	2.258	0.330	−0.504	0.000	0.014	0.133	−0.017	−0.013	0.006	0.084	−0.007	−0.016	−0.015	−0.246	−0.489
Hδ A	3.106	0.640	−0.196	−0.019	0.008	0.118	−0.319	0.011	0.007	0.095	−0.009	−0.073	0.021	−0.086	−0.186
Hδ F	2.748	0.400	−0.039	−0.004	0.004	0.056	−0.149	0.028	0.003	0.042	−0.024	−0.056	0.020	−0.017	−0.035

Table 14. Spectral index response: Cool giant (4255/1.90/0.00/0.00).

(1)	(2)	(3)	(4)	(5)	(6)	(7)	(8)	(9)	(10)	(11)	(12)	(13)	(14)	(15)	(16)
Index	I_0	Error	C	N	O	Mg	Fe	Ca	Na	Si	Cr	Ti	[Z/H]	C0.15	C+O0.3
CN_1	0.145	0.021	0.173	0.067	−0.072	−0.014	−0.019	−0.002	0.000	0.014	−0.012	0.004	0.030	0.062	0.014
CN_2	0.231	0.023	0.187	0.072	−0.078	−0.022	−0.025	−0.005	−0.001	0.025	−0.013	0.006	0.043	0.068	0.016
Ca4227	2.704	0.270	−0.805	−0.185	0.401	0.109	0.087	1.479	0.053	−0.038	−0.132	−0.012	1.124	−0.317	−0.063
G4300	6.912	0.390	1.139	0.079	−0.566	0.007	−0.300	0.212	0.045	0.091	−0.118	0.292	−0.162	0.394	−0.060
Fe4383	8.705	0.530	0.387	−0.001	−0.077	−0.597	1.961	−0.245	−0.037	−0.141	−0.206	0.072	1.015	0.144	0.133
Ca4455	1.372	0.250	−0.041	0.007	0.018	0.001	−0.192	−0.015	0.000	0.007	0.153	0.071	0.047	−0.018	−0.015
Fe4531	6.333	0.420	0.009	0.010	0.005	−0.204	0.290	0.010	0.025	−0.031	0.102	0.638	0.929	0.000	−0.003
C_2 4668	3.279	0.640	8.289	0.098	−1.230	−0.380	0.058	0.126	−0.037	−0.226	−0.219	0.186	0.733	2.683	2.454
Hβ	0.887	0.220	0.006	0.024	0.028	−0.030	0.017	0.008	0.016	0.031	−0.072	0.080	0.048	−0.007	−0.010
Fe5015	7.071	0.460	−0.114	0.059	0.090	−0.736	0.692	0.140	0.100	0.038	0.142	0.751	1.075	−0.055	−0.041
Mg_1	0.246	0.007	0.107	0.000	−0.019	0.041	−0.020	−0.005	−0.004	−0.007	0.000	0.001	0.050	0.035	0.029
Mg_2	0.381	0.008	0.041	−0.001	−0.010	0.087	−0.025	−0.007	−0.006	−0.009	−0.005	0.002	0.066	0.015	0.011
Mg *b*	3.694	0.230	−0.261	−0.013	0.006	1.577	−0.423	−0.077	−0.108	−0.085	−0.407	0.008	0.620	−0.068	−0.069
Fe5270	4.560	0.280	0.016	0.014	0.015	−0.147	0.548	0.111	−0.005	−0.022	−0.101	0.057	0.428	0.000	0.005
Fe5270(Sauron)	3.537		0.009	0.008	0.009	−0.135	0.505	0.095	−0.008	−0.023	−0.031	0.009	0.374	0.000	0.003
Fe5335	4.320	0.260	−0.002	−0.001	−0.001	−0.196	0.563	−0.021	−0.026	−0.046	0.171	0.059	0.716	−0.001	0.000
Fe5406	2.984	0.200	−0.029	0.003	0.007	−0.106	0.329	−0.012	−0.010	−0.028	0.089	0.046	0.421	−0.011	−0.008
Fe5709	1.832	0.180	0.009	0.009	0.009	0.005	0.074	0.025	−0.017	0.015	0.038	0.105	0.306	0.000	0.000
Fe5782	1.135	0.200	0.008	0.006	0.006	0.035	−0.124	−0.005	0.005	0.019	0.276	−0.042	0.208	0.001	0.002
Na D	3.247	0.240	−0.005	−0.008	−0.005	−0.105	−0.022	−0.054	1.282	−0.058	0.014	−0.063	1.068	0.000	0.010
TiO_1	0.000	0.007	0.000	0.000	0.000	0.000	0.000	−0.001	0.000	0.000	0.000	0.003	0.000	0.000	0.000
TiO_2	0.019	0.006	0.000	0.000	0.000	0.000	0.001	−0.001	0.000	0.000	0.000	0.002	0.000	0.000	0.000
Hγ A	−14.427	0.480	−0.413	−0.058	0.451	0.560	−1.953	−0.145	−0.011	−0.023	−0.070	−0.330	−1.820	−0.158	0.248
Hγ F	−4.041	0.330	−0.295	−0.005	0.269	0.171	−0.556	−0.048	0.015	0.001	−0.071	0.012	−0.534	−0.116	0.101
Hδ A	−8.164	0.640	−0.018	0.395	0.344	0.372	−2.568	−0.110	0.053	0.571	0.063	−0.344	−1.533	−0.089	−0.021
Hδ F	−5.224	0.400	−0.180	0.042	0.219	0.341	−0.975	0.024	0.069	0.146	−0.017	−0.279	−1.252	−0.112	−0.032

Table 15. Spectral index response: Cool dwarf (5297/4.56/0.00/0.00).

(1)	(2)	(3)	(4)	(5)	(6)	(7)	(8)	(9)	(10)	(11)	(12)	(13)	(14)
Index	I_0	Error	C	N	O	Mg	Fe	Ca	Na	Si	Cr	Ti	[Z/H]
CN_1	−0.015	0.021	0.069	0.054	−0.024	−0.009	−0.009	−0.002	−0.001	0.002	−0.005	0.003	0.034
CN_2	0.012	0.023	0.072	0.058	−0.025	−0.011	−0.010	−0.003	−0.001	0.006	−0.006	0.004	0.040
Ca4227	0.864	0.270	−0.498	−0.269	0.189	0.045	0.061	0.583	0.004	−0.013	−0.102	−0.006	0.125
G4300	5.206	0.390	0.779	0.000	−0.525	−0.221	−0.460	0.128	−0.035	−0.090	−0.099	0.122	−0.074
Fe4383	5.973	0.530	0.438	0.000	−0.101	−0.450	1.260	−0.222	0.002	−0.171	−0.063	0.134	0.710
Ca4455	0.669	0.250	−0.035	0.000	0.008	−0.027	−0.017	−0.037	−0.009	−0.008	0.047	0.035	0.131
Fe4531	3.001	0.420	0.015	0.000	−0.004	−0.133	0.171	−0.018	0.008	−0.045	0.113	0.316	0.470
C_2 4668	1.984	0.640	3.881	0.000	−0.525	−0.032	0.059	0.025	0.246	−0.179	0.239	0.119	0.841
Hβ	1.797	0.220	−0.009	0.000	0.004	−0.061	−0.009	−0.014	−0.005	−0.019	−0.046	0.047	0.178
Fe5015	3.866	0.460	−0.101	0.000	0.015	−0.396	0.370	0.049	0.019	−0.052	−0.012	0.352	0.638
Mg_1	0.048	0.007	0.062	0.000	−0.009	0.020	−0.007	−0.001	−0.001	−0.003	0.000	0.001	0.032
Mg_2	0.215	0.008	0.031	0.000	−0.005	0.067	−0.016	−0.002	−0.001	−0.007	−0.002	0.001	0.047
Mg *b*	4.655	0.230	−0.097	0.001	0.015	1.502	−0.373	−0.029	−0.051	−0.123	−0.209	−0.018	0.692
Fe5270	2.807	0.280	−0.001	0.000	0.003	−0.130	0.439	0.139	−0.010	−0.052	0.020	0.051	0.460
Fe5270(Sauron)	2.424		−0.001	0.000	0.003	−0.118	0.386	0.129	−0.009	−0.048	0.033	0.017	0.377
Fe5335	2.504	0.260	−0.004	0.000	0.003	−0.132	0.487	−0.007	−0.011	−0.055	0.092	0.018	0.446
Fe5406	1.374	0.200	−0.023	0.000	0.004	−0.058	0.282	−0.006	−0.005	−0.031	0.064	0.009	0.249
Fe5709	0.836	0.180	−0.001	0.000	0.000	0.017	0.092	0.004	−0.038	−0.005	0.015	0.022	0.178
Fe5782	0.367	0.200	0.002	0.000	0.000	0.031	−0.069	−0.013	0.000	0.007	0.150	−0.015	0.108
Na D	2.210	0.240	−0.001	0.000	0.004	−0.113	−0.098	−0.047	0.863	−0.065	0.002	−0.008	0.491
TiO_1	−0.001	0.007	0.000	0.000	0.000	0.000	0.000	−0.001	0.000	0.000	0.000	0.001	−0.001
TiO_2	0.000	0.006	0.000	0.000	0.000	0.000	0.000	−0.001	0.000	0.000	0.000	0.000	0.000
Hγ A	−7.829	0.480	−0.712	0.000	0.525	0.653	−0.800	−0.095	0.019	0.187	0.032	−0.213	−0.620
Hγ F	−1.733	0.330	−0.328	0.000	0.252	0.216	−0.234	−0.042	0.012	0.058	0.023	−0.008	−0.064
Hδ A	−4.019	0.640	−0.577	−0.068	0.233	0.456	−1.483	0.018	0.038	0.264	0.004	−0.142	−0.681
Hδ F	−0.908	0.400	−0.160	−0.037	0.058	0.162	−0.558	0.034	0.014	0.093	−0.023	−0.114	−0.286

Table 16. Spectral index response: Turnoff star (8048/3.91/0.00/0.00).

(1)	(2)	(3)	(4)	(5)	(6)	(7)	(8)	(9)	(10)	(11)	(12)	(13)	(14)
Index	I_0	Error	C	N	O	Mg	Fe	Ca	Na	Si	Cr	Ti	[Z/H]
CN_1	−0.299	0.021	0.000	0.000	0.000	0.000	0.002	0.000	0.000	−0.001	−0.001	0.002	−0.001
CN_2	−0.257	0.023	0.000	0.000	0.000	0.000	0.003	0.000	0.000	−0.001	−0.001	0.002	0.000
Ca4227	0.151	0.270	0.018	0.002	0.000	0.000	0.005	0.017	0.000	0.000	−0.025	0.009	0.037
G4300	−2.942	0.390	−0.008	0.000	0.001	−0.007	0.020	0.055	−0.002	−0.009	−0.038	0.133	0.092
Fe4383	−2.126	0.530	−0.026	−0.001	−0.039	0.028	−0.011	−0.031	0.006	−0.004	−0.021	0.116	0.001
Ca4455	0.089	0.250	0.000	0.000	0.000	−0.015	−0.026	0.006	−0.001	0.000	0.010	0.009	0.051
Fe4531	0.923	0.420	0.001	0.000	0.000	−0.011	0.105	−0.009	0.001	0.002	0.063	0.168	0.327
C_2 4668	−0.307	0.640	−0.019	0.000	0.000	0.016	0.085	0.035	0.007	−0.033	−0.094	0.023	−0.003
Hβ	8.504	0.220	−0.005	0.000	0.001	0.003	−0.059	−0.001	0.000	0.028	−0.004	0.018	0.109
Fe5015	1.193	0.460	0.014	0.000	−0.030	−0.006	0.236	0.054	0.014	−0.045	−0.014	0.151	0.471
Mg_1	−0.022	0.007	0.000	0.000	0.000	0.000	0.001	0.000	0.000	0.000	−0.002	0.000	0.000
Mg_2	0.006	0.008	0.000	0.000	0.000	0.002	0.002	0.000	0.000	0.000	−0.002	0.001	0.003
Mg *b*	0.315	0.230	0.000	0.000	0.000	0.072	−0.050	0.000	−0.004	0.000	−0.031	0.009	−0.021
Fe5270	0.630	0.280	0.008	0.000	0.000	−0.002	0.095	0.068	0.000	0.002	0.001	0.041	0.196
Fe5270(Sauron)	0.656		0.006	0.000	0.000	−0.002	0.077	0.063	0.000	0.002	0.004	0.027	0.170
Fe5335	0.359	0.260	−0.025	0.000	0.014	−0.001	0.073	−0.015	0.000	0.001	0.006	0.015	0.076
Fe5406	0.137	0.200	−0.023	0.000	0.000	−0.001	0.076	0.000	0.000	−0.001	0.017	−0.015	0.048
Fe5709	0.113	0.180	−0.005	0.000	0.000	0.018	0.049	0.001	−0.017	0.004	−0.001	0.001	0.059
Fe5782	0.041	0.200	0.013	0.000	0.000	0.010	−0.020	−0.002	0.000	0.001	0.033	−0.001	0.031
Na D	0.223	0.240	−0.002	0.000	0.000	0.000	−0.016	−0.015	0.035	−0.008	0.003	0.000	0.009
TiO_1	0.001	0.007	0.000	0.000	0.000	0.000	0.000	0.000	0.000	0.001	0.000	0.000	0.000
TiO_2	−0.001	0.006	0.000	0.000	0.000	0.000	0.000	0.000	0.000	0.000	0.000	0.000	0.000
Hγ A	13.220	0.480	0.020	0.001	0.005	0.010	−0.082	−0.026	−0.001	0.039	−0.010	−0.092	0.066
Hγ F	8.812	0.330	0.013	0.000	−0.002	0.006	−0.033	−0.009	0.000	0.024	−0.006	−0.009	0.083
Hδ A	13.588	0.640	−0.001	0.001	0.005	−0.001	−0.128	−0.007	0.000	0.034	−0.008	−0.024	0.027
Hδ F	8.526	0.400	0.006	0.000	0.001	0.003	−0.092	0.001	0.000	0.015	−0.006	−0.013	0.000

Table 17. Spectral index response: Cool giant (4336/1.83/0.00/0.00).

(1)	(2)	(3)	(4)	(5)	(6)	(7)	(8)	(9)	(10)	(11)	(12)	(13)	(14)
Index	I_0	Error	C	N	O	Mg	Fe	Ca	Na	Si	Cr	Ti	[Z/H]
CN_1	0.162	0.021	0.165	0.069	−0.075	−0.017	−0.021	−0.006	−0.002	0.009	−0.012	0.002	0.032
CN_2	0.238	0.023	0.178	0.075	−0.082	−0.024	−0.027	−0.008	−0.003	0.020	−0.013	0.004	0.046
Ca4227	2.050	0.270	−0.842	−0.222	0.406	0.091	0.064	1.333	0.023	−0.060	−0.139	−0.031	1.038
G4300	7.165	0.390	0.908	0.000	−0.610	−0.077	−0.384	0.116	−0.035	0.006	−0.176	0.172	−0.195
Fe4383	8.111	0.530	0.421	0.000	−0.085	−0.513	1.737	−0.197	−0.013	−0.140	−0.194	0.092	0.989
Ca4455	1.326	0.250	−0.049	0.000	0.011	−0.008	−0.201	−0.017	−0.008	−0.001	0.142	0.067	0.062
Fe4531	6.161	0.420	−0.009	0.000	−0.004	−0.193	0.271	0.005	0.016	−0.044	0.088	0.543	0.878
C_2 4668	3.937	0.640	8.827	−0.001	−1.440	−0.480	−0.095	0.014	−0.138	−0.366	−0.288	0.091	1.043
Hβ	1.021	0.220	−0.018	0.000	0.003	−0.064	−0.014	−0.014	−0.007	0.008	−0.095	0.068	0.059
Fe5015	7.417	0.460	−0.266	0.000	0.047	−0.702	0.614	0.070	0.032	−0.029	0.073	0.571	1.036
Mg_1	0.195	0.007	0.127	0.000	−0.020	0.047	−0.006	−0.003	−0.002	−0.007	0.010	0.010	0.065
Mg_2	0.321	0.008	0.044	0.000	−0.011	0.081	−0.021	−0.004	−0.003	−0.008	−0.004	0.003	0.067
Mg *b*	3.051	0.230	−0.349	0.001	0.038	1.565	−0.378	−0.044	−0.080	−0.070	−0.348	0.017	0.647
Fe5270	4.427	0.280	−0.001	0.000	0.001	−0.148	0.500	0.098	−0.015	−0.041	−0.112	0.038	0.436
Fe5270(Sauron)	3.403		−0.001	0.000	0.001	−0.130	0.465	0.086	−0.013	−0.036	−0.039	−0.001	0.379
Fe5335	4.130	0.260	−0.003	0.000	0.001	−0.169	0.527	−0.012	−0.018	−0.045	0.153	0.058	0.716
Fe5406	2.818	0.200	−0.040	0.000	0.005	−0.095	0.306	−0.011	−0.009	−0.035	0.074	0.045	0.422
Fe5709	1.779	0.180	−0.001	0.000	0.000	−0.002	0.064	0.014	−0.025	0.006	0.030	0.092	0.308
Fe5782	1.080	0.200	0.002	0.000	0.000	0.030	−0.132	−0.011	−0.001	0.013	0.269	−0.049	0.216
Na D	2.751	0.240	0.000	0.001	0.003	−0.087	−0.007	−0.045	1.098	−0.054	0.017	−0.059	0.938
TiO_1	0.000	0.007	0.000	0.000	0.000	0.000	0.000	−0.001	0.000	0.000	0.000	0.003	0.000
TiO_2	0.018	0.006	0.000	0.000	0.000	0.000	0.000	−0.001	0.000	0.000	0.000	0.001	0.000
Hγ A	−13.729	0.480	−0.240	0.000	0.482	0.508	−1.645	−0.082	0.023	0.036	0.020	−0.243	−1.669
Hγ F	−3.646	0.330	−0.230	0.000	0.263	0.130	−0.436	−0.041	0.012	0.003	−0.058	0.024	−0.458
Hδ A	−7.909	0.640	0.117	0.470	0.286	0.302	−2.423	−0.070	0.032	0.554	0.060	−0.033	−1.338
Hδ F	−4.884	0.400	−0.152	0.036	0.173	0.235	−0.974	0.000	0.025	0.087	−0.044	−0.303	−1.201

Table 18. Spectral index response: Cool dwarf (4466/4.60/−0.35/0.00).

(1)	(2)	(3)	(4)	(5)	(6)	(7)	(8)	(9)	(10)	(11)	(12)	(13)	(14)
Index	I_0	Error	C	N	O	Mg	Fe	Ca	Na	Si	Cr	Ti	[Z/H]
CN_1	−0.040	0.021	0.096	0.027	−0.020	−0.001	−0.004	−0.006	0.000	0.010	−0.019	0.003	0.006
CN_2	0.021	0.023	0.102	0.028	−0.021	−0.006	−0.006	−0.009	−0.001	0.017	−0.019	0.004	0.013
Ca4227	3.836	0.270	−0.589	−0.111	0.149	−0.098	−0.083	1.073	−0.035	−0.057	−0.182	−0.007	0.626
G4300	4.639	0.390	1.821	0.000	−0.802	−0.198	−0.475	0.301	−0.060	−0.031	−0.224	0.477	0.070
Fe4383	10.513	0.530	0.180	0.000	0.007	−1.050	2.560	−0.659	−0.209	−0.155	−0.158	0.029	0.862
Ca4455	0.868	0.250	−0.053	0.000	0.012	−0.049	−0.005	−0.108	−0.022	−0.007	0.046	−0.008	0.060
Fe4531	4.672	0.420	0.040	0.000	−0.010	−0.416	0.250	−0.131	−0.053	−0.049	0.169	0.901	0.655
C_2 4668	0.447	0.640	1.653	0.000	−0.148	−0.182	0.276	0.120	−0.004	−0.065	−0.196	0.158	0.050
Hβ	0.563	0.220	−0.009	0.000	0.002	−0.063	0.032	−0.032	−0.009	−0.013	−0.065	0.018	0.038
Fe5015	3.599	0.460	−0.010	0.000	−0.001	−0.785	0.310	0.004	−0.003	−0.040	−0.010	1.221	0.808
Mg_1	0.230	0.007	0.022	0.000	−0.002	0.032	−0.019	−0.006	−0.005	−0.002	−0.003	0.000	0.016
Mg_2	0.494	0.008	0.012	0.000	−0.001	0.084	−0.030	−0.014	−0.012	−0.006	−0.005	0.003	0.046
Mg *b*	6.990	0.230	−0.031	0.000	0.006	1.494	−0.632	−0.146	−0.150	−0.057	−0.530	−0.110	0.263
Fe5270	4.667	0.280	0.001	0.000	0.002	−0.334	0.695	0.178	−0.091	−0.047	0.051	0.037	0.478
Fe5270(Sauron)	4.019		0.000	0.000	0.002	−0.288	0.576	0.175	−0.079	−0.041	0.050	0.000	0.405
Fe5335	4.211	0.260	0.000	0.000	0.002	−0.371	0.798	−0.104	−0.101	−0.056	0.233	0.020	0.531
Fe5406	2.600	0.200	−0.004	0.000	0.001	−0.211	0.454	−0.069	−0.060	−0.031	0.156	0.029	0.334
Fe5709	0.954	0.180	0.000	0.000	0.000	−0.011	0.129	−0.011	−0.089	−0.004	0.020	0.051	0.182
Fe5782	0.562	0.200	0.000	0.000	0.000	−0.003	−0.062	−0.028	−0.009	0.000	0.233	−0.027	0.117
Na D	6.427	0.240	0.001	0.001	0.006	−0.306	−0.200	−0.167	1.713	−0.051	−0.008	−0.038	1.089
TiO_1	−0.002	0.007	0.000	0.000	0.000	0.000	0.000	−0.001	0.000	0.000	0.000	0.002	−0.001
TiO_2	0.003	0.006	0.000	0.000	0.000	0.000	0.001	−0.003	0.000	0.000	0.000	0.001	0.000
Hγ A	−13.875	0.480	−1.386	−0.001	0.711	1.396	−2.188	−0.083	0.276	0.151	0.156	−0.582	−1.290
Hγ F	−4.187	0.330	−0.618	0.000	0.325	0.378	−0.680	−0.067	0.079	0.035	0.228	−0.096	−0.249
Hδ A	−9.800	0.640	−1.123	−0.089	0.337	1.088	−3.209	0.331	0.265	0.472	0.054	−0.208	−0.983
Hδ F	−4.325	0.400	−0.294	−0.034	0.073	0.460	−1.053	0.200	0.116	0.121	−0.009	−0.201	−0.489

Table 19. Spectral index response: Turnoff star (5822/4.22/−0.35/0.00).

(1)	(2)	(3)	(4)	(5)	(6)	(7)	(8)	(9)	(10)	(11)	(12)	(13)	(14)
Index	I_0	Error	C	N	O	Mg	Fe	Ca	Na	Si	Cr	Ti	[Z/H]
CN_1	−0.078	0.021	0.004	0.013	0.000	−0.001	−0.003	−0.002	0.000	0.000	−0.002	0.001	0.002
CN_2	−0.054	0.023	0.003	0.014	0.000	−0.001	−0.003	−0.002	0.000	0.000	−0.002	0.002	0.003
Ca4227	0.449	0.270	−0.129	−0.074	0.011	0.014	0.050	0.201	0.001	0.007	−0.054	0.004	0.045
G4300	4.399	0.390	0.937	0.000	−0.110	−0.250	−0.356	0.059	−0.021	−0.179	−0.052	0.089	0.277
Fe4383	2.943	0.530	0.362	0.000	−0.024	−0.131	0.529	−0.088	0.009	−0.076	−0.021	0.129	0.560
Ca4455	0.343	0.250	−0.014	0.000	0.001	−0.010	−0.031	−0.012	−0.004	0.001	0.028	0.016	0.106
Fe4531	2.071	0.420	0.010	0.000	−0.001	−0.028	0.101	0.000	0.004	−0.007	0.108	0.207	0.435
C_2 4668	0.609	0.640	1.012	0.000	−0.050	0.223	0.150	0.023	0.004	−0.096	−0.071	0.097	0.578
Hβ	2.619	0.220	−0.007	0.000	0.001	−0.005	−0.060	−0.004	−0.001	−0.004	−0.018	0.050	0.188
Fe5015	2.940	0.460	−0.019	0.000	−0.001	−0.034	0.222	0.040	0.020	−0.009	−0.033	0.240	0.629
Mg_1	0.000	0.007	0.017	0.000	−0.001	0.002	−0.005	0.000	0.000	0.000	−0.001	0.000	0.007
Mg_2	0.076	0.008	0.010	0.000	0.000	0.025	−0.003	0.000	0.000	−0.002	−0.001	0.001	0.021
Mg *b*	1.818	0.230	−0.048	0.000	0.004	0.814	−0.094	−0.004	−0.017	−0.044	−0.074	−0.013	0.370
Fe5270	1.390	0.280	0.000	0.000	0.000	−0.011	0.240	0.085	−0.001	−0.008	0.023	0.055	0.364
Fe5270(Sauron)	1.241		0.000	0.000	0.000	−0.015	0.199	0.079	−0.001	−0.011	0.027	0.030	0.282
Fe5335	1.206	0.260	−0.004	0.000	0.001	−0.015	0.256	0.004	−0.001	−0.010	0.036	0.016	0.291
Fe5406	0.633	0.200	−0.016	0.000	0.001	0.002	0.160	0.000	0.000	−0.002	0.029	0.002	0.165
Fe5709	0.475	0.180	−0.001	0.000	0.000	0.027	0.089	0.003	−0.021	0.007	0.006	0.005	0.152
Fe5782	0.160	0.200	0.003	0.000	0.000	0.026	−0.036	−0.005	0.000	0.010	0.099	−0.007	0.084
Na D	0.781	0.240	−0.001	0.000	0.001	−0.023	−0.028	−0.027	0.327	−0.029	0.002	−0.007	0.185
TiO_1	0.001	0.007	0.000	0.000	0.000	0.000	0.000	0.000	0.000	0.000	0.000	0.001	0.000
TiO_2	−0.001	0.006	0.000	0.000	0.000	0.000	0.000	0.000	0.000	0.000	0.000	0.000	0.000
Hγ A	−3.160	0.480	−1.045	0.000	0.112	0.392	−0.133	−0.037	0.012	0.225	0.003	−0.167	−0.522
Hγ F	0.406	0.330	−0.507	0.000	0.052	0.176	−0.005	−0.013	0.009	0.107	0.005	−0.009	−0.051
Hδ A	0.785	0.640	−0.239	−0.032	0.022	0.154	−0.462	0.019	0.010	0.119	−0.001	−0.072	−0.159
Hδ F	1.413	0.400	−0.069	−0.007	0.006	0.069	−0.195	0.032	0.004	0.056	−0.016	−0.055	−0.041

Table 20. Spectral index response: Cool giant (4414/1.77/−0.35/0.00).

(1)	(2)	(3)	(4)	(5)	(6)	(7)	(8)	(9)	(10)	(11)	(12)	(13)	(14)
Index	I_0	Error	C	N	O	Mg	Fe	Ca	Na	Si	Cr	Ti	[Z/H]
CN_1	0.117	0.021	0.145	0.078	−0.063	−0.019	−0.022	−0.011	−0.002	0.004	−0.008	0.004	0.046
CN_2	0.169	0.023	0.158	0.085	−0.068	−0.025	−0.027	−0.014	−0.002	0.014	−0.008	0.005	0.058
Ca4227	0.698	0.270	−0.902	−0.322	0.423	0.129	0.099	0.859	0.013	−0.032	−0.120	−0.025	0.556
G4300	7.545	0.390	0.707	0.000	−0.570	−0.086	−0.368	0.079	−0.029	−0.005	−0.124	0.104	−0.144
Fe4383	6.857	0.530	0.523	0.000	−0.117	−0.405	1.173	−0.129	0.006	−0.141	−0.115	0.147	0.855
Ca4455	1.129	0.250	−0.055	0.000	0.013	−0.008	−0.159	−0.009	−0.009	−0.001	0.107	0.054	0.126
Fe4531	5.094	0.420	0.011	0.000	−0.007	−0.131	0.153	0.010	0.011	−0.039	0.107	0.355	0.663
C_2 4668	3.092	0.640	6.699	0.000	−0.905	−0.294	0.028	0.010	−0.082	−0.273	−0.135	0.149	1.061
Hβ	1.047	0.220	−0.010	0.000	0.001	−0.053	−0.021	−0.009	−0.004	−0.005	−0.073	0.064	0.094
Fe5015	6.476	0.460	−0.236	0.000	0.042	−0.470	0.511	0.044	0.024	−0.029	0.030	0.360	0.891
Mg_1	0.118	0.007	0.099	0.000	−0.015	0.026	−0.013	−0.002	−0.001	−0.005	0.000	0.000	0.043
Mg_2	0.209	0.008	0.043	0.000	−0.009	0.061	−0.014	−0.002	−0.001	−0.006	−0.002	0.002	0.053
Mg *b*	2.038	0.230	−0.326	0.000	0.027	1.262	−0.248	−0.022	−0.059	−0.061	−0.228	−0.019	0.477
Fe5270	3.677	0.280	−0.001	0.000	0.000	−0.110	0.422	0.094	−0.009	−0.040	−0.058	0.049	0.494
Fe5270(Sauron)	2.773		0.000	0.000	0.001	−0.093	0.377	0.086	−0.008	−0.033	−0.006	0.012	0.403
Fe5335	3.200	0.260	−0.002	0.000	0.001	−0.110	0.423	−0.001	−0.009	−0.038	0.096	0.038	0.585
Fe5406	2.139	0.200	−0.032	0.000	0.004	−0.060	0.277	−0.006	−0.005	−0.028	0.058	0.046	0.399
Fe5709	1.400	0.180	0.000	0.000	0.000	0.002	0.063	0.005	−0.024	0.005	0.033	0.059	0.248
Fe5782	0.757	0.200	0.001	0.000	0.000	0.033	−0.108	−0.009	0.000	0.012	0.247	−0.040	0.204
Na D	1.669	0.240	0.000	0.000	0.001	−0.059	−0.008	−0.040	0.665	−0.043	0.008	−0.040	0.546
TiO_1	−0.001	0.007	0.000	0.000	0.000	0.000	0.000	0.000	0.000	0.000	0.000	0.002	0.000
TiO_2	0.015	0.006	0.000	0.000	0.000	0.000	0.000	−0.001	0.000	0.000	0.000	0.001	0.002
Hγ A	−11.941	0.480	−0.425	0.000	0.468	0.343	−1.060	−0.047	0.001	0.034	0.095	−0.213	−1.195
Hγ F	−3.307	0.330	−0.157	0.000	0.258	0.099	−0.326	−0.027	0.007	0.005	−0.001	0.025	−0.281
Hδ A	−6.145	0.640	−0.208	0.247	0.410	0.340	−1.426	0.205	0.029	0.487	0.050	−0.296	−1.092
Hδ F	−3.404	0.400	−0.225	−0.028	0.153	0.202	−0.518	0.176	0.017	0.131	−0.035	−0.269	−0.866

Table 21. Spectral index response: Cool dwarf (4385/4.83/−1.35/0.00).

(1)	(2)	(3)	(4)	(5)	(6)	(7)	(8)	(9)	(10)	(11)	(12)	(13)	(14)
Index	I_0	Error	C	N	O	Mg	Fe	Ca	Na	Si	Cr	Ti	[Z/H]
CN_1	−0.035	0.021	0.015	0.006	0.000	−0.002	−0.002	−0.004	−0.001	0.014	−0.013	0.001	−0.009
CN_2	0.006	0.023	0.014	0.007	0.001	−0.004	−0.003	−0.005	−0.001	0.023	−0.013	0.002	0.000
Ca4227	2.230	0.270	−0.281	−0.036	0.067	0.031	−0.039	0.905	0.017	−0.069	−0.112	−0.003	0.704
G4300	3.900	0.390	2.188	0.000	−0.971	−0.069	−0.374	0.189	0.002	−0.022	−0.182	0.316	0.100
Fe4383	7.041	0.530	0.218	0.000	−0.005	−0.453	1.979	−0.313	−0.049	−0.099	−0.044	0.054	1.349
Ca4455	0.436	0.250	−0.041	0.000	0.010	−0.020	0.030	−0.058	−0.005	−0.004	0.019	0.008	0.131
Fe4531	2.748	0.420	0.051	0.000	−0.011	−0.179	0.252	−0.028	−0.004	−0.027	0.154	0.532	0.702
C_2 4668	−0.031	0.640	0.219	0.000	−0.010	−0.124	0.216	0.057	0.025	−0.005	−0.080	0.124	0.044
Hβ	0.312	0.220	−0.001	0.000	0.001	−0.007	−0.014	−0.008	0.002	−0.007	−0.027	0.021	0.033
Fe5015	1.528	0.460	−0.005	0.000	0.000	−0.610	0.311	0.037	0.044	−0.006	−0.035	0.706	0.572
Mg_1	0.161	0.007	0.002	0.000	0.000	0.040	−0.008	−0.002	−0.002	−0.003	0.000	0.001	0.035
Mg_2	0.344	0.008	0.001	0.000	0.000	0.084	−0.017	−0.003	−0.003	−0.004	−0.002	0.002	0.064
Mg *b*	5.141	0.230	0.010	0.000	−0.001	1.346	−0.313	−0.038	−0.038	−0.052	−0.327	−0.031	0.724
Fe5270	3.063	0.280	0.000	0.000	0.000	−0.145	0.554	0.154	−0.017	−0.032	0.082	0.036	0.633
Fe5270(Sauron)	2.657		0.000	0.000	0.000	−0.126	0.481	0.148	−0.016	−0.028	0.060	0.009	0.531
Fe5335	2.697	0.260	0.000	0.000	0.000	−0.164	0.622	−0.017	−0.023	−0.035	0.141	0.013	0.550
Fe5406	1.601	0.200	−0.001	0.000	0.000	−0.094	0.371	−0.016	−0.013	−0.020	0.098	0.013	0.355
Fe5709	0.394	0.180	0.000	0.000	0.000	0.016	0.103	−0.003	−0.050	−0.003	0.007	0.013	0.143
Fe5782	0.187	0.200	0.000	0.000	0.000	0.000	−0.015	−0.002	0.000	−0.001	0.130	−0.011	0.108
Na D	3.802	0.240	0.000	0.000	0.000	−0.065	−0.100	−0.032	1.330	−0.032	0.001	−0.015	1.115
TiO_1	−0.001	0.007	0.000	0.000	0.000	0.000	0.000	−0.001	0.000	0.000	0.000	0.001	0.000
TiO_2	0.002	0.006	0.000	0.000	0.000	0.000	0.001	−0.002	0.000	0.000	0.000	0.000	0.001
Hγ A	−9.406	0.480	−1.814	0.000	0.870	0.535	−1.385	−0.164	0.036	0.089	0.044	−0.397	−1.582
Hγ F	−3.293	0.330	−0.865	0.000	0.413	0.195	−0.482	−0.063	0.017	0.029	0.149	−0.071	−0.337
Hδ A	−6.547	0.640	−0.852	−0.027	0.238	0.446	−2.228	0.092	0.060	0.383	0.008	−0.088	−1.207
Hδ F	−2.870	0.400	−0.184	−0.005	0.050	0.207	−0.802	0.087	0.029	0.084	−0.011	−0.087	−0.583

Table 22. Spectral index response: Turnoff star (6383/4.16/−1.35/0.00).

(1)	(2)	(3)	(4)	(5)	(6)	(7)	(8)	(9)	(10)	(11)	(12)	(13)	(14)
Index	I_0	Error	C	N	O	Mg	Fe	Ca	Na	Si	Cr	Ti	[Z/H]
CN_1	−0.091	0.021	−0.001	0.000	0.000	0.000	0.001	0.000	0.000	0.000	−0.001	0.001	−0.002
CN_2	−0.066	0.023	−0.002	0.000	0.000	0.000	0.002	0.000	0.000	0.000	0.000	0.001	−0.001
Ca4227	0.128	0.270	−0.001	0.000	0.000	0.000	0.007	0.038	0.000	0.000	−0.008	0.004	0.037
G4300	−0.259	0.390	0.296	0.000	0.000	−0.008	0.023	0.052	−0.001	−0.003	−0.015	0.111	0.388
Fe4383	0.323	0.530	0.027	0.000	−0.001	−0.004	0.129	−0.029	0.001	0.000	−0.010	0.078	0.211
Ca4455	0.105	0.250	−0.001	0.000	0.000	−0.009	−0.019	−0.003	0.000	0.000	0.001	0.010	0.021
Fe4531	0.498	0.420	0.001	0.000	0.000	−0.011	0.085	−0.015	0.000	0.000	0.039	0.122	0.231
C_2 4668	0.021	0.640	0.001	0.000	0.000	0.096	0.038	0.044	0.039	−0.009	−0.031	0.008	−0.005
Hβ	3.692	0.220	−0.001	0.000	0.000	0.003	−0.032	−0.003	0.000	0.002	0.003	0.007	0.065
Fe5015	0.774	0.460	0.001	0.000	−0.001	−0.001	0.149	0.013	−0.015	0.002	−0.004	0.087	0.357
Mg_1	−0.004	0.007	0.000	0.000	0.000	0.000	0.000	0.000	0.000	0.000	−0.001	0.000	0.001
Mg_2	0.018	0.008	0.000	0.000	0.000	0.004	0.001	0.000	0.000	0.000	−0.001	0.001	0.005
Mg *b*	0.463	0.230	0.000	0.000	0.000	0.165	−0.063	0.000	−0.001	0.000	−0.021	0.011	0.074
Fe5270	0.403	0.280	0.000	0.000	0.000	0.000	0.058	0.061	0.000	0.000	0.001	0.012	0.122
Fe5270(Sauron)	0.414		0.000	0.000	0.000	0.000	0.050	0.059	0.000	0.000	0.005	0.007	0.116
Fe5335	0.352	0.260	−0.001	0.000	0.000	0.000	0.052	0.001	0.000	0.000	0.019	0.013	0.087
Fe5406	0.194	0.200	−0.003	0.000	0.000	0.000	0.052	0.000	0.000	0.000	0.014	−0.012	0.050
Fe5709	0.073	0.180	0.000	0.000	0.000	0.012	0.034	0.000	−0.010	0.002	0.000	0.000	0.045
Fe5782	0.011	0.200	0.001	0.000	0.000	0.002	−0.007	0.000	0.000	0.000	0.014	0.000	0.011
Na D	0.247	0.240	0.000	0.000	0.000	0.000	−0.015	−0.008	0.055	−0.003	0.000	−0.001	0.033
TiO_1	0.000	0.007	0.000	0.000	0.000	0.000	0.000	0.000	0.000	0.000	0.000	0.000	0.000
TiO_2	−0.001	0.006	0.000	0.000	0.000	0.000	0.000	0.000	0.000	0.000	0.000	0.000	0.000
Hγ A	3.669	0.480	−0.236	0.000	0.000	0.032	−0.114	−0.036	0.000	0.006	0.018	−0.088	−0.305
Hγ F	3.440	0.330	−0.099	0.000	0.000	0.015	−0.034	−0.013	0.000	0.004	0.013	−0.010	−0.052
Hδ A	4.226	0.640	−0.016	0.000	0.000	0.007	−0.147	0.000	0.000	0.012	0.006	−0.018	−0.048
Hδ F	3.464	0.400	−0.004	0.000	0.000	0.005	−0.084	0.002	0.000	0.010	0.002	−0.010	−0.038

Table 23. Spectral index response: Cool giant (4662/1.83/−1.35/0.00).

(1)	(2)	(3)	(4)	(5)	(6)	(7)	(8)	(9)	(10)	(11)	(12)	(13)	(14)
Index	I_0	Error	C	N	O	Mg	Fe	Ca	Na	Si	Cr	Ti	[Z/H]
CN_1	−0.021	0.021	0.025	0.030	−0.005	0.000	−0.007	−0.002	0.000	0.002	−0.002	0.001	0.021
CN_2	−0.004	0.023	0.025	0.032	−0.005	0.000	−0.008	−0.002	0.000	0.006	−0.002	0.002	0.025
Ca4227	0.149	0.270	−0.364	−0.200	0.103	0.000	0.064	0.196	0.004	0.019	−0.041	0.004	−0.015
G4300	7.853	0.390	0.401	0.000	−0.333	−0.008	−0.243	0.043	−0.010	−0.073	−0.044	0.071	0.118
Fe4383	3.683	0.530	0.628	0.000	−0.123	−0.004	0.316	−0.061	−0.005	−0.110	−0.005	0.165	0.650
Ca4455	0.475	0.250	−0.036	0.000	0.007	−0.009	−0.046	−0.003	−0.002	0.002	0.024	0.005	0.135
Fe4531	2.863	0.420	0.037	0.000	−0.008	−0.011	0.092	0.002	0.000	−0.015	0.141	0.252	0.561
C_2 4668	0.747	0.640	1.165	0.000	−0.136	0.096	0.211	0.021	0.006	−0.067	−0.124	0.148	0.502
Hβ	0.853	0.220	0.004	0.000	−0.002	0.003	−0.083	−0.004	−0.001	−0.007	0.001	0.070	0.100
Fe5015	3.725	0.460	−0.042	0.000	0.006	−0.001	0.214	0.020	0.020	−0.001	−0.042	0.346	0.777
Mg_1	0.012	0.007	0.020	0.000	−0.002	0.000	−0.001	0.000	0.000	0.000	−0.001	0.000	0.011
Mg_2	0.059	0.008	0.013	0.000	−0.002	0.004	−0.002	0.000	0.000	−0.001	−0.002	0.001	0.016
Mg *b*	0.525	0.230	−0.055	0.000	0.005	0.165	−0.111	−0.003	−0.009	−0.019	−0.059	−0.037	0.092
Fe5270	1.624	0.280	0.000	0.000	0.000	0.000	0.208	0.081	0.000	−0.007	0.008	0.082	0.373
Fe5270(Sauron)	1.281		0.000	0.000	0.000	0.000	0.154	0.077	−0.001	−0.007	0.013	0.039	0.257
Fe5335	1.464	0.260	0.000	0.000	0.000	0.000	0.200	0.008	−0.001	−0.009	0.046	0.020	0.304
Fe5406	0.879	0.200	−0.007	0.000	0.001	0.000	0.169	0.000	0.000	−0.001	0.027	0.002	0.216
Fe5709	0.588	0.180	0.000	0.000	0.000	0.012	0.110	0.001	−0.022	0.009	0.005	0.005	0.198
Fe5782	0.173	0.200	0.000	0.000	0.000	0.002	−0.019	−0.001	0.000	0.005	0.098	−0.009	0.095
Na D	0.580	0.240	0.000	0.000	0.000	0.000	−0.030	−0.029	0.162	−0.018	0.001	−0.010	0.099
TiO_1	0.000	0.007	0.000	0.000	0.000	0.000	0.000	0.000	0.000	0.000	0.000	0.001	0.000
TiO_2	0.004	0.006	0.000	0.000	0.000	0.000	0.001	0.000	0.000	0.000	0.000	0.001	0.002
Hγ A	−8.376	0.480	−0.192	0.000	0.305	0.032	−0.228	−0.041	0.005	0.076	0.071	−0.203	−0.676
Hγ F	−2.629	0.330	−0.112	0.000	0.169	0.015	−0.026	−0.014	0.005	0.044	0.055	0.013	−0.052
Hδ A	−2.538	0.640	−0.667	−0.132	0.179	0.007	−0.240	0.016	0.013	0.132	0.025	−0.100	−0.572
Hδ F	−1.151	0.400	−0.160	−0.032	0.043	0.005	−0.124	0.031	0.004	0.064	−0.005	−0.078	−0.342

Table 24. Spectral index response: Cool dwarf (4385/4.83/−1.35/+0.30).

(1)	(2)	(3)	(4)	(5)	(6)	(7)	(8)	(9)	(10)	(11)	(12)	(13)	(14)
Index	I_0	Error	C	N	O	Mg	Fe	Ca	Na	Si	Cr	Ti	[Z/H]
CN_1	−0.016	0.021	0.012	0.007	0.001	−0.003	−0.001	−0.004	−0.001	0.014	−0.010	0.001	−0.004
CN_2	0.025	0.023	0.010	0.007	0.002	−0.005	−0.002	−0.005	−0.001	0.022	−0.010	0.002	0.003
Ca4227	2.395	0.270	−0.271	−0.037	0.073	0.035	−0.034	0.901	0.020	−0.073	−0.089	−0.003	0.721
G4300	4.197	0.390	1.981	0.000	−0.943	−0.087	−0.328	0.209	0.001	−0.028	−0.162	0.332	0.122
Fe4383	5.305	0.530	0.260	0.000	−0.030	−0.440	1.686	−0.335	−0.045	−0.100	−0.025	0.057	1.039
Ca4455	0.268	0.250	−0.036	0.000	0.009	−0.025	0.032	−0.064	−0.006	−0.005	0.011	0.008	0.091
Fe4531	2.420	0.420	0.048	0.000	−0.012	−0.181	0.231	−0.029	−0.002	−0.029	0.123	0.563	0.667
C_2 4668	0.010	0.640	0.186	0.000	−0.008	−0.139	0.169	0.060	0.028	−0.004	−0.069	0.130	0.056
Hβ	0.290	0.220	0.001	0.000	0.001	−0.004	−0.010	−0.008	0.003	−0.008	−0.014	0.023	0.024
Fe5015	1.165	0.460	−0.003	0.000	0.000	−0.579	0.257	0.047	0.050	−0.002	−0.033	0.739	0.546
Mg_1	0.163	0.007	0.003	0.000	0.000	0.038	−0.002	−0.002	−0.002	−0.002	0.002	0.002	0.038
Mg_2	0.361	0.008	0.000	0.000	0.000	0.081	−0.012	−0.004	−0.003	−0.005	−0.002	0.002	0.065
Mg *b*	5.611	0.230	0.008	0.000	0.000	1.262	−0.235	−0.046	−0.044	−0.067	−0.242	−0.032	0.788
Fe5270	2.560	0.280	0.000	0.000	0.000	−0.139	0.478	0.176	−0.016	−0.033	0.059	0.037	0.552
Fe5270(Sauron)	2.227		0.000	0.000	0.000	−0.122	0.418	0.169	−0.014	−0.029	0.040	0.009	0.465
Fe5335	2.096	0.260	0.000	0.000	0.000	−0.150	0.553	−0.014	−0.021	−0.034	0.107	0.014	0.430
Fe5406	1.227	0.200	−0.001	0.000	0.000	−0.082	0.313	−0.013	−0.011	−0.019	0.071	0.015	0.281
Fe5709	0.272	0.180	0.000	0.000	0.000	0.020	0.080	−0.003	−0.051	−0.003	0.004	0.014	0.108
Fe5782	0.105	0.200	0.000	0.000	0.000	0.002	−0.009	−0.002	0.000	−0.001	0.088	−0.011	0.074
Na D	3.929	0.240	0.000	0.000	0.000	−0.081	−0.074	−0.031	1.352	−0.040	0.001	−0.015	1.126
TiO_1	0.000	0.007	0.000	0.000	0.000	0.000	0.000	−0.001	0.000	0.000	0.000	0.001	0.000
TiO_2	0.000	0.006	0.000	0.000	0.000	0.000	0.001	−0.002	0.000	0.000	0.000	0.000	0.000
Hγ A	−8.157	0.480	−1.687	0.000	0.870	0.521	−1.091	−0.187	0.032	0.089	0.036	−0.410	−1.254
Hγ F	−2.944	0.330	−0.825	0.000	0.421	0.197	−0.398	−0.072	0.016	0.031	0.110	−0.077	−0.272
Hδ A	−4.938	0.640	−0.769	−0.023	0.237	0.397	−1.818	0.062	0.054	0.365	0.001	−0.093	−0.924
Hδ F	−2.165	0.400	−0.173	−0.005	0.053	0.188	−0.684	0.074	0.026	0.089	−0.008	−0.091	−0.472

Table 25. Spectral index response: Turnoff star (6383/4.16/−1.35/+0.30).

(1)	(2)	(3)	(4)	(5)	(6)	(7)	(8)	(9)	(10)	(11)	(12)	(13)	(14)
Index	I_0	Error	C	N	O	Mg	Fe	Ca	Na	Si	Cr	Ti	[Z/H]
CN_1	−0.090	0.021	−0.002	0.000	0.000	0.000	0.002	0.000	0.000	0.000	0.000	0.001	−0.001
CN_2	−0.066	0.023	−0.002	0.000	0.000	0.000	0.003	0.000	0.000	0.000	0.000	0.001	0.000
Ca4227	0.134	0.270	−0.001	0.000	0.000	0.000	0.006	0.040	0.000	0.000	−0.005	0.005	0.038
G4300	−0.227	0.390	0.314	0.000	0.000	−0.011	0.024	0.050	−0.001	−0.004	−0.010	0.113	0.412
Fe4383	0.232	0.530	0.017	0.000	−0.001	−0.004	0.085	−0.028	0.001	0.000	−0.018	0.068	0.175
Ca4455	0.089	0.250	−0.001	0.000	0.000	−0.009	−0.010	−0.005	0.000	0.000	0.000	0.007	0.012
Fe4531	0.404	0.420	0.001	0.000	0.000	−0.011	0.071	−0.015	0.000	0.000	0.027	0.126	0.207
C_2 4668	0.126	0.640	0.001	0.000	0.000	−0.057	−0.056	−0.070	−0.001	−0.010	−0.126	−0.072	−0.069
Hβ	3.647	0.220	−0.001	0.000	0.000	0.003	−0.015	−0.003	0.000	0.002	0.002	0.008	0.058
Fe5015	0.605	0.460	0.001	0.000	−0.016	−0.002	0.133	0.013	0.006	0.003	−0.018	0.112	0.299
Mg_1	−0.004	0.007	0.000	0.000	0.000	0.000	0.000	0.000	0.000	0.000	0.000	0.000	0.001
Mg_2	0.018	0.008	0.000	0.000	0.000	0.005	0.001	0.000	0.000	0.000	0.000	0.001	0.006
Mg *b*	0.546	0.230	0.000	0.000	0.000	0.172	−0.050	0.000	−0.001	−0.001	−0.021	0.011	0.098
Fe5270	0.366	0.280	0.000	0.000	0.000	0.000	0.049	0.063	0.000	0.000	0.002	0.013	0.119
Fe5270(Sauron)	0.375		0.000	0.000	0.000	0.000	0.046	0.060	0.000	0.000	0.004	0.008	0.113
Fe5335	0.295	0.260	−0.001	0.000	0.000	0.000	0.047	0.001	0.000	0.000	0.014	0.013	0.075
Fe5406	0.142	0.200	−0.003	0.000	0.000	0.000	0.044	0.000	0.000	0.000	0.012	−0.013	0.039
Fe5709	0.047	0.180	0.000	0.000	0.000	0.012	0.025	0.000	−0.010	0.002	0.000	0.000	0.033
Fe5782	0.007	0.200	0.001	0.000	0.000	0.002	−0.004	0.000	0.000	0.000	0.008	0.000	0.007
Na D	0.257	0.240	0.000	0.000	0.000	−0.001	−0.011	−0.009	0.057	−0.003	0.000	−0.001	0.035
TiO_1	0.000	0.007	0.000	0.000	0.000	0.000	0.000	0.000	0.000	0.000	0.000	0.000	0.000
TiO_2	−0.001	0.006	0.000	0.000	0.000	0.000	0.000	0.000	0.000	0.000	0.000	0.000	0.000
Hγ A	3.655	0.480	−0.250	0.000	0.000	0.034	−0.081	−0.036	0.000	0.007	0.012	−0.101	−0.318
Hγ F	3.410	0.330	−0.104	0.000	0.000	0.016	−0.023	−0.013	0.000	0.004	0.010	−0.010	−0.067
Hδ A	4.268	0.640	−0.017	0.000	0.000	0.008	−0.125	0.000	0.000	0.013	0.004	−0.019	−0.058
Hδ F	3.495	0.400	−0.004	0.000	0.000	0.006	−0.067	0.002	0.000	0.010	0.002	−0.010	−0.029

Table 26. Spectral index response: Cool giant (4662/1.83/−1.35/+0.30).

(1)	(2)	(3)	(4)	(5)	(6)	(7)	(8)	(9)	(10)	(11)	(12)	(13)	(14)
Index	I_0	Error	C	N	O	Mg	Fe	Ca	Na	Si	Cr	Ti	[Z/H]
CN_1	−0.010	0.021	0.030	0.034	−0.007	−0.005	−0.005	−0.003	0.000	0.002	−0.002	0.002	0.028
CN_2	0.008	0.023	0.030	0.036	−0.006	−0.006	−0.006	−0.003	−0.001	0.006	−0.001	0.002	0.033
Ca4227	0.085	0.270	−0.391	−0.224	0.119	0.081	0.049	0.205	0.006	0.027	−0.027	0.003	−0.032
G4300	7.885	0.390	0.333	0.000	−0.326	−0.128	−0.157	0.040	−0.010	−0.071	−0.033	0.071	0.115
Fe4383	3.316	0.530	0.670	0.000	−0.148	−0.209	0.284	−0.067	−0.007	−0.129	−0.005	0.165	0.607
Ca4455	0.346	0.250	−0.037	0.000	0.008	−0.001	−0.041	−0.003	−0.002	0.002	0.014	0.005	0.121
Fe4531	2.586	0.420	0.043	0.000	−0.010	−0.039	0.115	0.002	0.000	−0.014	0.115	0.247	0.531
C_2 4668	0.762	0.640	1.254	0.000	−0.151	−0.032	0.167	0.020	0.006	−0.074	−0.135	0.149	0.510
Hβ	0.833	0.220	0.004	0.000	−0.003	−0.014	−0.092	−0.004	−0.001	−0.008	0.007	0.070	0.075
Fe5015	3.356	0.460	−0.043	0.000	0.007	−0.053	0.194	0.021	0.020	0.004	−0.035	0.335	0.728
Mg_1	0.011	0.007	0.021	0.000	−0.003	0.005	−0.001	0.000	0.000	−0.001	−0.001	0.000	0.012
Mg_2	0.062	0.008	0.013	0.000	−0.002	0.017	−0.001	0.000	0.000	−0.001	−0.002	0.001	0.019
Mg *b*	0.763	0.230	−0.060	0.000	0.005	0.455	−0.120	−0.004	−0.010	−0.029	−0.043	−0.035	0.133
Fe5270	1.487	0.280	0.000	0.000	0.000	−0.003	0.154	0.081	0.000	−0.003	0.003	0.082	0.306
Fe5270(Sauron)	1.185		0.000	0.000	0.000	−0.007	0.111	0.076	0.000	−0.005	0.007	0.039	0.209
Fe5335	1.244	0.260	0.000	0.000	0.000	−0.009	0.157	0.009	−0.001	−0.007	0.042	0.019	0.247
Fe5406	0.711	0.200	−0.007	0.000	0.001	0.004	0.135	0.000	0.000	0.001	0.023	0.005	0.180
Fe5709	0.448	0.180	0.000	0.000	0.000	0.028	0.093	0.001	−0.022	0.010	0.003	0.007	0.173
Fe5782	0.111	0.200	0.000	0.000	0.000	0.010	−0.011	−0.002	0.000	0.005	0.066	−0.009	0.071
Na D	0.583	0.240	0.000	0.000	0.000	−0.015	−0.037	−0.029	0.173	−0.021	0.001	−0.009	0.094
TiO_1	0.001	0.007	0.000	0.000	0.000	0.000	0.000	0.000	0.000	0.000	0.000	0.001	0.001
TiO_2	0.003	0.006	0.000	0.000	0.000	0.000	0.001	0.000	0.000	0.000	0.000	0.001	0.002
Hγ A	−8.063	0.480	−0.079	0.000	0.286	0.155	−0.219	−0.039	0.004	0.066	0.073	−0.205	−0.561
Hγ F	−2.611	0.330	−0.043	0.000	0.160	0.083	−0.035	−0.014	0.004	0.041	0.056	0.011	−0.019
Hδ A	−2.338	0.640	−0.680	−0.134	0.199	0.194	−0.221	0.009	0.014	0.146	0.021	−0.105	−0.519
Hδ F	−0.904	0.400	−0.165	−0.034	0.049	0.063	−0.131	0.029	0.005	0.065	0.001	−0.080	−0.314

Table 27. Spectral index response: Cool dwarf (5124/4.70/−2.25).

(1)	(2)	(3)	(4)	(5)	(6)	(7)	(8)	(9)	(10)	(11)	(12)	(13)	(14)
Index	I_0	Error	C	N	O	Mg	Fe	Ca	Na	Si	Cr	Ti	[Z/H]
CN_1	−0.038	0.021	−0.009	0.001	0.003	0.000	0.001	0.000	0.000	0.002	−0.002	0.000	−0.005
CN_2	−0.032	0.023	−0.011	0.001	0.003	0.001	0.002	0.000	0.000	0.004	−0.002	0.001	−0.004
Ca4227	0.301	0.270	−0.056	−0.005	0.011	0.004	0.014	0.163	0.000	−0.008	−0.018	0.001	0.095
G4300	4.313	0.390	1.148	0.000	−0.408	−0.107	−0.224	0.046	−0.007	−0.052	−0.032	0.096	0.559
Fe4383	1.702	0.530	0.231	0.000	−0.023	−0.048	0.562	−0.062	−0.003	−0.022	−0.015	0.041	0.649
Ca4455	0.099	0.250	−0.010	0.000	0.002	−0.001	0.009	−0.012	0.000	0.000	0.000	0.010	0.037
Fe4531	0.530	0.420	0.015	0.000	−0.003	−0.027	0.106	−0.018	0.000	−0.002	0.025	0.137	0.246
C_2 4668	0.094	0.640	0.019	0.000	−0.001	0.050	0.096	0.004	0.001	−0.002	−0.041	0.011	0.060
Hβ	1.062	0.220	0.000	0.000	0.000	0.004	−0.006	−0.004	0.000	0.002	−0.001	0.000	0.029
Fe5015	0.549	0.460	−0.002	0.000	0.000	−0.038	0.142	0.005	0.003	0.004	−0.004	0.143	0.330
Mg_1	−0.004	0.007	0.000	0.000	0.000	0.004	−0.002	0.000	0.000	0.000	−0.001	0.000	0.001
Mg_2	0.046	0.008	0.000	0.000	0.000	0.021	−0.001	0.000	0.000	0.000	−0.001	0.001	0.018
Mg *b*	1.393	0.230	−0.001	0.000	0.000	0.590	−0.064	−0.002	−0.002	−0.012	−0.048	0.010	0.449
Fe5270	0.639	0.280	0.000	0.000	0.000	0.002	0.200	0.061	0.000	−0.002	0.015	0.004	0.268
Fe5270(Sauron)	0.605		0.000	0.000	0.000	0.000	0.175	0.059	−0.001	−0.003	0.010	0.002	0.234
Fe5335	0.641	0.260	0.000	0.000	0.000	−0.003	0.204	0.000	−0.001	−0.004	0.028	0.005	0.215
Fe5406	0.312	0.200	0.000	0.000	0.000	0.000	0.095	0.000	0.000	−0.002	0.017	−0.003	0.111
Fe5709	0.070	0.180	0.000	0.000	0.000	0.008	0.036	0.000	−0.006	0.001	0.000	0.000	0.051
Fe5782	0.010	0.200	0.000	0.000	0.000	0.001	−0.003	0.000	0.000	0.000	0.009	0.000	0.010
Na D	0.584	0.240	0.000	0.000	0.000	−0.002	−0.015	−0.006	0.226	−0.004	0.000	−0.002	0.192
TiO_1	0.000	0.007	0.000	0.000	0.000	0.000	0.000	0.000	0.000	0.000	0.000	0.000	0.000
TiO_2	−0.001	0.006	0.000	0.000	0.000	0.000	0.000	0.000	0.000	0.000	0.000	0.000	0.000
Hγ A	−4.280	0.480	−1.150	0.000	0.390	0.170	−0.214	−0.041	0.008	0.061	0.033	−0.099	−0.948
Hγ F	−1.464	0.330	−0.594	0.000	0.198	0.084	−0.077	−0.015	0.004	0.032	0.033	−0.006	−0.373
Hδ A	−1.119	0.640	−0.263	−0.003	0.053	0.061	−0.543	0.000	0.003	0.042	0.001	−0.010	−0.546
Hδ F	−0.046	0.400	−0.068	−0.001	0.014	0.029	−0.208	0.003	0.002	0.034	0.000	−0.008	−0.199

Table 28. Spectral index response: Turnoff star (6724/4.15/−2.25).

(1)	(2)	(3)	(4)	(5)	(6)	(7)	(8)	(9)	(10)	(11)	(12)	(13)	(14)
Index	I_0	Error	C	N	O	Mg	Fe	Ca	Na	Si	Cr	Ti	[Z/H]
CN_1	−0.124	0.021	0.000	0.000	0.000	0.000	0.001	0.000	0.000	0.000	0.000	0.000	0.000
CN_2	−0.097	0.023	0.000	0.000	0.000	0.000	0.002	0.000	0.000	0.000	0.000	0.000	0.001
Ca4227	0.069	0.270	0.000	0.000	0.000	0.000	0.015	0.009	0.000	0.000	−0.003	0.001	0.011
G4300	−1.475	0.390	0.016	0.000	0.000	0.000	0.017	0.037	0.000	0.000	−0.004	0.060	0.109
Fe4383	−0.330	0.530	0.001	0.000	0.000	−0.001	0.043	−0.020	0.000	0.000	−0.001	0.031	0.059
Ca4455	0.035	0.250	0.000	0.000	0.000	−0.004	0.010	−0.005	0.000	0.000	0.000	0.009	0.017
Fe4531	0.098	0.420	0.000	0.000	0.000	−0.001	0.037	−0.006	0.000	0.000	0.007	0.018	0.063
C_2 4668	−0.014	0.640	0.000	0.000	0.000	0.016	−0.007	0.001	0.000	−0.001	0.014	0.030	−0.001
Hβ	4.485	0.220	0.000	0.000	0.000	0.000	0.001	−0.001	0.000	0.000	0.000	0.001	0.035
Fe5015	0.102	0.460	0.000	0.000	0.000	0.000	0.063	0.002	0.001	0.000	0.000	0.016	0.095
Mg_1	−0.006	0.007	0.000	0.000	0.000	0.000	−0.001	0.000	0.000	0.000	0.000	0.000	−0.001
Mg_2	0.006	0.008	0.000	0.000	0.000	0.001	0.000	0.000	0.000	0.000	0.000	0.000	0.002
Mg *b*	0.298	0.230	0.000	0.000	0.000	0.050	0.001	0.000	0.000	0.000	−0.019	0.005	0.036
Fe5270	0.110	0.280	0.000	0.000	0.000	0.000	0.034	0.019	0.000	0.000	0.000	0.001	0.052
Fe5270(Sauron)	0.125		0.000	0.000	0.000	0.000	0.038	0.019	0.000	0.000	0.001	0.001	0.057
Fe5335	0.112	0.260	0.000	0.000	0.000	0.000	0.045	0.000	0.000	0.000	0.003	0.003	0.050
Fe5406	0.052	0.200	−0.001	0.000	0.000	0.000	0.029	0.000	0.000	0.000	0.004	−0.002	0.029
Fe5709	0.007	0.180	0.000	0.000	0.000	0.002	0.006	0.000	−0.002	0.001	0.000	0.000	0.007
Fe5782	0.001	0.200	0.000	0.000	0.000	0.000	−0.001	0.000	0.000	0.000	0.001	0.000	0.001
Na D	0.147	0.240	0.000	0.000	0.000	0.000	−0.003	−0.001	0.030	0.000	0.000	0.000	0.026
TiO_1	0.000	0.007	0.000	0.000	0.000	0.000	0.000	0.000	0.000	0.000	0.000	0.000	0.000
TiO_2	0.000	0.006	0.000	0.000	0.000	0.000	0.000	0.000	0.000	0.000	0.000	0.000	0.000
Hγ A	5.781	0.480	−0.011	0.000	0.000	0.011	−0.035	−0.024	0.000	0.001	−0.004	−0.044	−0.063
Hγ F	4.539	0.330	−0.005	0.000	0.000	0.005	−0.011	−0.009	0.000	0.000	0.000	−0.005	0.003
Hδ A	5.984	0.640	−0.001	0.000	0.000	0.001	−0.069	0.000	0.000	0.002	−0.003	−0.003	−0.022
Hδ F	4.548	0.400	0.000	0.000	0.000	0.000	−0.034	0.000	0.000	0.001	0.001	−0.001	−0.010

Table 29. Spectral index response: Cool giant (4822/1.83/−2.25).

(1)	(2)	(3)	(4)	(5)	(6)	(7)	(8)	(9)	(10)	(11)	(12)	(13)	(14)
Index	I_0	Error	C	N	O	Mg	Fe	Ca	Na	Si	Cr	Ti	[Z/H]
CN_1	−0.027	0.021	−0.010	0.001	0.001	0.001	0.002	0.000	0.000	0.001	−0.001	0.002	−0.005
CN_2	−0.017	0.023	−0.012	0.001	0.001	0.001	0.003	0.000	0.000	0.001	0.000	0.002	−0.003
Ca4227	0.107	0.270	−0.053	−0.008	0.003	0.004	0.023	0.051	0.000	0.001	−0.010	0.009	0.026
G4300	5.319	0.390	1.200	0.000	−0.101	−0.092	−0.078	0.049	−0.005	−0.073	−0.022	0.127	1.069
Fe4383	1.480	0.530	0.164	0.000	−0.003	−0.013	0.175	−0.036	0.000	−0.008	−0.020	0.146	0.519
Ca4455	0.198	0.250	−0.008	0.000	0.000	−0.001	−0.024	−0.004	0.000	0.000	0.001	0.012	0.053
Fe4531	1.078	0.420	0.011	0.000	−0.001	−0.021	0.120	−0.020	0.000	0.003	0.048	0.257	0.426
C_2 4668	0.106	0.640	0.037	0.000	−0.001	0.095	0.068	0.006	0.001	−0.005	−0.112	0.061	0.082
Hβ	0.916	0.220	0.002	0.000	0.000	0.000	−0.038	−0.004	0.000	0.000	0.007	0.019	0.023
Fe5015	1.391	0.460	−0.003	0.000	0.000	0.003	0.145	0.008	0.004	0.008	−0.008	0.233	0.561
Mg_1	−0.005	0.007	0.000	0.000	0.000	0.001	0.000	0.000	0.000	0.000	−0.001	0.000	0.001
Mg_2	0.023	0.008	0.000	0.000	0.000	0.004	0.000	0.000	0.000	0.000	−0.001	0.002	0.005
Mg *b*	0.410	0.230	−0.002	0.000	0.000	0.124	−0.120	0.000	−0.001	−0.002	−0.025	0.016	−0.022
Fe5270	0.690	0.280	0.000	0.000	0.000	0.004	0.114	0.068	0.000	0.004	0.004	0.026	0.204
Fe5270(Sauron)	0.617		0.000	0.000	0.000	0.002	0.071	0.066	0.000	0.002	0.005	0.016	0.156
Fe5335	0.709	0.260	0.000	0.000	0.000	0.002	0.075	0.002	0.000	0.002	0.034	0.023	0.152
Fe5406	0.378	0.200	−0.001	0.000	0.000	0.003	0.076	0.000	0.000	0.002	0.018	−0.028	0.092
Fe5709	0.134	0.180	0.000	0.000	0.000	0.012	0.050	0.000	−0.007	0.003	0.000	0.001	0.080
Fe5782	0.022	0.200	0.000	0.000	0.000	0.001	−0.004	0.000	0.000	0.000	0.015	−0.001	0.020
Na D	0.357	0.240	0.000	0.000	0.000	0.000	−0.021	−0.008	0.053	−0.002	0.000	−0.003	0.042
TiO_1	0.000	0.007	0.000	0.000	0.000	0.000	0.001	0.000	0.000	0.000	0.000	0.000	0.001
TiO_2	0.000	0.006	0.000	0.000	0.000	0.000	0.001	0.000	0.000	0.000	0.000	0.000	0.001
Hγ A	−4.620	0.480	−1.212	0.000	0.097	0.119	−0.077	−0.046	0.005	0.074	0.081	−0.155	−1.246
Hγ F	−1.334	0.330	−0.637	0.000	0.049	0.059	0.004	−0.016	0.003	0.039	0.055	0.013	−0.468
Hδ A	−0.508	0.640	−0.260	−0.005	0.012	−0.017	−0.231	−0.002	0.001	0.027	−0.018	−0.070	−0.428
Hδ F	0.080	0.400	−0.059	−0.001	0.003	0.005	−0.113	0.003	0.000	0.022	0.005	−0.024	−0.234

Table 30. Spectral index response: Cool dwarf (5124/4.70/−2.25/+0.30).

(1)	(2)	(3)	(4)	(5)	(6)	(7)	(8)	(9)	(10)	(11)	(12)	(13)	(14)
Index	I_0	Error	C	N	O	Mg	Fe	Ca	Na	Si	Cr	Ti	[Z/H]
CN_1	−0.037	0.021	−0.009	0.001	0.003	0.001	0.001	0.000	0.000	0.003	−0.001	0.000	−0.004
CN_2	−0.032	0.023	−0.011	0.001	0.004	0.001	0.002	0.000	0.000	0.005	−0.001	0.001	−0.002
Ca4227	0.327	0.270	−0.058	−0.006	0.012	0.005	0.009	0.172	0.000	−0.009	−0.013	0.001	0.100
G4300	4.526	0.390	1.128	0.000	−0.439	−0.120	−0.163	0.048	−0.007	−0.057	−0.024	0.099	0.581
Fe4383	1.303	0.530	0.240	0.000	−0.027	−0.053	0.434	−0.065	−0.002	−0.024	−0.009	0.043	0.488
Ca4455	0.072	0.250	−0.010	0.000	0.002	−0.001	0.008	−0.012	0.000	0.000	−0.001	0.008	0.018
Fe4531	0.442	0.420	0.018	0.000	−0.004	−0.026	0.083	−0.018	0.000	−0.001	0.018	0.142	0.206
C_2 4668	0.093	0.640	0.019	0.000	−0.001	0.057	0.047	0.005	0.001	−0.001	−0.019	0.011	0.075
Hβ	1.040	0.220	−0.001	0.000	0.000	0.004	0.005	−0.004	0.001	0.002	0.000	0.000	0.028
Fe5015	0.438	0.460	−0.003	0.000	0.000	−0.050	0.098	0.006	0.003	0.003	−0.002	0.149	0.258
Mg_1	−0.002	0.007	0.000	0.000	0.000	0.005	−0.002	0.000	0.000	0.000	0.000	0.000	0.002
Mg_2	0.049	0.008	0.000	0.000	0.000	0.021	−0.001	0.000	0.000	−0.001	0.000	0.001	0.020
Mg *b*	1.546	0.230	−0.001	0.000	0.000	0.585	−0.053	−0.002	−0.002	−0.019	−0.038	0.009	0.482
Fe5270	0.509	0.280	0.000	0.000	0.000	−0.008	0.152	0.065	0.000	−0.003	0.010	0.004	0.220
Fe5270(Sauron)	0.493		0.000	0.000	0.000	−0.009	0.133	0.063	0.000	−0.004	0.008	0.002	0.192
Fe5335	0.495	0.260	0.000	0.000	0.000	−0.011	0.151	0.001	0.000	−0.005	0.022	0.006	0.163
Fe5406	0.242	0.200	0.000	0.000	0.000	−0.005	0.067	0.000	0.000	−0.002	0.016	−0.003	0.075
Fe5709	0.045	0.180	0.000	0.000	0.000	0.006	0.024	0.000	−0.006	0.000	0.000	0.000	0.033
Fe5782	0.006	0.200	0.000	0.000	0.000	0.000	−0.002	0.000	0.000	0.000	0.005	−0.001	0.005
Na D	0.619	0.240	0.000	0.000	0.000	−0.012	−0.013	−0.007	0.238	−0.007	0.000	−0.002	0.198
TiO_1	0.000	0.007	0.000	0.000	0.000	0.000	0.000	0.000	0.000	0.000	0.000	0.000	0.000
TiO_2	−0.001	0.006	0.000	0.000	0.000	0.000	0.000	0.000	0.000	0.000	0.000	0.000	0.000
Hγ A	−4.187	0.480	−1.115	0.000	0.416	0.185	−0.174	−0.043	0.008	0.065	0.026	−0.103	−0.858
Hγ F	−1.448	0.330	−0.579	0.000	0.211	0.092	−0.066	−0.015	0.005	0.035	0.027	−0.006	−0.327
Hδ A	−0.781	0.640	−0.268	−0.003	0.059	0.053	−0.432	−0.002	0.003	0.043	0.001	−0.011	−0.438
Hδ F	0.104	0.400	−0.070	−0.001	0.016	0.026	−0.162	0.003	0.001	0.034	0.000	−0.008	−0.144

Table 31. Spectral index response: Turnoff star (6724/4.15/−2.25/+0.30).

(1)	(2)	(3)	(4)	(5)	(6)	(7)	(8)	(9)	(10)	(11)	(12)	(13)	(14)
Index	I_0	Error	C	N	O	Mg	Fe	Ca	Na	Si	Cr	Ti	[Z/H]
CN_1	−0.123	0.021	0.000	0.000	0.000	0.000	0.001	0.000	0.000	0.000	0.000	0.000	0.000
CN_2	−0.097	0.023	0.000	0.000	0.000	0.000	0.001	0.000	0.000	0.000	0.000	0.000	0.000
Ca4227	0.067	0.270	0.000	0.000	0.000	0.000	0.017	0.009	0.000	0.000	−0.003	0.001	0.013
G4300	−1.460	0.390	0.016	0.000	0.000	0.000	0.007	0.038	0.000	0.000	−0.006	0.063	0.103
Fe4383	−0.366	0.530	0.001	0.000	0.000	−0.001	0.039	−0.020	0.000	0.000	−0.001	0.032	0.052
Ca4455	0.025	0.250	0.000	0.000	0.000	−0.004	0.008	−0.005	0.000	0.000	0.000	0.009	0.013
Fe4531	0.066	0.420	0.000	0.000	0.000	−0.001	0.028	−0.006	0.000	0.000	0.004	0.019	0.048
C_2 4668	−0.002	0.640	0.000	0.000	0.000	0.016	0.025	0.001	0.000	−0.001	−0.007	0.001	0.006
Hβ	4.462	0.220	0.000	0.000	0.000	0.000	0.001	−0.001	0.000	0.000	0.000	0.001	0.026
Fe5015	0.060	0.460	0.000	0.000	0.000	0.000	0.040	0.002	0.001	0.000	0.000	0.017	0.066
Mg_1	−0.005	0.007	0.000	0.000	0.000	0.000	−0.001	0.000	0.000	0.000	0.000	0.000	−0.001
Mg_2	0.006	0.008	0.000	0.000	0.000	0.001	0.000	0.000	0.000	0.000	0.000	0.000	0.002
Mg *b*	0.307	0.230	0.000	0.000	0.000	0.050	0.008	0.000	0.000	0.000	−0.014	0.005	0.049
Fe5270	0.087	0.280	0.000	0.000	0.000	0.000	0.027	0.020	0.000	0.000	0.000	0.001	0.047
Fe5270(Sauron)	0.096		0.000	0.000	0.000	0.000	0.032	0.020	0.000	0.000	0.001	0.001	0.052
Fe5335	0.076	0.260	0.000	0.000	0.000	0.000	0.038	0.000	0.000	0.000	0.002	0.003	0.042
Fe5406	0.030	0.200	−0.001	0.000	0.000	0.000	0.022	0.000	0.000	0.000	0.002	−0.002	0.021
Fe5709	0.004	0.180	0.000	0.000	0.000	0.002	0.003	0.000	−0.002	0.000	0.000	0.000	0.004
Fe5782	0.001	0.200	0.000	0.000	0.000	0.000	0.000	0.000	0.000	0.000	0.001	0.000	0.001
Na D	0.151	0.240	0.000	0.000	0.000	0.000	−0.002	−0.002	0.030	0.000	0.000	0.000	0.026
TiO_1	0.000	0.007	0.000	0.000	0.000	0.000	0.000	0.000	0.000	0.000	0.000	0.000	0.000
TiO_2	0.000	0.006	0.000	0.000	0.000	0.000	0.000	0.000	0.000	0.000	0.000	0.000	0.000
Hγ A	5.776	0.480	−0.012	0.000	0.000	0.012	−0.026	−0.025	0.000	0.001	−0.005	−0.046	−0.067
Hγ F	4.528	0.330	−0.005	0.000	0.000	0.005	−0.008	−0.009	0.000	0.000	−0.001	−0.005	−0.001
Hδ A	5.999	0.640	−0.001	0.000	0.000	0.001	−0.052	0.000	0.000	0.002	−0.002	−0.003	−0.018
Hδ F	4.555	0.400	0.000	0.000	0.000	0.001	−0.025	0.000	0.000	0.001	0.000	−0.001	−0.006

Table 32. Spectral index response: Cool giant (4822/1.83/−2.25/+0.30).

(1)	(2)	(3)	(4)	(5)	(6)	(7)	(8)	(9)	(10)	(11)	(12)	(13)	(14)
Index	I_0	Error	C	N	O	Mg	Fe	Ca	Na	Si	Cr	Ti	[Z/H]
CN_1	−0.028	0.021	−0.010	0.001	0.001	0.001	0.003	0.000	0.000	0.001	−0.001	0.002	−0.003
CN_2	−0.021	0.023	−0.012	0.001	0.001	0.001	0.004	0.000	0.000	0.002	0.000	0.002	−0.001
Ca4227	0.102	0.270	−0.053	−0.009	0.003	0.003	0.016	0.053	0.000	0.001	−0.006	0.010	0.016
G4300	5.377	0.390	1.175	0.000	−0.108	−0.097	−0.030	0.047	−0.006	−0.077	−0.015	0.128	1.082
Fe4383	1.247	0.530	0.168	0.000	−0.003	−0.014	0.134	−0.037	0.000	−0.009	−0.017	0.148	0.479
Ca4455	0.168	0.250	−0.008	0.000	0.000	−0.002	−0.015	−0.004	0.000	0.000	−0.001	0.010	0.039
Fe4531	0.948	0.420	0.012	0.000	−0.001	−0.021	0.097	−0.020	0.000	0.003	0.035	0.261	0.386
C_2 4668	0.128	0.640	0.039	0.000	−0.001	0.022	0.119	0.006	0.001	−0.005	−0.073	0.061	0.097
Hβ	0.905	0.220	0.002	0.000	0.000	0.000	−0.013	−0.005	0.000	0.000	0.004	0.020	0.027
Fe5015	1.175	0.460	−0.003	0.000	0.000	0.003	0.161	0.009	0.004	0.009	−0.005	0.238	0.508
Mg_1	−0.006	0.007	0.000	0.000	0.000	0.001	0.001	0.000	0.000	0.000	−0.001	0.000	0.002
Mg_2	0.023	0.008	0.000	0.000	0.000	0.004	0.001	0.000	0.000	0.000	−0.001	0.002	0.006
Mg b	0.542	0.230	−0.002	0.000	0.000	0.128	−0.102	0.000	−0.001	−0.002	−0.024	0.016	0.003
Fe5270	0.605	0.280	0.000	0.000	0.000	0.004	0.103	0.071	0.000	0.003	0.005	0.028	0.202
Fe5270(Sauron)	0.558		0.000	0.000	0.000	0.002	0.067	0.069	0.000	0.002	0.005	0.017	0.155
Fe5335	0.615	0.260	0.000	0.000	0.000	0.002	0.065	0.002	0.000	0.002	0.032	0.022	0.132
Fe5406	0.293	0.200	−0.001	0.000	0.000	0.003	0.060	0.000	0.000	0.002	0.019	−0.029	0.068
Fe5709	0.087	0.180	0.000	0.000	0.000	0.012	0.039	0.000	−0.008	0.003	0.000	0.001	0.060
Fe5782	0.012	0.200	0.000	0.000	0.000	0.001	−0.003	0.000	0.000	0.000	0.008	−0.001	0.011
Na D	0.360	0.240	0.000	0.000	0.000	0.000	−0.014	−0.008	0.053	−0.002	0.000	−0.004	0.039
TiO_1	0.000	0.007	0.000	0.000	0.000	0.000	0.000	0.000	0.000	0.000	0.000	0.000	0.000
TiO_2	−0.001	0.006	0.000	0.000	0.000	0.000	0.001	0.000	0.000	0.000	0.000	0.000	0.000
Hγ A	−4.572	0.480	−1.172	0.000	0.104	0.124	−0.084	−0.044	0.005	0.077	0.069	−0.159	−1.218
Hγ F	−1.354	0.330	−0.620	0.000	0.052	0.062	−0.007	−0.016	0.003	0.041	0.050	0.011	−0.474
Hδ A	−0.376	0.640	−0.234	−0.005	0.013	0.014	−0.178	−0.003	0.001	0.027	0.008	−0.040	−0.380
Hδ F	0.216	0.400	−0.061	−0.001	0.003	0.006	−0.088	0.002	0.000	0.022	0.003	−0.024	−0.194